Pontifícia Universidade Católica
do Rio de Janeiro

Alandmara Rosa Dionizio Leôncio

Injectivity and stability of oil-in-water emulsions with lipophilic natural surfactants

Dissertação de Mestrado

Dissertation presented to the Programa de Pós-Graduação em Engenharia Mecânica of PUC-Rio in partial fulfillment of the requirements for the degree of Mestre em Engenharia Mecânica.

Advisor : Prof. Márcio da Silveira Carvalho
Co-advisor: Dra. Ranena Verónica Ponce Flores

Rio de Janeiro
November 2019

Pontifícia Universidade Católica
do Rio de Janeiro

Alandmara Rosa Dionizio Leôncio

Injectivity and stability of oil-in-water emulsions with lipophilic natural surfactants

Dissertation presented to the Programa de Pós-Graduação em Engenharia Mecânica of PUC-Rio in partial fulfillment of the requirements for the degree of Mestre em Engenharia Mecânica. Approved by the Examination Committee.

Prof. Márcio da Silveira Carvalho
Advisor
Departamento de Engenharia Mecânica – PUC-Rio

Dra. Ranena Verónica Ponce Flores
Co-advisor
Laboratório de Microhidrodinâmica e Escoamento em Meios Porosos (LMMP) – PUC-Rio

Prof. Aurora Pérez Gramatages
Departamento de Química – PUC-Rio

Prof. Mônica Feijó Naccache
Departamento de Engenharia Mecânica – PUC-Rio

Rio de Janeiro, November the 19th, 2019

Alandmara Rosa Dionizio Leôncio

Bachelor in Production Engineering with emphasis in Mechanics by University of the State of Rio de Janeiro (UERJ) - 2017.

Bibliographic data

Leôncio, Alandmara Rosa Dionizio

Injectivity and stability of oil-in-water emulsions with lipophilic natural surfactants / Alandmara Rosa Dionizio Leôncio; advisor: Márcio da Silveira Carvalho; co-advisor: Ranena Verónica Ponce Flores. - 2019.

139 f.: il. color. ; 30 cm

Dissertação (mestrado) - Pontifícia Universidade Católica do Rio de Janeiro, Departamento de Engenharia Mecânica, 2019.

Inclui bibliografia

1. Engenharia Mecânica – Teses. 2. Emulsões. 3. Estabilidade de emulsões. 4. Meios porosos. 5. Injetividade. I. Carvalho, Márcio da Silveira. II. Ponce Flores, Ranena Verónica. III. Pontifícia Universidade Católica do Rio de Janeiro. Department of Engenharia Mecânica. IV. Título.

CDD: 621

To God and my family for their love.

Acknowledgments

Above all, I thank God for his infinite and unconditional love.

I especially would like to demonstrate my gratitude for my wonderful mother, Rosa, for the sacrifices she made for me and my brothers, for her immense love and friendship.

To my brothers, Alandina, Alina, Adordema and Alice, and babies for the constant smiles that make my life smooth and pleasurable.

To all my teachers from Uerj, especially Alzira, who supported and encouraged me, was friendly, kind and has an immeasurable heart.

To my friends Fernanda, Joyce, Kayza, Moacyr, Thaís, and others that Uerj gives me. Thank you for your kindness, encouragement, for listening to all my complaints and for never letting me give up.

To my advisor, Prof. Marcio Carvalho and my co-adviser Ranena for the great opportunity to work in his group, for the trust and transmission of knowledge.

To Felicle, Leo, Pedro, Tálita, and Thiago for being patient with me every time and for all the knowledge I gained in the lab.

To my friends from the residence, especially Kelly, Rose, Thayline, and Tuane for the beers and good times we shared.

To all whom I have had the honor of meeting in the Lmmp group during these two years, for all their advice, help and friendship.

To Repsol Sinopec for financing in part the project.

This study was financed in part by the Coordenação de Aperfeiçoamento de Pessoal de Nível Superior - Brasil (CAPES) - Finance Code 001.

Abstract

Leôncio, Alandmara Rosa Dionizio; Carvalho, Márcio da Silveira (Advisor); Ponce Flores, Ranena Verónica (Co-Advisor). **Injectivity and stability of oil-in-water emulsions with lipophilic natural surfactants**. Rio de Janeiro, 2019. 139p. Dissertação de Mestrado – Departamento de Engenharia Mecânica, Pontifícia Universidade Católica do Rio de Janeiro.

Stable oil-in-water (O/W) and water-in-oil (W/O) emulsions are created in different processes of oil production due to the presence of natural crude oil surfactants, such as asphaltenes, resins, oil-soluble organic acids, solids, and waxes. An interfacial film is formed causing chemical interactions between the surfactants and other species in the water phase. This work aims to study the formation and stability of emulsions stabilized by a fatty acid as natural surfactant, under ambient and high-pressure conditions, and their flow behavior through injectivity tests in sandstones. To this end, study of emulsion stability and interfacial rheology analysis were performed by evaluating the droplet size distribution and interfacial viscoelastic modulus as a function of the surfactant concentration, aqueous composition, and flow conditions. In the rheological tests, results showed that the presence of the fatty acid in the oil phase promoted a reduction in the oil-water interfacial tension and elastic modulus larger than the viscous modulus, evidencing important surface activity. All emulsions formed with an alkaline solution without salts were stable under ambient conditions. During emulsion injection in single-phase flow, water mobility control was observed through the reduction of the absolute permeability as a strong function of emulsion drop size distribution and capillary number.

Keywords

Emulsions; Emulsion stability; Porous media; Injectivity

Resumo

Leôncio, Alandmara Rosa Dionizio; Carvalho, Márcio da Silveira; Ponce Flores, Ranena Verónica. **Injetividade e Estabilidade de emulsões óleo em água com surfactantes naturais oleosos**. Rio de Janeiro, 2019. 139p. Dissertação de Mestrado – Departamento de Engenharia Mecânica, Pontifícia Universidade Católica do Rio de Janeiro.

Emulsões estáveis de óleo-em-água (O/A) e água-em-óleo (A/O) são criadas em diferentes processos de produção de óleo devido à presença de tensoativos naturais, tais como asfaltenos, resinas, ácidos orgânicos solúveis em óleo, sólidos e ceras. Um filme interfacial é formado causando interações químicas entre os surfactantes e outras espécies na fase aquosa. Este trabalho tem como objetivo estudar a formação e estabilidade de emulsões estabilizadas por um ácido graxo como um surfactante natural, sob condições ambientes e de alta pressão, bem como seu comportamento de fluxo através de testes de injetividade em arenitos. Para este fim, o estudo da estabilidade da emulsão e análise de reologia interfacial foram realizadas através da avaliação da distribuição do tamanho de gotas e do módulo viscoelástico da interface em função da concentração de surfactante, composição aquosa e condições de fluxo. Nos testes reológicos, os resultados mostraram que a presença do ácido graxo na fase oleosa promoveu redução na tensão interfacial óleo-água e módulo elástico maior que o módulo viscoso, evidenciando importante atividade superficial. Todas as emulsões formadas com uma solução alcalina sem sais foram estáveis sob condições ambientes. Durante a injeção de emulsão em fluxo monofásico, o controle da mobilidade da água foi observado através da redução da permeabilidade absoluta como uma função forte da distribuição do tamanho da gota da emulsão e do número de capilaridade.

Palavras-chave

Emulsões; Estabilidade de emulsões; Meios porosos; Injetividade

Table of contents

List of figures

List of tables

List of Abreviations

Greek Symbols

ϕ - Effective porosity

ρ - Density

Acronyms

Ca - Capillary number

CFS - Core flooding system

CMC - Critical micelle concentration

EOR - Enhanced Oil Recovery

HD - Hexadecane

IFT - Dynamic interfacial tension

k - Absolute permeability

NA - Naphthenic Acids

O/W - Oil-in-water emulsion

PSD - Particle size distribuition

q - Flow rate

RF - Oil recovery factor

SA - Stearic acid

S_{oi} - Initial oil saturation

S_{or} - Residual oil saturation

SSW - Synthetic seawater

S_{wi} - Irreducible water saturation

TL - Toluene

V_p - Pore Volume

W/O - Water-in-oil emulsion

"The best way for man to perfect himself is to draw closer to God."

Pitágoras, .

1
Introduction

1.1
Motivation

Oil is considered the main component of the world energy matrix and studies indicate that over time, disregarding the rapid development of new energy resources, the world will still depend significantly on fossil energy sources [1, 2], as shown in fig. 1.1. To increase production, it is necessary to discover new oil fields or improve production in the current reservoirs. To meet this demand, conventional methods are employed, called primary and secondary recovery, which produce only a small fraction of hydrocarbons ranging from 20 to 40%, implying that most of the oil remains in the reservoirs trapped in the rock pores. Although these methods are used in the industry, they are not very efficient due to the low sweep efficiency caused by the high mobility ratio between water and the high costs related to water treatment [3] so that it can be properly disposed of in accordance with the legislation.

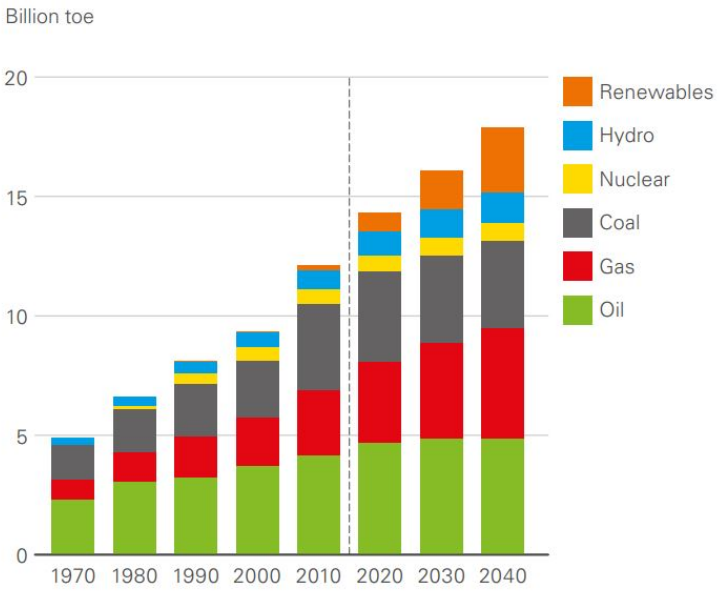

Figure 1.1: Primary energy consumption by fuel (BP Energy Outlook, 2019).

Many wells that have started production in recent decades are in declining process, so oil companies are applying and improving oil recovery tech-

niques. Several oil fields have been confronted with Enhanced Oil Recovery (EOR), due to the advances in exploration stages [4, 5]. Reservoir engineers have studied fluid flow in oil reservoirs applying more effective EOR methods to maximize oil production and economic viability, and minimize environmental impacts.

Emulsion injection is one of the most promising EOR methods. Displacement experiments have shown that more than 15% of the residual oil can be recovered by emulsion flooding in comparison to the water flooding [6, 7]. Emulsion flooding results in an improvement in oil recovery factor (RF) due to many reasons such as reduced interfacial tension (IFT) and the effective oil-water mobility ratio. Emulsions effectively block high permeability paths and improves flow through low permeability paths mobilizing the residual oil.

Emulsions are created in different oil production processes due to the presence of natural crude oil surfactant. The oil is present as dispersed phase in the large amount of produced water, and 80% of the crude oil recovered is produced in the form of emulsion [8]. Some studies in the literature argue that this water containing oil droplets can be re-injected into the reservoir as emulsion flooding, and several experimental works in the literature have been performed by adding chemicals in water to achieve emulsion stability in injection tests. Recovery process has great economic and environmental benefits as it would not be necessary to spend resources in designing stable emulsions and the produced water would be used, avoiding disposal in the environment and treatment of this water.

1.2 Dissertation goals

This study was carried out at Laboratory of Micro-hydrodynamics and Flow in Porous Media (LMMP) with the objective to study the formation, stability and flow behavior of emulsions stabilized by a fatty acid as oily surfactant.

The purpose of this work was to experimentally form oil-in-water emulsions by intentionally choosing the oily phase and aqueous phase with compositions similar to those found in oil production processes. To stabilize the emulsions, stearic acid was selected as a lipophilic surfactant with characteristics similar to natural crude oil surfactants to simulate production water with oil droplets. Stability of the emulsions were analyzed through the evolution of drop size measurements at ambient and under pressure conditions, and through interfacial rheology by studying the properties of the drops interfacial film considering the effect of salinity, pH variation, temperature and other factors that

influence the interface rheology. Analyzes of the elastic and viscoelastic modulus as a function of surfactant concentration were investigated to understand the emulsion characteristics. Flow behavior of stable emulsions were studied through sandstone injectivity tests and the efficiency of the emulsions as an EOR method through Water-alternated-emulsion (WAE) injection.

1.3 Dissertation structure

This dissertation is composed of six chapters, where the chapter §1 gives a brief introduction of the theme addressed, motivations, objectives, and present the scope of work. Chapter §2 presents the fundamental concepts associated with the problem. An overview of previous work on the topic as flow in porous media, emulsion injection and natural surfactants is discussed in chapter §3. Chapter §4 presents the methodology used in the experiments, a description of the workbenches and step-by-step procedures of the experiments. Chapter §5 presents the results and discussion. Finally, chapter §6 summarizes the main results of the research and suggests future work.

2
Fundamental Concepts

2.1
Enhanced oil recovery (EOR)

Crude oil comes from deposited organic material and consists of a complex mixture of hydrocarbons with a significant amount of isomers and compounds containing nitrogen, oxygen and sulfur [9, 10]. It contains hundreds of chemical and is generally separated into fractions according to their boiling point [1].

Due to oil complexity, the chemical compounds are classified by a technique called SARA analysis, examples displayed in fig. 2.1. SARA is an abbreviation for saturated (alkanes and cycloparaffins), aromatics (hydrocarbons, mono, di and polyaromatics), resins (fractions consisting of polar molecules containing heteroatoms such as N, O or S) and asphaltenes (resins but with higher molecular weight and polyaromatic nucleus) [11]. These analyses exhibit the oil properties and composition and are separated according to the solubility in solvents with different polarities.

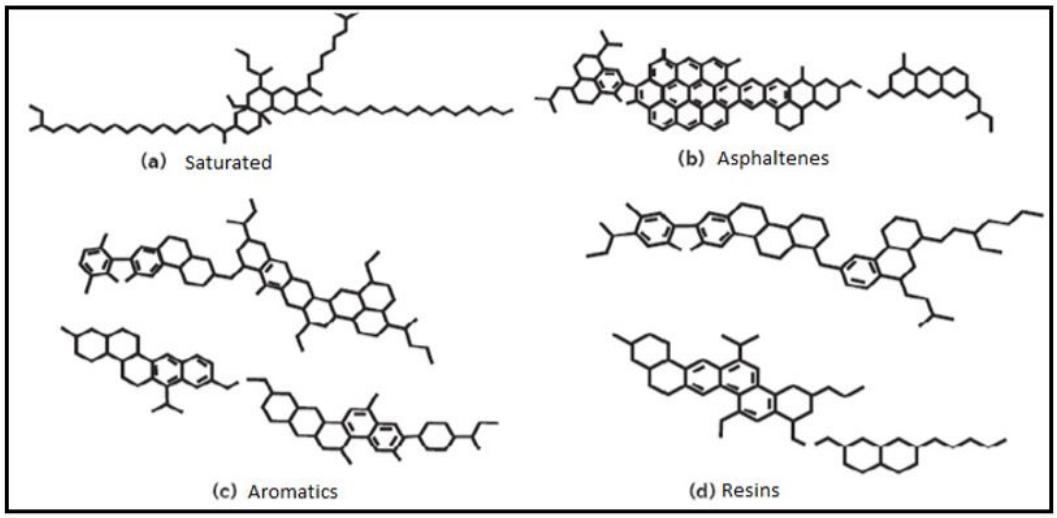

Figure 2.1: Structures representing the SARA compounds (Abdel *et al.*, 2012).

Most produced oils contain hundreds of chemical compounds, which

makes it difficult to separate them. Oils obtained from different reservoirs have different characteristics, such as their flammability at ambient conditions, their odor and the density difference that conventionally classifies them according to American Petroleum Institute standards, designated as API gravity.

The oil production process can be divided into three stages, being primary, secondary and enhanced oil recovery. When an oil reserve is identified, a producing well is installed and causes decompression of the reservoir. Generally, the reservoir pressure is sufficient to displace the oil to the surface. Primary recovery is the process at which this internal energy is used to oil recovery. However, after producing a certain amount of oil, the reservoir pressure decreases until it becomes insufficient to move the fluids to the surface, turning primary recovery not economical [12]. Hence, implementation of external energy is necessary, processes known as secondary recovery. It consists of injecting one or more fluids into the reservoir through the injection wells, and thus continue with the displacement of oil to the producing wells [12, 13].

Water flooding is the most commonly secondary recovery used technique, which is usually quite inefficient due to unfavorable mobility ratio that forms preferential paths and early water breakthrough [14]. Breakthrough is the early arrival of injected water into the producing well, which is due to the high mobility of water compared to oil. These preferential paths, as shown in fig. 2.2, are known as viscous fingerings, and the higher the oil/water viscosity ratio, the more likely they are to occur [15].

The heterogeneity of the reservoir is another factor that influences fingerings formation, as a heterogeneous rock has more or less permeable zones. This phenomenon is observed in mature fields subjected to prolonged water flooding processes or heterogeneous reservoirs with high permeability zones, which may lead to premature abandonment of producing wells. Reservoirs may contain impermeable layer e/or fracture between production and injection wells, which may also increase the formation of viscous fingerings [16, 17].

Figure 2.2: Viscous fingerings formation (Van *et al.*, 1958).

Preferential water paths generally lead to low sweep efficiency in the water flooding process. Sweep efficiency is a parameter used to analyze a recovery process and is evaluated as the ratio between the volume invaded by the injected fluid and the total reservoir volume. The effectiveness of water flooding in a given oilfield depends on a number of aspects, but especially the reservoir geology, the mobility relationship between oil and water and its wettability. Besides, at high interfacial tension between displacing and displaced fluid, the ability of the injected fluid to move reservoir oil out of the pores is greatly reduced, leaving high residual oil saturation in regions already contacted by the injected fluid.

The main weakness of the primary and secondary recovery is the low volume of oil produced. By application of primary and second recovery methods, maximum oil production is usually 20% of the original oil in place in conventional oil reservoirs [18, 19]. Enhanced oil recovery (EOR) or tertiary recovery processes are techniques used to recover the remaining oil which can not be recovery by the primary and secondary recovery [12].

EOR processes modify the original rock/fluid interactions to improve oil recovery. They can be classified into miscible processes, thermal processes, biological or microbiological processes, and chemical processes (cEOR). In miscible processes, the goal is to inject fluids that are directly miscible with oil, that means, fluids that when mixed with oil, form a single phase such as carbon dioxide or nitrogen. Thermal processes involve injection of thermal energy or heat generation in the reservoir to change the viscosity of the oil and improve its recovery, for example steam injection or in situ combustion through air or oxygen injection. Biological or microbiological processes consist of addition of bacteria in the injection water, which will perform chemical reactions in contact with the oil and will be able to break longer hydrocarbon chains, resulting in a lighter, less viscous oil. These bacteria can also cause changes in IFT between oil and water or alter the wettability of the rock. In cEOR methods, chemicals are injected causing improved microscopic efficiency by reducing the IFT between the injected fluid and the oil, maintaining a favorable mobility ratio and a more uniform sweep. Various methods can be used as cEOR in oil fields, such as gel blocking, foam flooding, polymer flooding, and emulsion flooding.

Emulsion flooding is an effective cEOR method [20], which aims to improve conformance by reducing the water mobility. The presence of oil droplets in water can block the preferential water paths, diverting flow to previously oil-saturated regions.

2.2 Fundamentals of rock properties

Rock characteristics

Oil is found in porous rocks called reservoir rocks, which are heterogeneous with pores of different sizes and shapes, and contain various types of fluids within it. The flow in porous media depends on several factors related to the physical and chemical properties of both rocks and fluids. Oil deposits usually occur in reservoirs formed by sedimentary rocks, especially sandstones and limestones. Sandstones are more easily found. Limestones are carbonated rocks and generally have greater porosity than sandstone [21]. The surfaces of the sandstone rocks generally are negatively charged according to the pH found in the reservoir conditions [22]. Sandstones are composed principally by silica with silicate minerals and limestones just have a small part of this. Sandstones are more homogeneous rock and is more adequate for cEOR.

Porosity

Porosity is an important physical parameter that directly affects the flow in porous media. This parameter measure the capacity of fluids storage and is defined as the relation between the empty rock volume and the total volume of the rock [1, 21]. It is represented by eq. 2-1,

$$\phi = V_v/V_t, \tag{2-1}$$

where ϕ is the porosity, V_v is the void volume, also known as porous volume (V_p), and V_t is the total volume of the rock which is the sum of pore volume and the volume of solid.

The volume of voids may or may not be interconnected and, accordingly, there are two types of porosity, the absolute and the effective. The ratio of the total pore space in the rock to the total volume of this medium is defined as the absolute porosity, that is the non-interconnected pores are considered. The effective porosity refers only to the interconnected pores and it represents the space occupied by the fluid, being used mainly by the reservoir engineering [23].

Saturation

Voids in a porous medium can be filled with fluids, usually various immiscible liquids and gas. Saturation is 100% if the porous medium contains only one fluid. The water saturation existing in the reservoir at the time of its discovery is called connate water and is determined from the formation samples. The reservoir phase saturation (S_f), defined by eq. 2-2, is the ratio

of phase volume (V_f) to the pore volume (V_p) of the reservoir [21]. Irreducible saturation and residual saturation are usual terms to refer to the volume of saturation phases that cannot be further mobilized during multi-phase flow.

$$S_f = V_f/V_p \tag{2-2}$$

Permeability

The permeability of a porous media is a property that measures the capacity to transmit fluids through the interconnected pores or fractures [1, 21, 23]. This parameter is a function of the geometry of the pores medium and grains. The concept of permeability is defined by the Darcy's Law, which describes the relation of the flow rate and the pressure gradient, as represented by eq. 2-3. k is the absolute permeability given in Darcy (D), q is the fluid flow (cm^3/s), A is the cross-sectional area (cm^2), Δp is the differential pressure (atm), μ is the fluid viscosity (cP), and L is the porous medium length (cm).

$$q = \frac{kA\Delta p}{\mu L} \tag{2-3}$$

There is a linear correlation between flow rate and pressure gradient in porous media, therefore Darcy's Law has some limitations in its use. It requires a stable regime, the porous media must be saturated with the fluid of interest and in low permeability porous media, flow characteristics show discrepancies when compared to Darcy's law [21, 24].

The permeability is classified in three types. Absolute permeability represents the conductivity in a porous medium when it is completely saturated by only one fluid. The absolute permeability may be calculated by aqueous phase solution injection. For this, obeying the Darcy conditions, several flow rates are examined and Δp are determined by the differential pressure transmitter [6, 25]. Although absolute permeability is invariable with the fluid that saturates the porous medium, certain factors may affect it, such as the klinkenberg effect [1], the fluid-rock reaction effect (which commonly occurs when the porous medium contains hydratable clay and permeability is measured with an aqueous phase with low salinity), and the overload pressure of the upper layers in the reservoir formation [21].

Effective permeability represents the conductivity when two or more phases are flowing in the porous media and measure the capacity of the medium

[1]Higher than actual permeability values is obtained due to gas slipping on porous media walls.

to allow one fluid to flow in the presence of other. The flow rate of a phase in a porous medium saturated with two or more fluids is usually less than the flow of a phase when it only saturates the porous medium. A reservoir is not completely saturated with a single fluid, usually flows occur with the presence of two or more immiscible fluids, such as oil and water. Its values ranging between 0 (no flow) and 1 (porous medium 100% saturated with a fluid). In case of a porous medium saturated with oil and water only, the effective permeability is described by eq. 2-4 and 2-5, where k_w and k_o are the effective permeability of water and oil respectively, and μ_w and μ_o are the viscosity of each fluid. Absolute permeability is a feature of the porous medium, and effective permeability is a function of the medium, fluid properties and saturation.

$$q_w = \frac{k_w A \Delta p}{\mu_w L} \tag{2-4}$$

$$q_o = \frac{k_o A \Delta p}{\mu_o L} \tag{2-5}$$

Relative permeability is defined as the ratio of the effective permeability of the fluid at a given saturation and the absolute permeability of the medium, $k_r = k_e/k$. Relative permeability in a rock saturated with oil and water is normally represented as a function of water saturation, as shown in fig. 2.3.

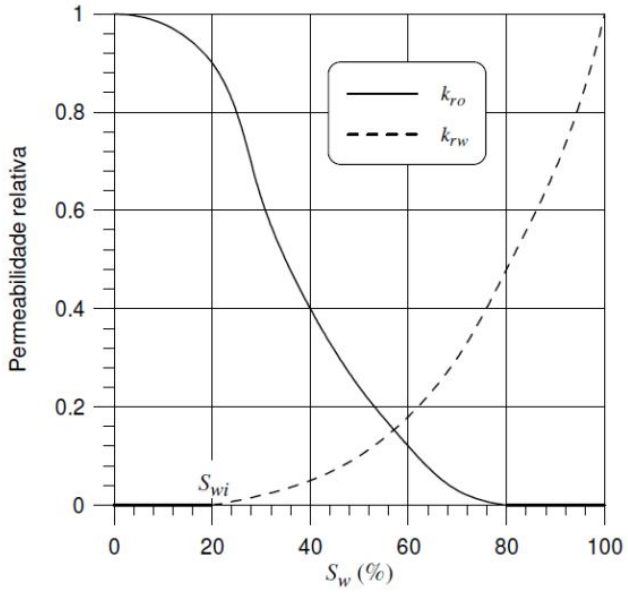

Figure 2.3: Relative permeability versus water saturation curves (Rosa *et al.*, 2006).

In the figure, initially, the relative oil permeability is 1, because the porous medium is fully saturated with oil ($S_w = 0$). Water saturation is gradually increased until it forms a continuous phase that flow, thus this saturation is called irreducible water saturation (S_{wi}). In this example, when water saturation reaches 20%, k_{rw} increases and k_{ro} decreases. The oil stops flowing when the porous medium reaches close to 80% water saturation. At this saturation only water flows and the oil saturation corresponds to the residual oil saturation (S_{or}). The reverse process is analogous from 100% water saturated porous medium [21, 26].

2.3 Properties of fluids

Capillary Number

Capillary phenomena are the result of attractive molecules of a fluid, due to different interactions of molecules in bulk and surface. When a molecule is located within a liquid, it is attracted equally in all directions by the surrounding molecules due to cohesive forces. However, if this molecule is located on the surface of the fluid, they attracted unequally to other molecules. Thus, a downward force network tends to pull these molecules back into the bulk making the surface behaves like an elastic film that offers resistance to the separation of molecules [21, 27].

The force that prevents the breakage of this film is called interfacial tension (σ). When this contact surface occurs between a liquid-gas, it is generally called surface tension. The fraction along the interface leads to a pressure jump between curved interfaces, called capillary pressure (p_c). According to the Young-Laplace equation, eq. 2-6, p_c in a spherical interface is inversely proportional to the radius of curvature (R) and directly proportional to the interfacial tension (σ) [21].

$$p_c = \frac{2\sigma}{R} \tag{2-6}$$

Capillary number (Ca) is a widely used dimensionless number in the oil industry for biphasic flows in porous media to describe the ratio of viscous to capillary forces, as defined in eq. 2-7, where μ is the viscosity of the displacing fluid, ν is the Darcy velocity, and σ is the oil–water interfacial tension.

$$Ca = \frac{\mu\nu}{\sigma} \tag{2-7}$$

Wettability

Wettability is the tendency of a fluid to spread on a solid surface in the presence of a second fluid. The contact angle (ranging from 0 to 180°) between a fluid drop and the surface is used to assess the wettability of this fluid on the surface [12, 27].

Most rocks and surfaces are commonly divided into hydrophilically when the surface has greater affinity for water and hydrophobic when the affinity is higher for oil. The shape of the interface between immiscible fluids is influenced by the interaction between the molecular forces acting on the interfaces. High surface tension compounds tend to behave like spherical drops on a surface, wetting it a little, as molecules are strongly attracted to each other and tend to bond together. If the surface tension is lower, the liquid spreads more over the surface, acquiring a lens, which has a certain contact angle with the solid surface, and depends directly on the surface tension of the liquid [28].

The phase that preferably wets the surface is called the wetting phase and the other phase is the non-wetting phase. Figure 2.4 shows a water drop in a rock surface in the presence of oil.

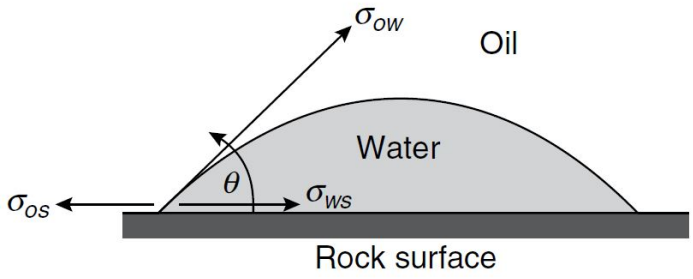

Figure 2.4: Interfacial forces between a water drop in a rock surface in the presence of oil (Green and Willhite, 1998).

The force balance between the solid and liquid, as well the contact angle θ between then, is described in eq. 2-8, where σ_{os}, σ_{ws}, and σ_{ow} are interfacial tension solid-oil, water-solid, and water-oil respectively. An oil droplet is used for a more general assessment, according to fig. 2.5. Angles between 0 and 90°C represent a water-wet rock and between 90 and 180°, an oil-wet rock [12, 27, 29]. When θ is closely to 0 oil do not contact with the surface directly, and if θ is closely to 180, the surface is completely oil-wet.

$$\sigma_{os} - \sigma_{ws} = \sigma_{ow} cos\theta \tag{2-8}$$

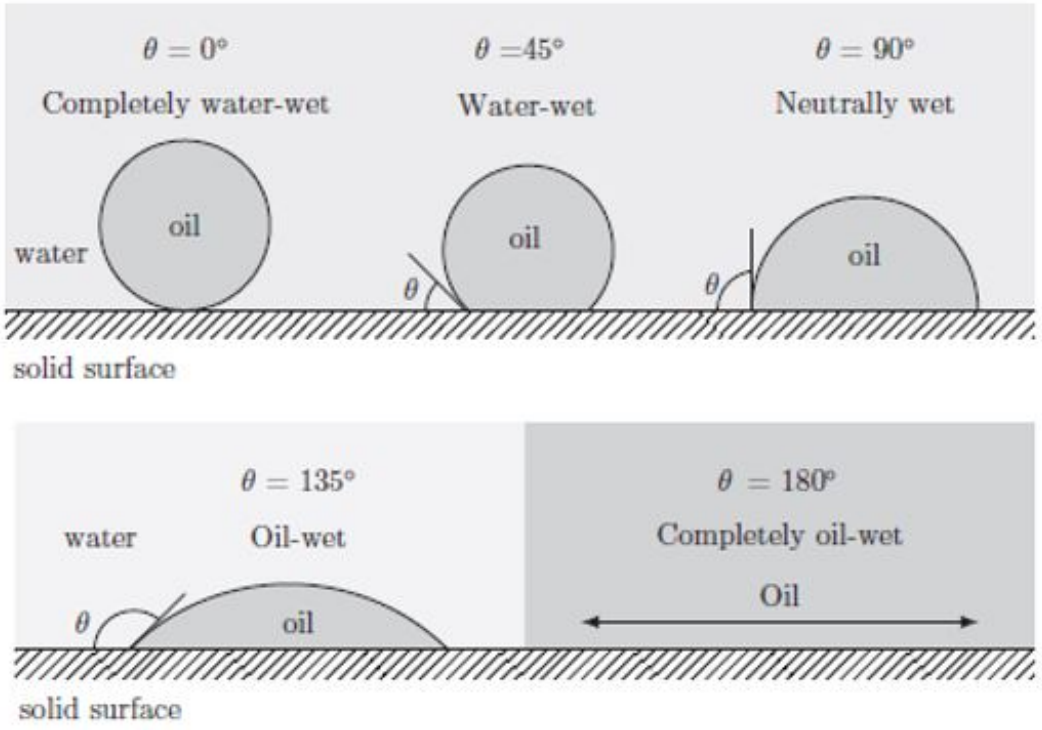

Figure 2.5: Different contact angles measured through water in an oil/water system (Blunt and Martin, 2001).

Imbibition and Drainage

Imbibition process consists of an increase in the saturation of the fluid that preferably wets the rock and drainage occurs when there is an increase of the non-wetting fluid saturation [1, 21].

Mobility ratio

Mobility ratio (M), shown in eq. 2-9, is an important parameter to consider during water flooding process. It determines the displacement efficiency of the fluids present in the reservoir, and is defined as the ratio between water and the oil phase mobility under reservoir conditions [21].

$$M = \frac{\lambda_w}{\lambda_o} \tag{2-9}$$

λ_w and λ_o represents the mobility of the aqueous and oil phase, respectively, being that mobility of a phase is the ratio between its effective permeability $k_e(mD)$ and viscosity μ (cP), accordingly to the eq. 2-10. For water flooding, the mobility ratio is generally greater than 1 due to the low viscosity of the water leading to the viscous fingering phenomenon. When the mobility ratio has very high values, typically greater than 50, sweep will not be very

efficient due to non-uniform displacement and formation of viscous fingering, preventing many areas of the reservoir from contacting the injection fluid [21].

$$\lambda = \frac{k_e}{\mu} \tag{2-10}$$

2.4 Surfactants

Surfactants (surface-active agents) are amphiphilic molecules, generally organic in nature, with a hydrophilic part (head group) and a hydrophobic part (tail group). They acts as an interfacial tension (IFT) reducers when adsorbed at the interface [30]. Figure 2.6 shows the stabilization of a drop of water in a continuous oil phase by the presence of surfactant [31]. The hydrophobic part is nonpolar and has its origin in carbonic parts (linear, branched or cyclic) [28].

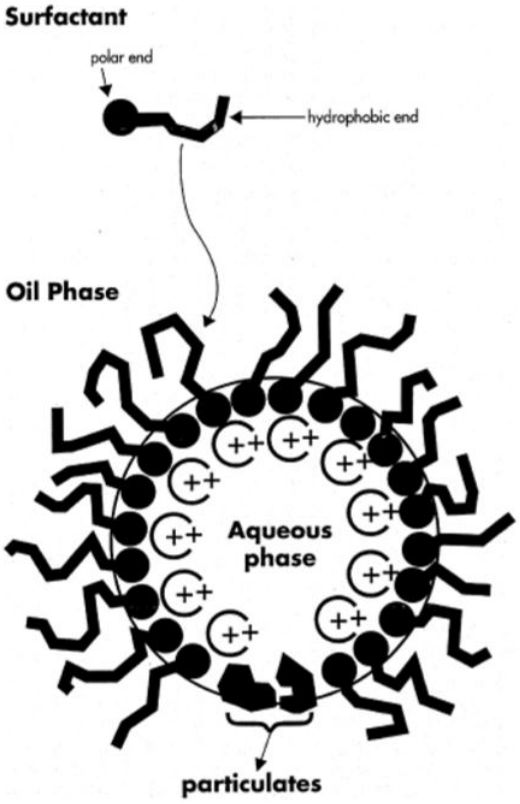

Figure 2.6: Emulsion W/O stabilized by surfactants (Lee *et al.*, 1999).

The hydrophilic part is water-soluble and a surfactant can be classified according to their polarity as anionic, cationic, nonionic , and zwitterionic: If a polar region is negatively charged, the surfactant is anionic. This type

is very soluble in water and have low adsorption on sandstone rocks, hence they are the most widely used in cEOR process. Cationic surfactants have the polar region positively charged molecule, are more tolerant with high salinity, and can adsorb in sandstone rocks due their positively charged, and they are more applied in carbonate rocks. Anionic and cationic surfactants cannot be mixed in the same solution due to the risk of neutralizing and forming an uncharged compound, therefore insoluble in water and precipitating in solution during their application. The surfactant is called nonionic when it has no actual charges, that means, are not originated from dissociated salts and do not ionize in aqueous solution. Another classification is zwitterionic or amphoteric surfactants, which behave anionic or cationic depending on the pH of the solution in which they are found. They behave as anionic surfactants in alkaline medium because the high concentration of hydroxyls neutralizes a positive charge and as cationic surfactants in acidic medium [12, 28, 30].

Hydrophile–lipophile balance (HLB)

Hydrophilic-lipophilic balance (HLB) is used to characterize surfactants indicating their tendency to solubilize in water or oil and whether the emulsion formed tends to be W/O or O/W. Thus, low HLB values indicate that surfactants are more oil soluble and form W/O emulsions, whereas emulsifiers with high HLB do the opposite [28, 30]. Due to their hydrophilic and lipophilic characteristics, surfactants show interactions when in contact with both oil and aqueous phases. They seek the interaction of their small soluble part in each of the solutions [28].

Critical Micelle Concentration (CMC)

Critical Micelle Concentration (CMC) is considered the concentration from which micelles are formed. In this concentration the entire fluid interface is saturated with surfactants and the surface tension no longer varies with the addition of surfactants, as can be seen in fig. 2.7. The investigation of interfacial properties is an essential tool to determine the ability of surfactants to reduce the tension by adsorption at the interface of the droplet. After introducing surfactants into a system, they will initially adsorb in the interface, reducing the free energy of the system by decreasing the interface energy and removing the hydrophobic parts of the surfactant from contact with water. As surfactant surface coverage increases and free surface energy decreases, surfactants begin to aggregate into micelles, thereby decreasing the free energy of the system by decreasing the contact area of the hydrophobic parts of the surfactant with water. Upon reaching CMC, any addition of surfactants will only increase the number of micelles. That means before reaching CMC, surface tension decreases markedly with surfactant concentration and after reaching the CMC,

the surface tension remains constant. For a given system, micellization occurs within a narrow concentration range [12, 30, 32, 33].

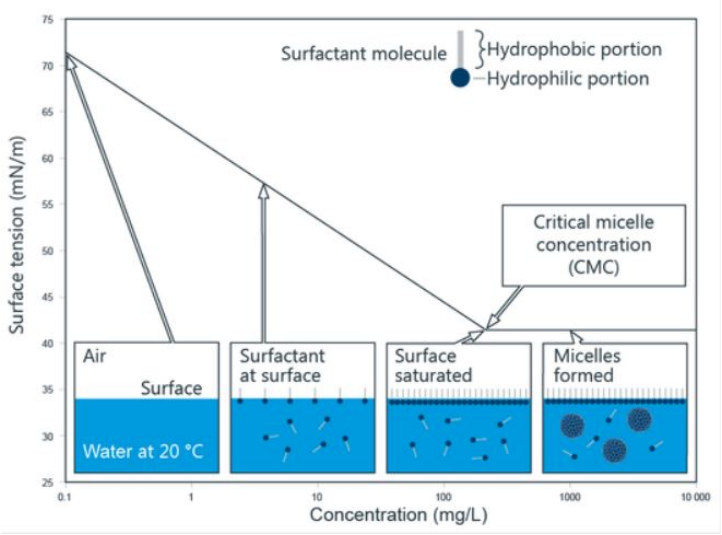

Figure 2.7: Surface tension behavior diagram between air and water as a function of surfactant concentration, indicating the CMC (Santos *et al.*, 2007) - adapted.

CMC depends on several parameters such as temperature and salinity [12]. It is generally determined by a tensiometer that measures the surface tension for different surfactant concentrations. Surface tension is linearly dependent on the logarithm of concentration over a wide range, and above CMC surface tension is completely independent of concentration, as shown in fig. 2.8. The CMC results from the intersection between the linear regression of the linearly dependent region and the line passing through the plateau.

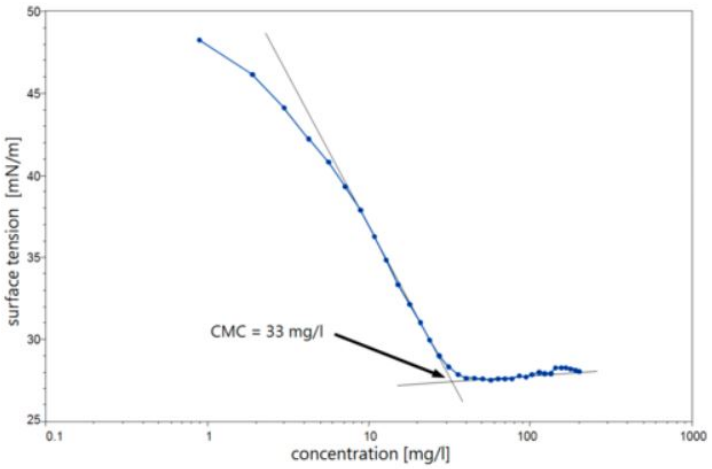

Figure 2.8: CMC determination by measuring surface tension for different surfactant concentrations (KRUSS Advancing your Surface Science, 2019).

3
Literature Review

3.1
Stability of emulsion by natural surfactants

An emulsion is a mixture of two immiscible liquids in which one of the phases is dispersed as drops within the other, called as continuous phase. Generally emulsions are stabilized by surfactants that reduce the IFT during emulsion formation and prevent coalescence between the drops. The necessary criteria to create an emulsion are the presence of two immiscible or mutually insoluble liquids, at least a surface-active component as the emulsifying agent, and a external energy, as a sufficient agitating effect to disperse one liquid into another as droplets. Emulsions are thermodynamically unstable, kinetically stable [20, 34, 35, 36, 37], and exhibit properties of a colloidal solution.

Emulsions are found in several areas such as pharmaceutical, food, cosmetics, pulp and paper, paints, coatings, and agricultural industry [34, 38, 39]. Also, they are common in the oil industry where they are generally undesirable, in particular when water is the dispersed phase, because droplets drastically increase the oil viscosity, can increase pumping costs, cause corrosion due to the presence of salt and brine in petroleum, reduce yield and may lead to equipment failure. Understanding their causes, physically and chemically, and predicting their formation are very important goals in the oil industry [34].

Depending on the dispersed phase nature, emulsions are divided into three groups: The most common type in the oil industry is the water-in-oil emulsion (W/O), which there are water droplets in an oil continuous phase; Oil-in-water (O/W) containing oil droplets in a water continuous phase; and multiple or complex emulsions (W/O/W or O/W/O), that consist of tiny droplets in a larger inside a continuous phase. Figure 3.1 exemplifies the types of emulsions. This classification depends on the volume fraction of the phases, for example when one phase is very small compared with the other, this phase normally will be the dispersed phase and the other will form the continuous phase. If both phases have the approximately the same volume, the type of emulsions will depend on others factors, like the surface-active structure and their interactions between water and oil phases [40].

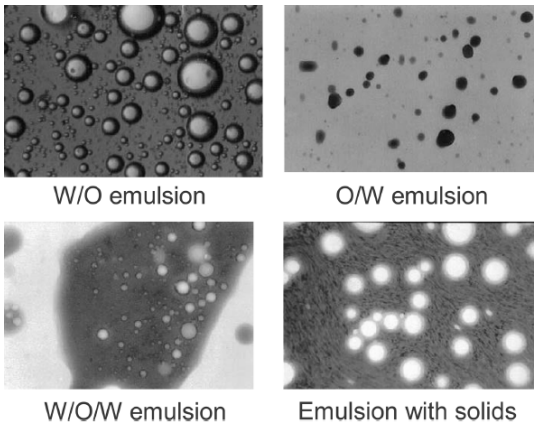

Figure 3.1: Emulsions photomicrographs (Kokal *et al.*, 2005).

Emulsions are classified as micro and macroemulsion. microemulsion is thermodynamically stable, that means, it will not be separated into oil and water phases even after a long period. The drops ranging in size between 1 to 100 nm in diameter. Macroemulsion is thermodynamically unstable, and will eventually be separated into two phases with temperature change or other thermodynamic variables. Their dispersed phase ranging between 1 to 100 μm in diameter [5, 41].

Emulsions may behave as Newtonian, dilatant, pseudoplastic or viscoelastic fluids. The behavior of a W/O emulsion is generally as a Newtonian fluid when the water cut is less than 30%. If the volume of water increases, the friction and the frequency of droplet collision increases, and an emulsion behaves as a non-Newtonian fluid and has thixotropic properties. However, there are many factors that influence the viscosity of emulsions, and it is difficult to describe it only by the volume fraction of the dispersed phase [7, 11, 40].

3.1.1 Emulsion stability

According to Kokal et al. (2005), emulsion stabilization is performed by surface agents that concentrate at the interface of droplets and create a film that reduces the IFT, avoiding coalescing droplets. When the continuous fluid between two approaching droplets drain to a point where random fluctuations and van der Waals forces destabilize the remainder of the film, droplet coalescence occurs. In this case, two or more droplets fuse together and form a single larger droplet [38], as shown in fig. 3.2. The stabilization of this film can be affected by some factors like temperature, droplet size, pH and composition of fluids used [11, 40].

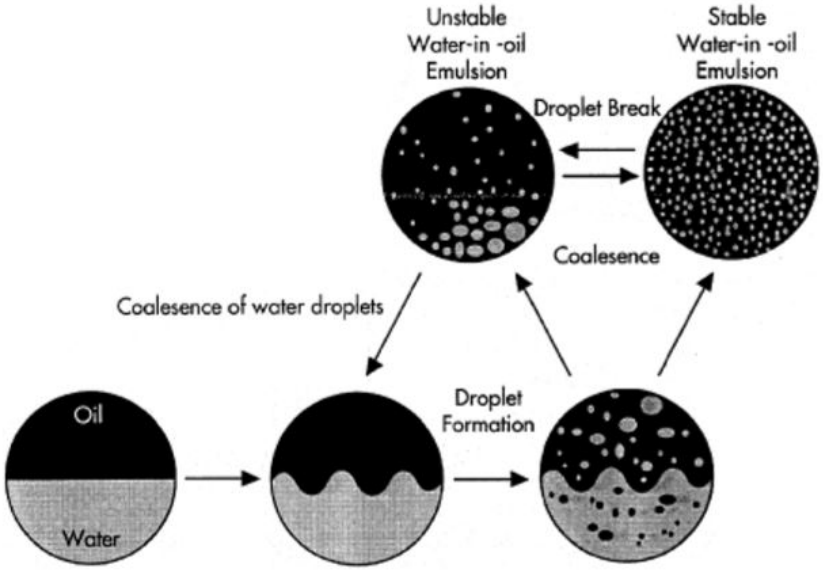

Figure 3.2: W/O emulsions formation (Lee *et al.*, 1999).

The stability of an emulsion depends mainly on the rate of aggregation and coalescing rate of a droplet, the lower the rate of aggregation and the coalescence rate, the more stable the emulsion. The resistance of crude-oil emulsion interfacial film is the key factor that influences its stability and it is closely related to the molecular structure of the emulsifier, its concentration, crude oil composition, emulsion droplet size, and water volume. In general, the larger the size of the emulsion droplet, the more likely the thim film between two drops will break [7].

The intensity of agitation may vary to produce emulsions with different drop size distribution. More efficient agitation produces a more stable emulsion, decreasing the size of the formed droplets. Temperature affects the emulsification process by changing the IFT values, the emulsifier adsorption rate and the viscosity of the emulsified system. Viscosity decreases with increasing temperature, which may favor the coalescence of drops, causing the destabilization of emulsions [37].

In general, emulsions with smaller droplets and smaller droplet size distribution shown higher stability and viscosity [42, 43]. The interfacial viscosity and the elasticity of the emulsions also greatly affect the stability, due to their influence on the rates of aggregation and drainage [7, 44]. The higher the interfacial viscosity and the interfacial elasticity of an interface, the lower the rates of aggregation and drainage and the more stable the emulsion is.

In the oil industry, the separation of crude oil emulsions is a big challenge when considering highly stable emulsions formed along oil pipelines and oil

production facilities. In addition to the decline in the commercial value of oil due to the presence of water, emulsions cause problems in many stages of oil production. Among these problems are corrosion in pipes, deactivation of catalysts and environmental impacts when the water produced is discarded [38, 45]. Hence, these can cause enormous financial losses if not treated correctly [38].

Emulsions can be destabilized by rising temperature, residence time, solids removal and emulsifier control [40]. Flocculation, creaming and coalescence are methods involved in the demulsification (breakdown of emulsions) [38, 40, 46], process shown in fig. 3.3. Flocculation is a response to brownian motion of molecules and agitation, that may occur when dispersed drops are grouped together and practically do not modify the total surface area, leading to coalescence and/or phase separation. Creaming results from the density difference between the dispersed phase and the continuous phase, resulting in the formation of two distinct layers. Coalescence occurs by a rupture effect of the interfacial film of a drop, promoting the fusion of one or more drops of the dispersed phase.

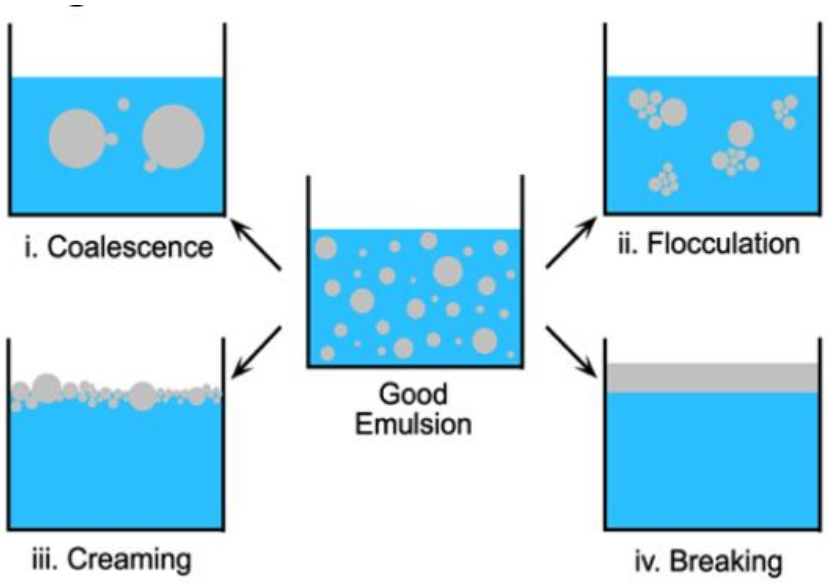

Figure 3.3: Emulsion breakdown (Djapan *et al.*, 2013).

3.1.2
Natural crude oil surfactants and crude oil emulsion

Natural surfactants or bio-surfactants (naphthenic acids) occur in crude oil containing higher boiling fractions, such as asphaltenes, resins, and organic acids and bases [40, 47]. Examples of structures found in crude oil are shown in fig. 3.4.

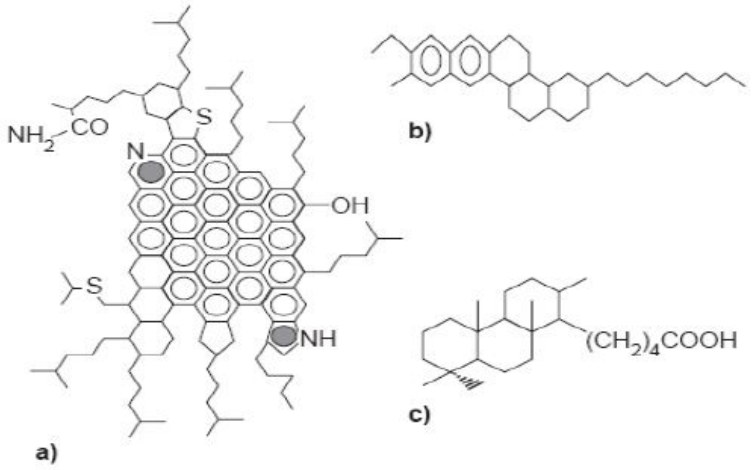

Figure 3.4: Examples of molecular structures found in crude oil: (a) Asphaltenes (b) Resins (c)Naphthenic acids (Abdel *et al.*, 2012).

Among this crude oil natural surfactants, there are acidic molecules that can ionize at the oil-water interface to form the acid anion and dramatically reduce IFT. This can lead to stabilized interfaces and emulsion stability. These acidic components include simple alkylcarboxylic acids, alkylbenzene carboxylic acids, naphthenic acids (NA) and fused aromatic acids [34].

NA are formed in the crude oil by bacterial degradation and are encountered, predominantly, in immature and biodegradable oils, in heavy oils and waste water generated in the bitumen extraction process [48, 49]. The bacteria attack the paraffin chain forming, preferably, compounds with naphthenic and aromatic shorter chain. The action of biodegradation is responsible for the increase of the acidic compounds. NA are defined as monobasic carboxylic acids of the general formula RCOOH, where R is a cycloaliphatic structure. The term generally represents all carboxylic acids present in crude oil, as acyclic and aromatic acids. They present a polydispersity in size and structure. The larger molecules are more oil-soluble than in water and most of them are dissolved in an aqueous phase at elevated pH [48].

The carboxylic part - COOH - are formed by many different components and is attached to the naphthenic structure or separated by a carbene - CH_2 -, besides may have an open chain or contain aromatic rings, depending on the origin of the oil. Mixtures of NA are difficult to understand, due the presence of polydispersity in stoichiometry and molecular weight, the fact that the physical-chemical behavior of naphthenic is different from normal fatty acids, and the complex distribution of different structures [50].

Asphaltenes are also a fraction of the crude oil and are composed of polyaromatic nuclei carrying aliphatic chains, rings and a number of heteroatoms

(including sulfur, oxygen, nitrogen, and metals such as vanadium, nickel, and iron), which account for a variety of polar groups, such as aldehyde, carbonyl, carboxylic acid, amine, and amide. They contribute to stabilizing water in crude oil emulsions, by the formation of a high mechanical rigidity at the oil/water interfaces [10, 38, 48]. Besides, they are the heaviest compounds in the crude oil, are the most polar and contain many functional groups, like acids and bases [11, 38]. Asphaltenes molecules interact strongly between each other generating aggregates that give rise to the formation of crude oil emulsions. The solubility characteristics define an asphaltene, for example, they are insoluble in n-heptane, n-hexane or n-pentane and are soluble in toluene or benzene. Therefore, the definition is as a class of solubility and, as a result, asphaltenes contain hundreds of thousands of chemically distinct molecules [11, 34, 47, 51, 52, 53].

The formation of stable emulsions during the production and transport stages is attributed to the interfacial activity of the asphaltenes [54]. The adsorption of asphaltenes at the W/O interface promotes a reduction of interfacial energy between the two phases creating strong interfacial films with viscoelastic properties [10, 55].

Kilpatrick *et al.* (2008) studied the stability of a model emulsion prepared with asphaltenes dissolved in toluene and found that the emulsion stability increased with increasing interfacial dilatational elasticity. Thus, asphaltenes are strongly attached to the interfacial film, probably through multiple intermolecular interactions of the asphaltene molecules. Analyzing the chemical composition of asphaltenes, the intermolecular interactions are probably π bonds between aromatic groups, hydrogen bonds, charge transfer interactions, multipolar forces, and van der Waals interactions. These interactions confer on adsorbed asphaltenic films elasticity, rigidity and enhanced emulsion stability [34, 56].

Unlike asphalthenes, resins are molecules soluble in light alkanes (pentane, hexane, or heptane) but insoluble in liquid propane [38, 53]. They are principally composed of naphthenic aromatics hydrocarbons and usually aromatic ring systems with alicyclic chains. Resins are effective as asphaltenes dispersants in crude oil. Components like fatty acids, resins, porphyrins, wax crystals cannot alone produce stable emulsions. However, their association with asphaltene can promote more stability. NA also do not seen be able to stabilize emulsions alone, but they are partly responsible on emulsion stability [38].

Together with the resins, asphaltenes form an interfacial film and delay the coalescence of the droplets [10, 55]. Once adsorbed onto an oil-water interface, there is densification and molecular rearrangement of asphaltene

molecules, as evidenced by many sources. During asphalthenes adsorption, many hours are needed in order that many interfacial properties reach a steady-state, including IFT, dilatational modulus of elasticity, and interfacial shear modulus. Even when all of the bulk asphaltenes in the oil phase have been replaced by pure oil, these properties change over time, indicating that the change is attributable to the consolidation or molecular rearrangement of the adsorbed asphaltenes [34]. The complexity of crude oil compositions can explain it. The variation in IFT is due to a combination of polar (acid-base) and nonpolar (lifshitz-van der waals) forces, so for pure nonpolar components, the IFT does not depend on the interfacial tension measurement time. On the other hand, if polar components are present, time dependence on interfacial tension values is expected and should lead to lower IFT values over time [57]. A schematic diagram made by MacKay *et al.* (1973), of stabilized droplets by crude oil compounds, as asphaltenes and waxes, is shown in fig. 3.5 [58].

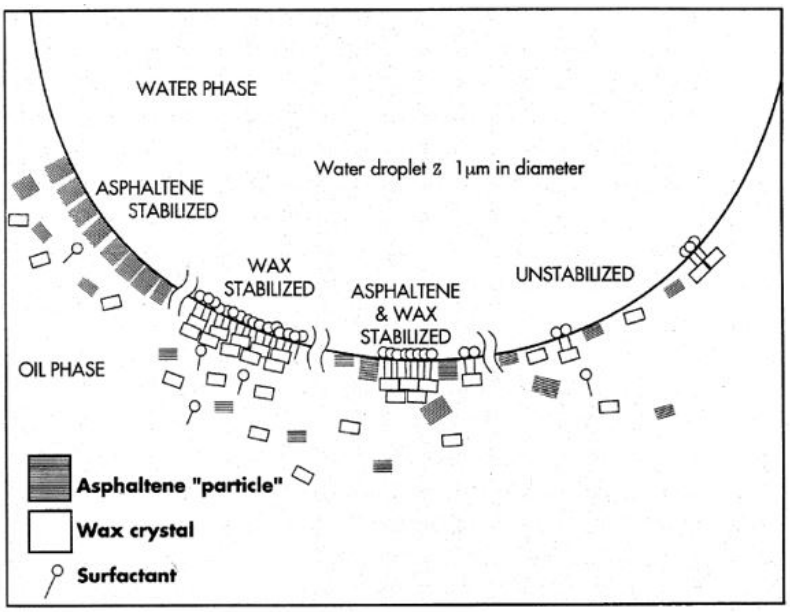

Figure 3.5: Schematic diagram showing a W/O emulsion droplet that is stabilized by asphaltenes, surfactants, and waxes. A region unstabilized is shown, where an incomplete barrier is formed (MacKay *et al.*, 1973).

Other elements can be found in the oil, such as particles of silica, clay, and oxides. They are naturally hydrophilic, however can become hydrophobic due to long time of exposure to the crude oil in the absence of water. They are particles much smaller than the droplets and act as mechanical stabilizers by adsorbing in the O/W interface [40]. Emulsions formed by this particles are called Pickering emulsions, which are assembled by stabilizing the droplets by solid particles in place of surfactants, providing a mechanical barrier to

droplet coalescence. They transmit electrostatic repulsion between droplets, further improving emulsion stability. Figure 3.6 shows a sketch of a classical emulsion (stabilized by surfactants) and a Pickering emulsion [59].

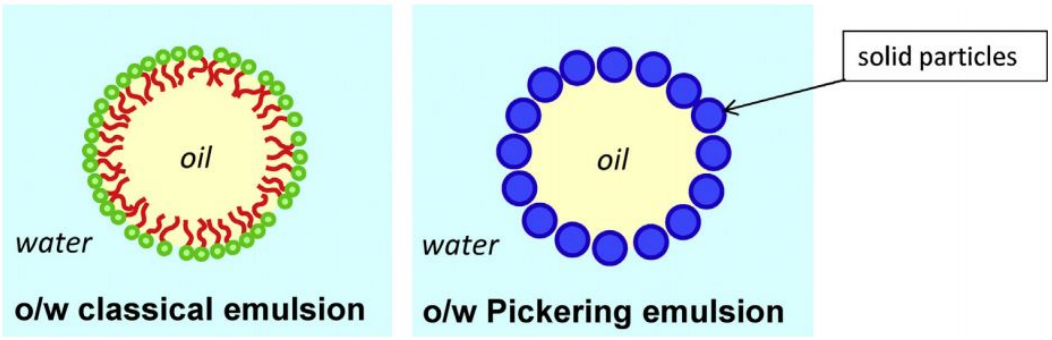

Figure 3.6: Sketch of a classical (surfactant-based) emulsion and a Pickering emulsion. The solid particles adsorbed at the oil–water interface stabilize the droplets in place of the surfactant molecules (Chevalier *et al.*, 2013).

Emulsions with combined asphaltenes and particles can be much more stable than those stabilized by just asphaltenes [38].

3.1.3 Rheological Behavior

The mechanical behavior of a fluid interface can be characterized by an interfacial rheological test [7], which are classified into two groups: shear and dilatational. The first one is based on the interfacial shear in which the interfacial area is maintained constant and it is used to measure shear rheological property. In the second one, the droplet area is sinusoidally oscillated by a defined extension while the interfacial tension is continuously measured. This technique includes the pendant drop method, the oscillating drop method, and the spinning drop method, to measure dynamic interfacial tension (IFT) and dilatational interfacial rheology with their respective viscoelastic moduli [7, 10].

Dynamic interfacial tension (IFT) considers the time of aging that depends on the diffusion and adsorption rates of the surfactants at the interface. Interfacial properties can be measured in a tensiometer through the pendant drop method, and the software of the equipment adjusts the Laplacian curve to the suspended droplet profile using a fourth-order Runge-Kuta integration algorithm. The IFT curves reduce interfacial tension over time without disturbing the interface and this is directly related to the time that the active molecules migrate and adsorb at the interface [10].

The Dilatational interfacial rheology, as the example show in fig. 3.7, is based on the interface dilation harmoniously oscillating the volume or interfacial area of a suspended drop. Changing the period of sinusoidal oscillations is one way of evaluating the speed at with which the interfacial film is recovered after being disturbed [10].

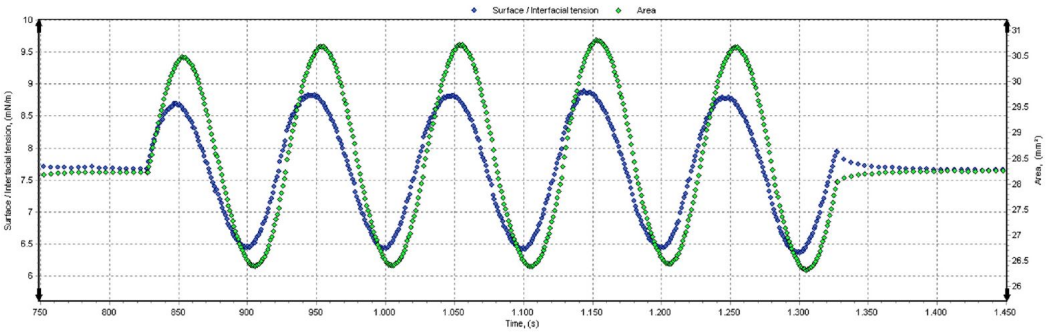

Figure 3.7: Example of experimental data of sinusoidal oscillations (Perles *et al.*, 2018).

The viscoelastic modulus ϵ has two components defined as ϵ=ϵ'+ϵ" : an elastic ϵ', and a viscous ϵ" moduli, and are defined by eq. 3-1, 3-2 and, 3-3. The modulus ϵ' regards the recoverable energy stored at the interface, and ϵ" considers the dissipation of energy over the relaxation processes [10, 60].

$$\epsilon = \left(\frac{d\gamma}{dlnA} \right) \tag{3-1}$$

$$\epsilon' = |\epsilon| \; cos \; \phi \tag{3-2}$$

$$\epsilon" = |\epsilon| \; sin \; \phi \tag{3-3}$$

In this equations, ϕ represents the phase angle displacement between the wave curves of the physical stimulus (area A variation), and γ is the interfacial tension response [10].

The presence of surfactants commonly found in crude oil limit the coalescence effect because they act by modifying the compressibility and rheology properties of the interfacial film [38, 45]. When a surface-active substance is added to water or oil, it spontaneously adsorbs at the surface

and lowers the surface tension. For small surfactant molecules, a monolayer is created, with the polar parts in contact with water, and the hydrophobic elements in contact with oil [38].

Havre and Sjöblom *et al.* (2003) evaluated the stability of emulsion including paraffinic, aromatic or naphthenic acids, as natural surfactants, with objectives to cover the emulsion droplet and increase the rigidity of the interfacial W/O layer and mimic real conditions of crude oils. This combination is relevant due to the impact in emulsion stability of acidic crude oils (including bitumen), and crude oils with high amounts of both resins and asphaltenes. The surface tension measurements were done using the ring method tensiometer, and the pH for the study of CMC was controlled by NaOH addition. The emulsions were prepared with systems containing carboxylic acid, water and heptane/toluene at different pH. It was concluded that at high pH, about 11.5, emulsions were stable for various days, about pH 5.6 they were destabilized, and at pH 7 the emulsions preserved some stability. This can be explained by the dissociation of carboxylic acids at higher pH, which creates an electrostatic stabilizing effect. The conclusions show that the emulsions have an increase in stability between pH 7 and 11.5.

Among the Carboxylic acids, it was observed that the smallest molecules are dissolved in the aqueous phase at pH 5, and the larger are preferably oil-soluble. However, at an aqueous phase with elevated pH, most of the molecules are dissolved. The variation of pH has an important role on the ability of NA monomers to stabilize emulsions. The NA become ionized as the water phase pH increases, rising electrostatic repulsion between droplets that may stabilize O/W emulsions. So, the acid salts behave as a micelle-forming surfactant at appropriate pH values [48].

Acidic pH usually produces W/O emulsions corresponding to oil-wetting solid films. On the other hand, basic pH produces O/W emulsion corresponding to water wetting mobile soap films. The pH of the aqueous phase has an important influence on the stability and type of emulsion formed, as it affects the rigidity of the interfacial film [11, 40].

In 2014, Alvarado *et al.* done several experiments to show a relation between dynamic interfacial viscoelasticity and oil recovery. Among them, it was evaluated the recovery factor on a core flooding test at low salinity and high salinity water flooding. 81% of the oil phase was produced by low salinity water injection compared to 52% with high salinity. It was also made a snap-off analysis by injecting oil at a constant pressure in a PDMS microfluidic device after saturating it with a brine solution to evaluate the water/oil interface at different brine salinities. The low salinity brine suppressed the snap-off, hence,

the droplets formed through snap-off depends on the viscoelasticity of the interface and the results show that in the presence of low salinity compared with high salinity brine, the elasticity is higher. Interfacial rheological tests also evidence that the interfacial viscoelasticity increases as brine salinity decreased, independent of the cations or anions presents in the brine solution. According to this, it was concluded that the film formed is more elastic in the presence of low salinity than of high salinity brine [61].

Moradi *et al.* (2016) evaluated the influence of aqueous-phase ionic strength and ionic composition on viscoelastic properties of the water–crude oil interfacial film by interfacial rheological measurements. They used a crude oil with 5% hexane-asphaltene content and deionized water with Na_2SO_4, $CaCl_2$ and NaCl dissolved in different concentrations, in order to investigate the impact of different cations (monovalent and divalent) and anions (sulfate and chloride). It was demonstrated that the film formation depends on the time due to the diffusion, adsorption, and rearranging of the surfactant which control the rate of the film formation. It was concluded that the naphthenic components compete with asphaltenes to adsorb onto the interface, furthermore, in a previous study, they consider that the interfacial response is a combined effect of both asphaltene and naphthenic component adsorption [42].

Brandal *et al.* (2005) investigated the interactions between a model acid crude and divalent metallic cations in the interfacial properties. The oil phase used was a 1–9 volume mixture of toluene and n-hexadecane. The water phase was a ultrapure water buffered to pH 8.0 or pH 9.0 by using a mixture of sodium tetraborate and hydrochloric acid. The divalent cations involved was Ca^{2+}, Mg^{2+}, Sr^{2+}, and Ba^{2+}, commonly encountered in naftenates, and they were added in the aqueous phase. They defended that during flow transport from the reservoir to the top, the acid monomers dissociate at the water-oil interface, making them more interfacially active when the pH of the co-produced water increases due to the release of CO_2. In a solution with co-produced forming brine, the dissociated carboxylic acid groups can also react with cations in the brine to form soaps/metal naftenates, and, under certain conditions, these metal soaps can stabilize foams and emulsion [50].

The addition of divalent cations cause a IFT decrease to different phenomena such as electrostatic attraction forces between the cations presents in the aqueous phase, the structure of the carboxylic groups presents in the acid, type of divalent cations, as well as the pH of the medium.

Emulsion stability is an important factor influencing emulsion performance in porous media and is strongly related to the pH and composition of injected water, such as salinity. Co-produced water has a significant degree of

salinity. The composition of salt is variable, the most common being sodium, magnesium and calcium in the form of chlorides [62]. A large number of studies have reported that pH and salinity have a major influence on emulsion stability [35, 45, 50, 63, 64, 65]. Several authors studied droplet size distribution over time to estimate emulsion stability and found that emulsions were more stable at lower salinity [66, 67, 68]. The possible reason for the rise in IFT with increasing salinity is that cation concentration increases with salinity, which may affect the aggregation morphology of active materials and decrease their interface adsorption [60].

Soares (2017) studied the interfacial rheology of emulsion prepared with organic acids as a natural surfactant (stearic acid and a commercially available mixture of naphthenic acid, both with carboxylic nature), representing the naphthenic acid present in crude oil. A mixture of hexadecane and toluene was used as an oily phase for different models of aqueous phases such as deionized water, and monovalent and divalent salts solutions. The influence of pH and different concentration valence of metal ions (Na^+, K^+, Ca^{2+} e Ba^2) in the IFT, the elastic modulus and the stability of the emulsion formed were evaluated. It was observed that the presence of salts and high pH in the aqueous phase increase the elastic interfacial modulus as well as their individual components [63].

According to Sauerer (2018), asphaltene and stearic acid molecules compete for the adsorption sites at the interface [57]. Moreover, Wang *et al.* (2017) evaluated asphaltene - stearic acid interactions at the water-solvent interface and asphaltene emulsion stabilization mechanisms by pending drop tensiometer analysis. The authors found that stearic acid and asphaltenes interact strongly at the interface, decreasing film rigidity compared to pure asphaltene films. The higher the stearic acid concentration the bigger the decay in IFT [55].

Perles *et al.* (2018) evaluated the O/W interface and analyzed the effect of temperature and brine concentration on the rheological properties, which are related to emulsion stability and the coalescence process. It was used a crude oil and deionized water or brine solution as aqueous phase. The crude oil used in the experiments had low viscosity and low acidity and the brine solution was a synthetic brine at pH = 7.8, in such a way that the composition of the brine was similar to the water produced in the oil production. The oscillatory pendant drop technique was used to measure the interfacial rheology. The results show that temperature do not interfere in the interface properties and the salt content in the water phase increases the viscous modulus. On both, water and brine phase, the elastic modulus was similar, however the viscous

modulus was significantly higher for brine solution compared with water.

Alves *et al.* (2014) explored the effect of salinity on the interfacial properties of a system formed by a Brazilian crude oil and brine solutions. To measure the rheological dilatational properties, the pendant drop technique was used, and the viscoelastic properties were evaluated by tests that were performed up to 24 h. The values of the total interfacial elasticity and its components, viscous and elastic modulus, were enhanced as the salt was added to the aqueous phase solution [45].

From the results, the presence of salt leads to a stronger interfacial activity that improves the interfacial elasticity and compressibility, and the salt-induced the formation of a more rigid interfacial film. The evolution of the interfacial properties with time indicates that the aging time of the interfacial film is important, and as the salt is added to the aqueous phase, this effect is enhanced. Yang *et al.* (2007) evaluated systems containing ultra pure heptol/water and asphaltenes as surfactants and found an initial dependence on total dilatational modulus over time and stabilization occurred after 20 hours of testing [69]. Regarding the influence of aging time on interfacial film formation, the results are consistent with Borges and Verruto *et al.* (2009), in which it was identified that the systems involving brine presented a longer time for the consolidation of their interfacial film [67, 70].

3.2 Emulsion flow/formation in porous media and emulsion injectivity

Many factors such as pore-throat structure, rock wettability, crude oil properties, and the quantity of residual oil influence emulsion formation process in two-phase flow in porous media [7, 43]. Among the EOR techniques, water-soluble chemical components like polymer, surfactant, and alkaline are added to the injection water to mobilize the trapped oil. Emulsion may be formed form when oil contacts with the surface-active components of injected fluids [5, 71]. Emulsions can be encountered in almost all stages of oil production, transportation and processing, due the oil composition, particularly the surface-active contained in oil [40, 72]. Zhou *et al.* (2018) evaluated the emulsification process using core displacement experiments, to study the formation of emulsion in situ. Cores with different permeabilities were used, and through them, emulsions with different drop size were formed. After that, these emulsions were injected as an EOR method to study their effect on the displacement efficiency. As the saturation of the non-wetting phase is reduced it becomes discontinuous when the viscous forces increases, thus the oil is dispersed in the wetting phase in the form of droplets. According

to the authors, the formation mechanisms of emulsions are mainly the residual oil snapping-off process and the shearing action of the emulsifier solution, as shown in fig. 3.8 [7].

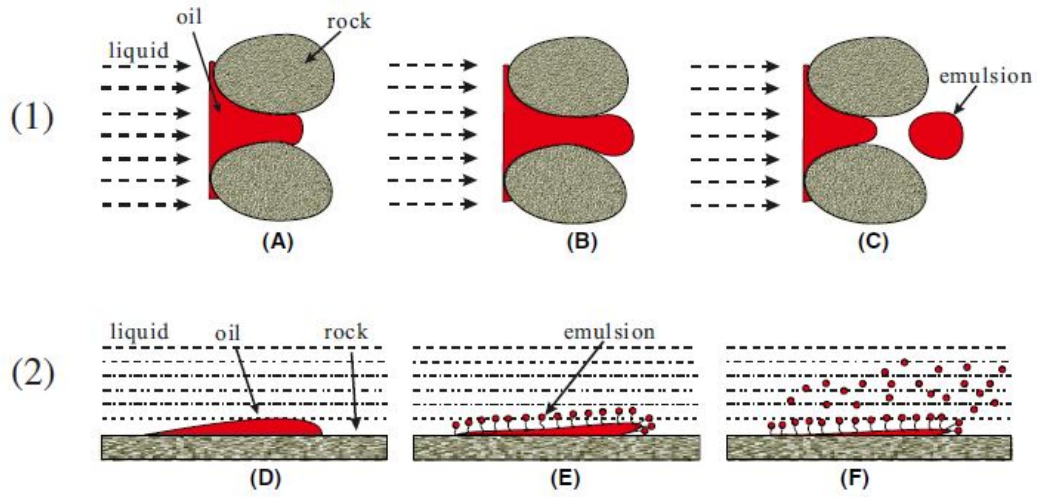

Figure 3.8: (1) The emulsion formation mechanism in porous media by the snap-off process: (A) The residual oil after water flooding; (B) The residual oil elongated; (C) The emulsion formed by the snap-off process. (2) The formation mechanism of emulsions in the porous media by shearing action: (D) The residual oil film after water flooding; (E) Small droplet size emulsion formed by shearing action of the emulsifier solution; (F) Oil film reducing and more emulsion formed (Zhou *et al.*, 2019).

When the emulsion drop size is much smaller than the throat diameter, the dispersed phase migrates within the porous medium and the emulsion can be considered as a continuous phase because the deformation of each drop is negligible. If the emulsion drop size is larger than the throat diameter but smaller than the pore diameter, the emulsion deforms when it migrates through the throat. The flow behavior of an oil drop at pore scale explains how emulsion can improve oil recovery. Figure 3.9 shows the flow of a drop through a pore throat, in which the drop is larger than the throat, and it needs to deform to pass through this pore. In this configuration, the radius of curvature at the front of the drop is smaller than at the rear, and an extra pressure is needed to force the droplet to flow into the porous medium. This process is known as Jamin effect [73], which is affected by emulsion droplet size, pore size and interfacial tension.

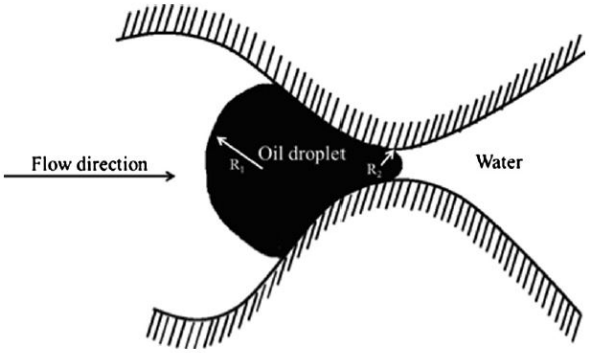

Figure 3.9: Capillary trapped drop: Jamin effect (Moradi *et al.*, 2014).

Cobos *et al.* (2009) studied experimentally the flow of O/W emulsions through a constricted quartz micro-capillary tube to mimic a connecting pore-throats of a high permeability porous media. The average drop diameter of the emulsions injected varied from smaller to larger than the constriction, and they were formed by a polymer solution as the aqueous phase, and a nonionic surfactant with a 10 times concentration in relation to its CMC. During the small drop emulsion injection, the inlet pressure kept almost constant and the presence of the dispersed phase did not alter the inlet pressure significantly, compared to the flow of the continuous phase. On the other hand, for emulsion with higher mean diameter, the presence of oil drops in the aqueous phase caused substantial fluctuations in the inlet pressure, as shown in fig. 3.10.

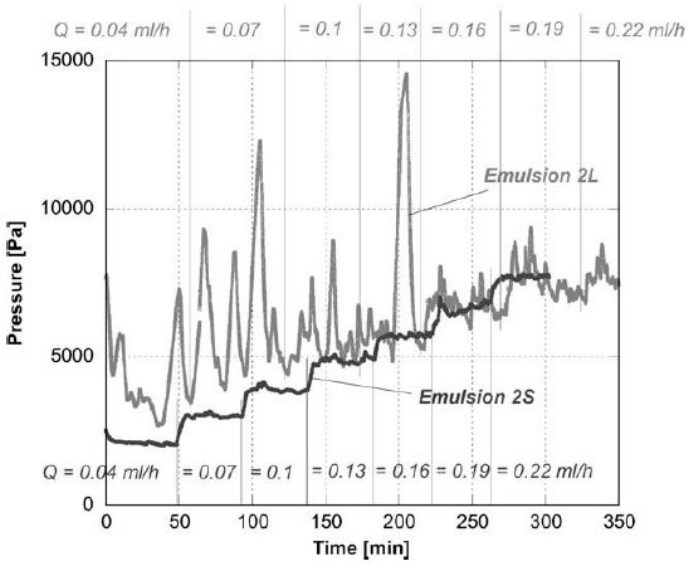

Figure 3.10: Evolution of the inlet pressure as the flow rate varies for one emulsion that contains drop size average smaller than the capillary constriction, 2S, and one emulsion that contains drop size average higher than the capillary constriction, 2L (Cobos *et al.*, 2009).

It was observed that the curvature radius in front of the drop goes down, and a higher pressure difference is required to overcome the capillary pressure [74].

The Capillary number (Ca) represents the ratio between viscous forces and capillary forces. At high Ca, viscous forces are stronger and the extra pressure needed to deform the drop as it flows through the constriction is negligible. At small Ca, the capillary forces are more important and, consequently, it is more difficult to deform the droplet, leading to a strong mobility change.

Several researchers reported that improved reservoir sweep occurs when Ca is below a critical value, and therefore there is pore blockage in the porous media. Above this critical value, the block mechanism is weak [25, 74, 73, 75]. Therefore, capillary forces are an important factor responsible for oil trapped and the Ca determines how strongly the trapped oil stays in a porous medium [76]. Guillen (2012) and Cobos *et al.* (2009) proposed a model to describe this behavior at pore scale through a mobility reduction factor f, defined as the ratio of the average pressure measured during continuous phase flow, Δp_c, to that of the emulsion flow, Δp_e [25, 74].

Figure 3.11 shows the mobility reduction factor f, by Guillen *et al.* when applied in a porous medium, as a function of Ca for the emulsions tested in the experiments. The results show that for the emulsion with drops smaller than the constriction, $f \sim 1$ and it is not a function of the Ca. On the other hand, when the drops have the same scale as the throat or higher, f strongly depended on the Ca. At high Ca, $f \to 1$.

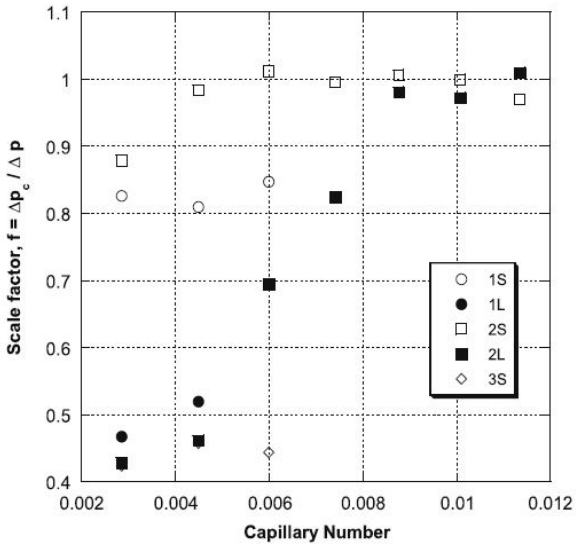

Figure 3.11: Scale factor in function of the Ca for flow of the emulsions (Cobos *et al.*, 2009).

Moradi *et al.* (2014) evaluated the efficiency of emulsion injection in single-phase flow experiments to understand their flow at pore scale. Crude O/W emulsions with stable drop-size distribution were injected in Berea sandstone cores, with different permeabilities, at increasing flow rate. In this tests, flow experiments were carried out with smaller and larger average drop size to pore size ratio. The effluent samples from each single-phase flow were collected, and according to fig. 3.12, the porous medium filtered the droplets and the larger ones got trapped in the pores. Hence, this portion that was trapped may block the pores. The droplet blocking mechanism becomes less effective when the water flow rate, and therefore Ca, increases above a critical value. The larger the droplet-to-pore size ratio the greater the Ca needed, that is, higher viscous forces are required to mobilize the droplets in the porous medium [73].

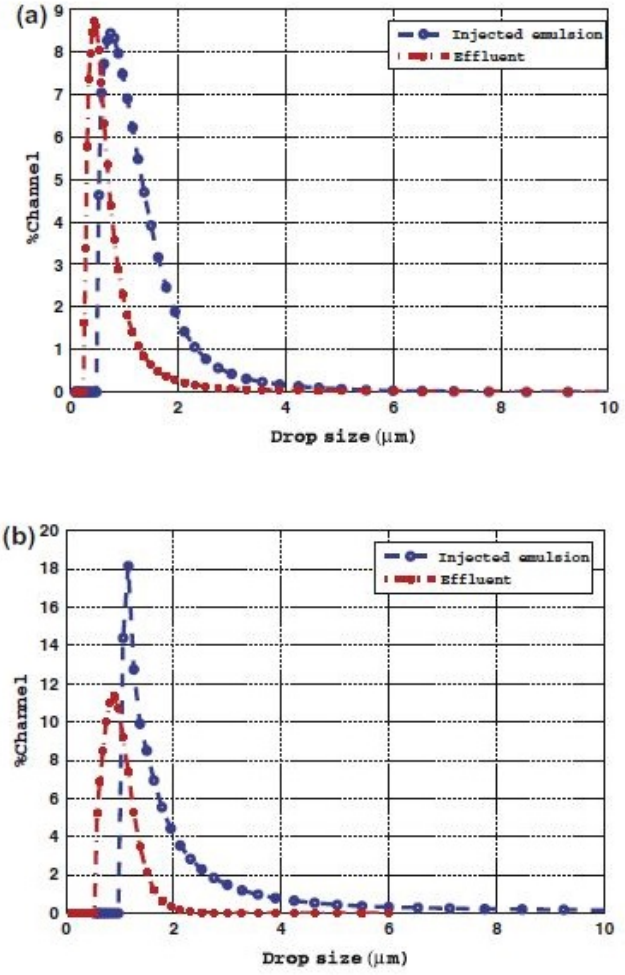

Figure 3.12: Filtering effect in the porous media: (a) Experiment with smaller average drop size to pore size ratio. (b) Experiment with larger average drop size to pore size ratio (Moradi *et al.*, 2014).

Fu *et al.* (2019) also studied emulsion injectivity in porous medium. The emulsion injection efficiency was rated by a resistance coefficient F_R, defined by eq. 3-4, where Δp_e is the pressure during emulsion injection, and Δp_w is the pressure in the post water injection. This factor quantifies the change in transport resistance of the emulsion system in porous media [8].

$$F_R = \frac{k_w \times \mu_e}{k_e \times \mu_w} = \frac{\Delta p_e}{\Delta p_w} \tag{3-4}$$

According to the results, F_R is the inverse of f, so similar conclusions was considered, as when $F_R > 1$ the drop is larger than the pore throat, it breaks or causes phase segregation due to increased pressure to deform the droplets as they pass into the pore. For $F_R < 1$ the emulsion can move freely in the pores and the blocking tendency is reduced. Maximum resistance to migration occurs when $F_R \sim 1$, in which case the droplet diameter is similar to the throat diameter and causes mobility control.

3.3 Emulsion injection as an EOR method

Emulsions have been an effective improved chemical oil recovery (cEOR) method [20]. Among the methods available for remaining and residual oil recovery, cEOR is one of the most promising methods designed to increase the microscopy (pore scale oil recovery), and macroscopic sweep efficiency [12].

Conventional light oil reserves is in decline and more attention has been paid to heavy oil reserves which are estimated to be twice the reserves of light crude, and the production is expected to increase significantly in the future. The average oil recovery for conventional oils is about 30%, however, for heavy oilfields, this value is reduced due to unfavorable mobility ratio [77]. It is hard to recover heavy oil, principally because of its high viscosity and poor mobility under reservoir conditions, that impairs water flooding. Hence, water flooding to heavy oil reservoir was generally characterized by low recovery and rapid increase in water cut. The two phase flow can lead to emulsion formation. W/O emulsions are more common than O/W emulsions mainly due to the lipophilic components present in heavy oil, and the fact that heavy oil is more viscous than water and is easier for water droplets to disperse on continuous oil phase [43, 78, 79]. A typical acidic heavy oil and viscous W/O emulsions formed with formation water was studied by Pu *et al.* (2018) [78]. The heavy oil was mixed with formation water without additional surfactants, and exhibited the emulsifying characteristics of natural heavy oil

surfactants such as asphaltene, resin, and petroleum oxide. Zhou *et al.* (2019) studied the flow of alkali/surfactant/polymer (ASP) through experiments and field applications and found out that oil recovery is 5% higher with emulsions compared with no emulsions [7].

Several authors proposed many mechanisms to explain the extra oil recovery with emulsion flooding such as modification of rock wettability [69, 80], modification of oil and water mobility [45], reducing water mobility and blocking large pores with dispersed emulsion phase [7, 81]. Emulsion injection may be performed between two water flooding cycles, a process called water-alternated-emulsion (WAE), resulting in an improvement in RF due to the mobility control of the aqueous phase by blocking pores in preferential paths, and reduction the effective permeability of these zones. Furthermore, emulsion injection after conventional water flooding can lead to an additional recovery of up to 20% [6]. With preferential paths blocked by the dispersed phase of the emulsion, water is diverted to different areas of the porous medium, resulting in better sweep efficiency of subsequent water flooding [82]. Figure 3.13 shows the deviation of the preferential water path after emulsion injection. Thus, emulsion injection causes an increase in pressure around the oil ganglia, which exceeds their capillary pressure, resulting in their mobilization [83].

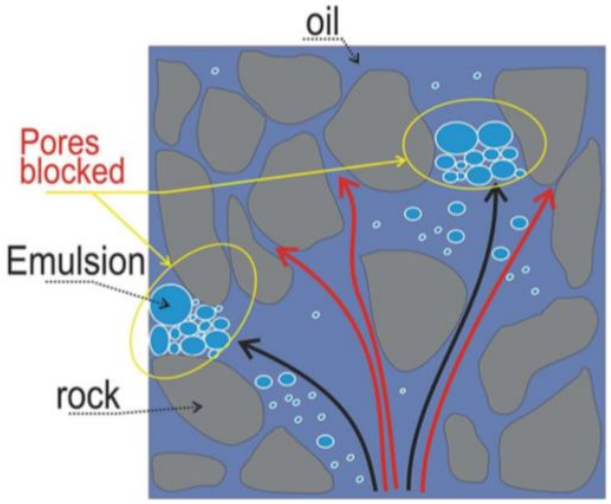

Figure 3.13: Pore blockage during emulsion flooding, altering the water preferential paths (Engelke *et al.*, 2012).

To mobilize the residual oil in an reservoir, interfacial tension reduction and/or effective mobility ratio between displacing fluid and residual oil is required [5, 35, 76, 77]. In EOR method, emulsion droplets compress each other in the flow process, blocking the high permeability path and forcing the wetting phase into low permeability paths [5].

The first experiments on emulsion injection as a EOR method was published by McAuliffe (1973a), which conducted laboratory studies with crude O/W emulsions prepared with dilute solutions of sodium hydroxide in sandstone cores [84]. Then a field test was reported by the same author (McAuliffe, 1973b) at Midway Sunset Oilfield, California, and until 2019 it is considered the most successful test. A total of 33,000 bbl emulsion bank (14 % oil content) was injected in this area and, among the results, a decreased fingering and a better volumetric sweep efficiency was reported. Reduction in the water production occurred and produced water salinity rose, indicating reduction of core permeability by emulsion injection. Additional oil recovery was estimated in 55,000 bbl indicating positive responses to emulsion flooding which was attributed to the improvement of the reservoir heterogeneity by the oil droplets that blocked high reservoir permeability zones [85].

McAuliffe (1973b) and Hofman *et al.* (1991) observed a reduction in permeability in their tests that strongly depends on the drop-to-pore size ratio. For fixed pore size, a very small droplet deforms and the radius of curvature ratio is close to 1 without blockage. For a big fall, it needs to warp, thus occurring the Jamin effect, and may or may not block the paths [85, 86].

Guillen *et al.* (2012) observed some benefits of mobility control by emulsion flow in porous media during WAE injection. They reported that emulsion injection changed the water phase path leading to higher volume of displaced oil. The O/W emulsion was injected at two different capillary numbers. Results are shown in fig. 3.14. At both Ca, oil was initially displaced by the injection of aqueous solution then, emulsion slugs were injected followed by aqueous solution. At low Ca, the volume of oil recovered after emulsion injection was considerably higher than at high Ca. At high Ca the emulsion drop have little effect on the fluid mobility, drops acts only as mobility control agent at low Ca. The results of applied O/W emulsion at low Ca after water flooding show that the RF increased from 35% to 55% [25].

Emulsion mobility control effect has been studied also by studying macroscopic rock-fluid properties. Engelke *et al.* (2013) compared the relative permeability curves of oil and water, and oil and emulsion. The residual oil saturation with emulsion injection was much lower than that obtained only with water injection, meaning that the droplets mobilize the oil ganglia, decrease the mobility of the aqueous phase, as well as delay the breakthrough of the water [87].

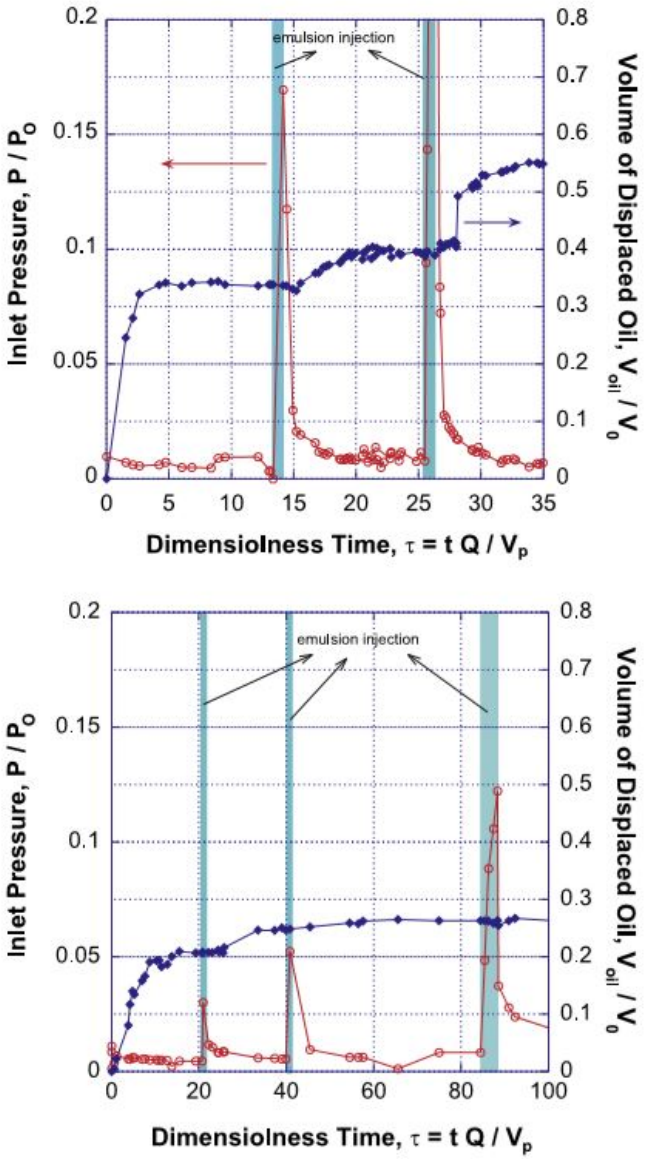

Figure 3.14: (a)Evolution of volume of oil displaced and inlet pressure at Ca below the critical Ca. (b) Evolution of volume of oil displaced and inlet pressure at Ca above the critical Ca. The equivalent continuous phase pressure is represented on the left axis, and the right axis corresponds to the oil recovery factor. The emulsion injection range is represented by the shaded area (Guillen *et al.*, 2012).

4
Experimental Procedure

4.1
Emulsions preparation and stability analysis

4.1.1
Working fluids

Model Oil

The model oil selected to compose the oil phase of the emulsions were mixtures of hexadecane (99% Sigma Aldrich) and toluene (99% Isofar). Hexadecane (cetane, $C_{16}H_{34}$), shown in fig. 4.1, is an alkane hydrocarbon, colorless liquid or leaflets and odorless. It is practically insoluble in water and generally used as an organic intermediate solvent, and an ingredient in gasoline, diesel and aviation fuels. It can be found in crude oil and naturally in many edible plants and can cause toxicity in humans [88, 89, 90].

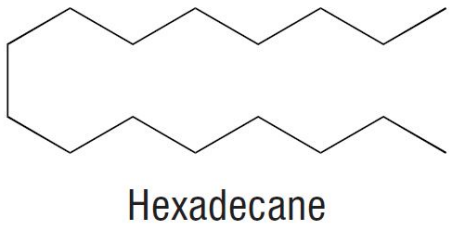

Figure 4.1: Hexadecane chemical structure (Haynes *et al.*, 2017).

Toluene (C_7H_8), shown in fig. 4.2, is an aromatic hydrocarbon, consisting of a nonpolar solvent, methylbenzene and volatile organic compound. It is clear, colorless and has a smell associated with paint thinners. In addition, it occurs naturally in crude oil, is produced in the process of manufacturing gasoline and other fuels, and is used predominantly as an industrial raw material and as a solvent [88, 89, 90].

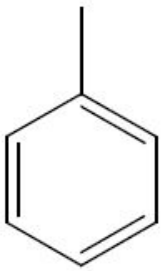

Figure 4.2: Toluene chemical structure (Haynes *et al.*, 2017).

In tensiometer tests performed by Soares (2017), it was found that there was dissolution of a drop of the oil phase in the aqueous phase in systems with a mixture of hexadecane and toluene, due to the solubility of toluene in water and high volatility which causes a decrease in the droplet volume throughout the experiment. To minimize this effect, the ideal blend was 90% hexadecane and 10% toluene [63]. Table 4.1 shows density and viscosity values at different temperatures of the model oils and its components.

Oil phase	T [°C]	ρ[g/cm³]	μ[cP]
Hexadecane	25	0.7699	3.0892
	45	0.7563	1.7129
Toluene	25	0.8670	0.5900
	45	0.8435	
Hexadecane + Toluene (9:1)	25	0.7768	3.0943
	45	0.7651	1.8812

Table 4.1: Properties of the fluids used as oil phase (model oil).

Aqueous phase

Different aqueous phase were used in the experiments: 1) Synthetic sea water solution prepared following ASTM norm (D1141-98 - Standard Practice for the Preparation of Substitute Ocean Water) with chemical composition showed in fig. 4.3 [91]; 2) Milli-Q water; 3) Buffer solution to maintain a basic pH of the solution.

Compound	Concentration, g/L
NaCl	24.53
$MgCl_2$	5.20
Na_2SO_4	4.09
$CaCl_2$	1.16
KCl	0.695
$NaHCO_3$	0.201
KBr	0.101
H_3BO_3	0.027
$SrCl_2$	0.025
NaF	0.003

Figure 4.3: Chemical Composition of the synthetic sea water solution prepared following ASTM norm.

The buffer solution was prepared with THAM base and HCl. Preparation was started with THAM base, reagent powder which was dissolved in water, and then the pH value was adjusted by the addition of HCl (hydrochloric acid).

THAM, abbreviation for Tris(hydroxymethyl)aminomethane, is classified as an amino alcohol in form of white crystalline solid, as shown in fig. 4.4. It is considered a weak base ($R-NH_2$), and in the presence of acid (HCl) reacts as shown in eq. 4-1 [92, 93, 94]. This compound is very soluble in water but poorly soluble in fats, with a buffering capacity dependent of temperature [92]. At 25°C it has a buffered capacity between 7 and 9.

Figure 4.4: Tris(hydroxymethyl)aminomethane.

$$(CH_2OH)_3C - NH_2 + HCl \rightleftharpoons (CH_2OH)_3C - NH_3^+ + Cl^- \qquad (4\text{-}1)$$

Calculations for buffer solution were based on the Henderson-Hasselbalch equation. To prepare $1L$, 12.114 g of the THAM compound and 56.85 ml of

$0.1M$ of HCl solution were added to approximately 800 ml of deionized water. Subsequently, the volume was completed until $1L$. The solution was stirred for 30 min and the pH measured was 8.0, as expected.

The aqueous phase properties are display in tab. 4.2.

Aqueous phase	T [°C]	ρ[g/cm³]	μ[cP]	pH
Synthetic sea water	45	1.0144	0.7760	8.23
	25	1.0212	0.9844	8.23
Milliq Water	45	0.9902	0.5437	6.62
	25	0.9900	0.5436	6.62
Buffer	45	1.0032	0.7554	8.00
	25	1.0041	1.1146	8.02
NaCl + Buffer	25	1.0027		8.19
	45	1.0013		8.18

Table 4.2: Aqueous phases properties at different temperatures.

4.1.2 Surfactant

Stearic acid (SA) was chosen for this study as the acidic oleic surfactant model, due to their simple molecular structure, and the fact that linear carboxylic fatty acids are preferentially adsorbed at the O/W interface than other naphthenic acids containing cyclic components [55]. SA is an octadecanoic acid with chemical formula $C_{18}H_{36}O_2$ as illustrated in fig. 4.5. It is a saturated fatty acid derived from animal and vegetable fats and oils, with high latent heat, excellent thermal stability, little overcooling, and with melting point between 67 and 70°C [95]. Besides, it is a relatively non-polar compound and is therefore more soluble in non-polar solvents [96, 97, 98, 99, 100, 101]. It is completely saturated and therefore has a straight chain that can be tightly packed into an interfacial monolayer. SA is a weak acid that dissociates little in aqueous medium, therefore, there is more acid in the nonionized form and it acts as a nonionic surfactant.

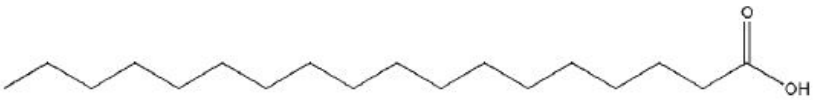

Figure 4.5: Stearic acid chemical Structure (Rowe *et al.*, 2009).

SA is applied mainly in the manufacture of pharmaceutical, cosmetics and food products, as it is considered inert, inexpensive, biocompatible and

has low toxicity. In general, it is used as an emulsifying and solubilizing agent, tablet and capsule lubrificant, and if it is neutralized with alkalis it can be used in the preparation of creams [102]. It is commercialized as white plate-shaped crystals, as shown in fig. 4.6 [103, 104].

Figure 4.6: Stearic acid.

SA has been found to associate strongly with asphaltene molecules at the interface and make films more expanded and flexible, and it is highly insoluble in water due to its long lipophilic chain length. In contact with oil and water phases, SA can adsorb on the the interface and will form a surface film with the hydrophilic group -carboxylic part - oriented towards the water phase and the lipophilic group - hydrocarbon chains - oriented away from water phase.

Stearic acid solubility

SA is a fatty acid distributed in the form of crystals under ambient conditions, so their solubility in the oil phase was analyzed. For this purpose, 10 ml of hexadecane were doped with 0.5% (wt/v) of SA. Such concentration was adopted in an exploratory way. The mixture was left under a stirr/heat plate for 20 minutes at 70°C, and after the plate was cooled to 25°C, the mixture stirred again for a further 20 minutes. The mixture was poured into a 100 ml Adonex becker attached to a thermostatic bath and was visualized in the Zeiss microscope. The temperature range was 25 to 45°C, enough to fully solubilize the acid.

Solubility of the SA in hexadecane at different temperatures is shown in fig. 4.7. It can be see that the acid is totally dissolved at around 40°C and in

order to keep solubility the temperature was set to 45°C during the oil phase preparation.

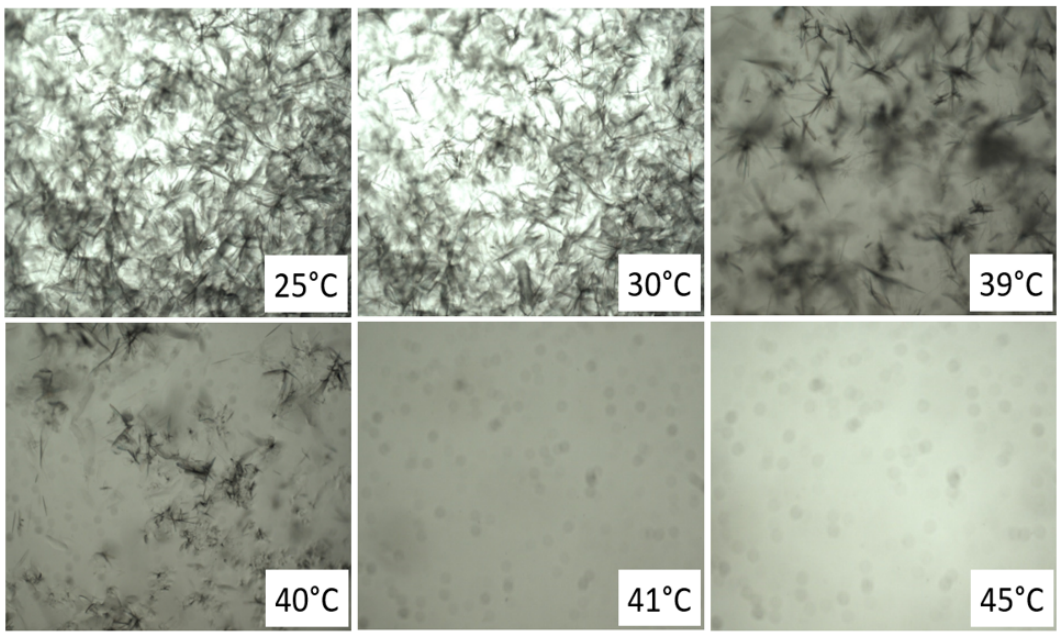

Figure 4.7: Stearic acid solubility in hexadecane.

The grey spots observed in fig. 4.7 at 41 and 45°C are dirt from the microscope camera, not from the analyzed solution. At these temperatures the solution was visually homogeneous.

4.1.3 Emulsions preparation

In all tests, the dispersed phase concentration of the emulsions was fixed at 5%, this means that emulsions were prepared with 95% of aqueous phase, 5% of oil and different SA concentrations were evaluated. Two model oil were tested: hexadecane and 9:1 mixture of hexadecane and toluene. Surfactant was added to reduce IFT and maintain the emulsion stability, and studies were performed at 45°C and ambient conditions.

At each test, a total volume of 100 ml of emulsion was prepared by homogenizing the fluids with an Ultra Turrax T-25, shown in fig. 4.8. The Turrax uses a rotor-stator type disperser, shown in fig. 4.9. Agitation time and speed were chosen to form emulsions with uniform appearance and without the presence of free water or oil at the end of agitation.

Figure 4.8: Ultra Turrax T-25.

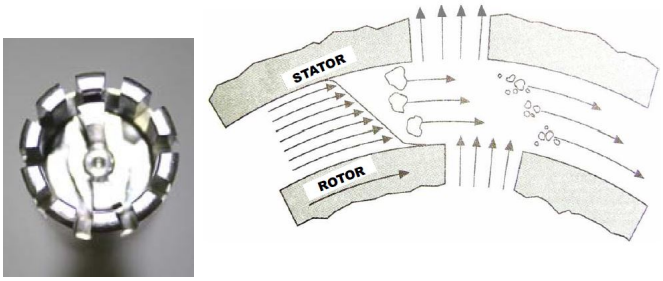

Figure 4.9: Ultra Turrax dispersing element.

Figure 4.10 shows the beakers used in emulsion preparation. For emulsions prepared at 45°C, a liner Adonex beaker, illustrated in the left of the figure, was used to maintain the temperature by bath circulation.

Figure 4.10: Emulsion preparation.

Stability analysis

Emulsion stability was studied by analyzing the evolution in time of the drop size distribution (DSD) and interfacial rheological properties. By carefully changing the time and the stirring rate, the size distribution of the emulsion droplets can be controlled. The stability behavior of emulsions was also studied by monitoring oil film formation over a certain period of aging time through bottle tests. The DSD determination was obtained using the MALVERN MASTERSIZER 2000 equipment, shown in fig. 4.11.

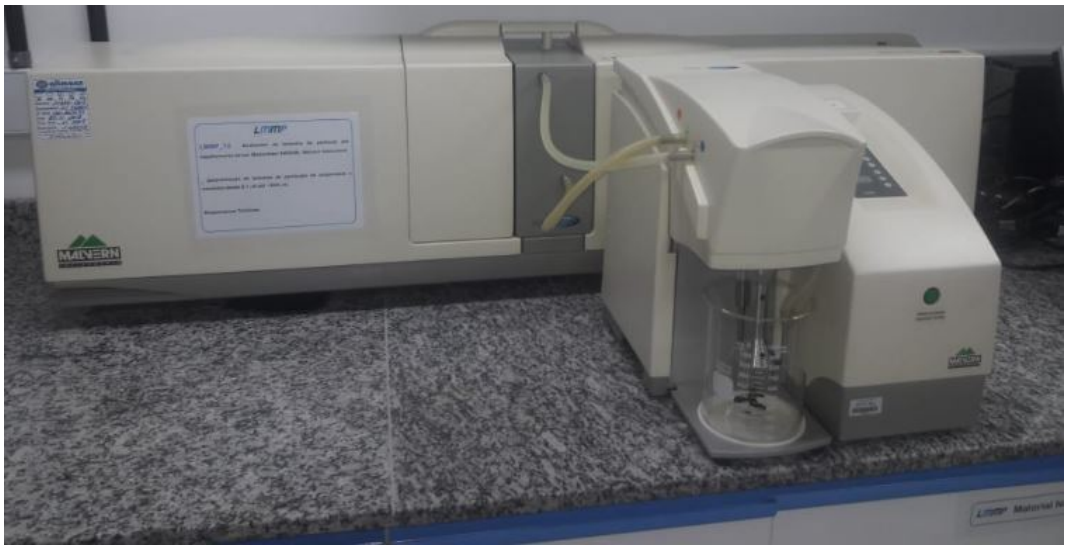

Figure 4.11: MALVERN MASTERSIZER 2000 equipment.

Laser diffraction technique is used, where a light beam emitted through the sample containing the droplets promotes the scattering of the incident light beam. The equipment provides some statistical parameters of the diameter measurements (D-values), among them d(0.1), the median d(0.5) and d(0.9) representing the diameters of which 10%, 50% and 90% of the drop population (total volume) has a diameter smaller than this value, respectively.

4.2 Characterization of fluids

Fluid viscosities were measured using the Ubbelohde viscometer for kinematic viscosity measurements of transparent liquids. Different capillary diameter may be used depending on the viscosity range. The 0 and 0B viscometers were used, which have a kinematic viscosity range of 0.3 - 1 and 1 - 5 mm^2/s, respectively. Temperature was set by an ECO SILVER - LAUDA Viscotemp thermostatic bath, displayed in fig. 4.12.

Figure 4.12: ECO SILVER - LAUDA Viscotemp thermostatic bath with an Ubbelohde capillary viscometer.

Working fluid densities were measured using the Density Meter for the Petroleum Industry DMA^{TH} 4200 M that measure petroleum samples including gas and high-viscosity fluids. This equipment is illustrated in fig. 4.13.

Figure 4.13: Density Meter DMA^{TH} 4200 M.

Emulsion analyzes were performed using the Zeiss AXIOVERT 40 MAT inverted microscope, ilustrated in fig. 4.14.

Figure 4.14: Zeiss AXIONET 40MAT inverted microscope

4.3 Interfacial properties

Interfacial properties of the emulsions were studied by using a TRACKER (Teclis) and a DCAT 25 (DataPhysics) tensiometers, both available at LMMP/PUC-Rio. The TRACKER tensiometer measures variations in surface tension or IFT over time, as well as dynamic oscillatory tests to estimate the total dilatation modulus (ϵ), the elastic dilatation modulus (ϵ') and the viscous dilatation module (ϵ"). It was used to investigate the performance of the fatty acid as oleic surfactant, as well as the acquired interfacial viscoelastic properties. The device, shown in fig. 4.15, consists of an optical support base with a light source, a cuvette and dropper syringe, a drop volume control motor, a camera, and a computer with a video monitor for viewing images and data processing.

For the O/W system, a U-shaped needle was used and the rising drop method, since the oil has a lower density than the aqueous solutions, the formed oil drop would tend to rise to the top of the cuvette. This method ensures that the drop of oil is suspended in the aqueous phase. During the tests, a 5 ml quartz cuvette, a 500 μL SGE syringe and a U-shaped needle number 22 were used.

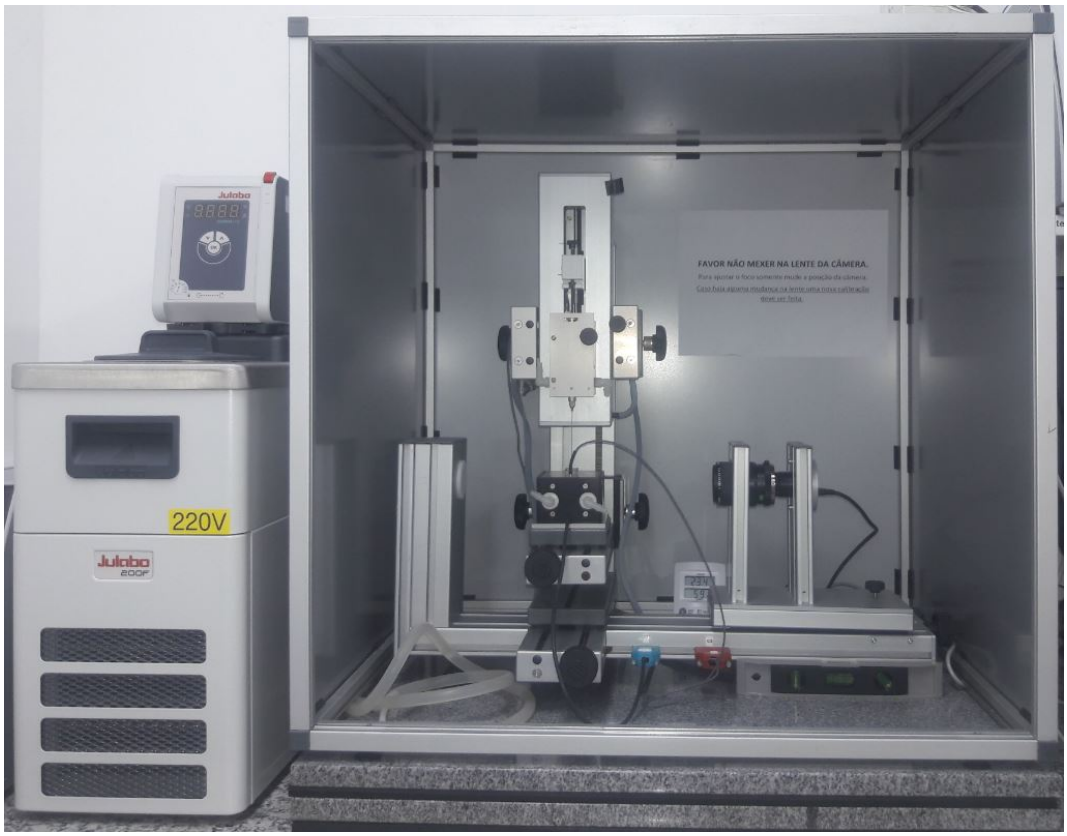

Figure 4.15: TRACKER (Teclis) tensiometer apparatus used to study viscoelastic properties trough oscillatory dynamic tests.

The TRACKER tensiometer internal software (WinDrop) has options to adjust the experiments and has statistical parameters such as needle vertically control, camera focus and drop volume and interfacial area adjustments. In all tests, the first drop is discarded to minimize the presence of air in the drop formed. Parameters such as delimited area where IFT is calculated, bulk density and drop density, drop volume and interfacial drop area, and the type of syringe used based on its volume, are required to calculate the IFT. In addition, drop amplitude and frequency oscillation, aging time, and measurement accuracy level are input values for the software for dilatational rheological tests. The drop formation rate directly influences the initial strain measurement, since the slower the drop formation rate, the longer the surfactant adsorption time until the first IFT measurement.

The type of procedure chosen to perform all the studied systems was the volume profile type, which consists in promoting sinusoidal variations in drop volume over time. The total elastic modulus and its individual components were determined by the IFT response to the interface area and volume disturbances. Figure 4.16 shows an example of the Windrop interface of an

oscillatory dynamic test.

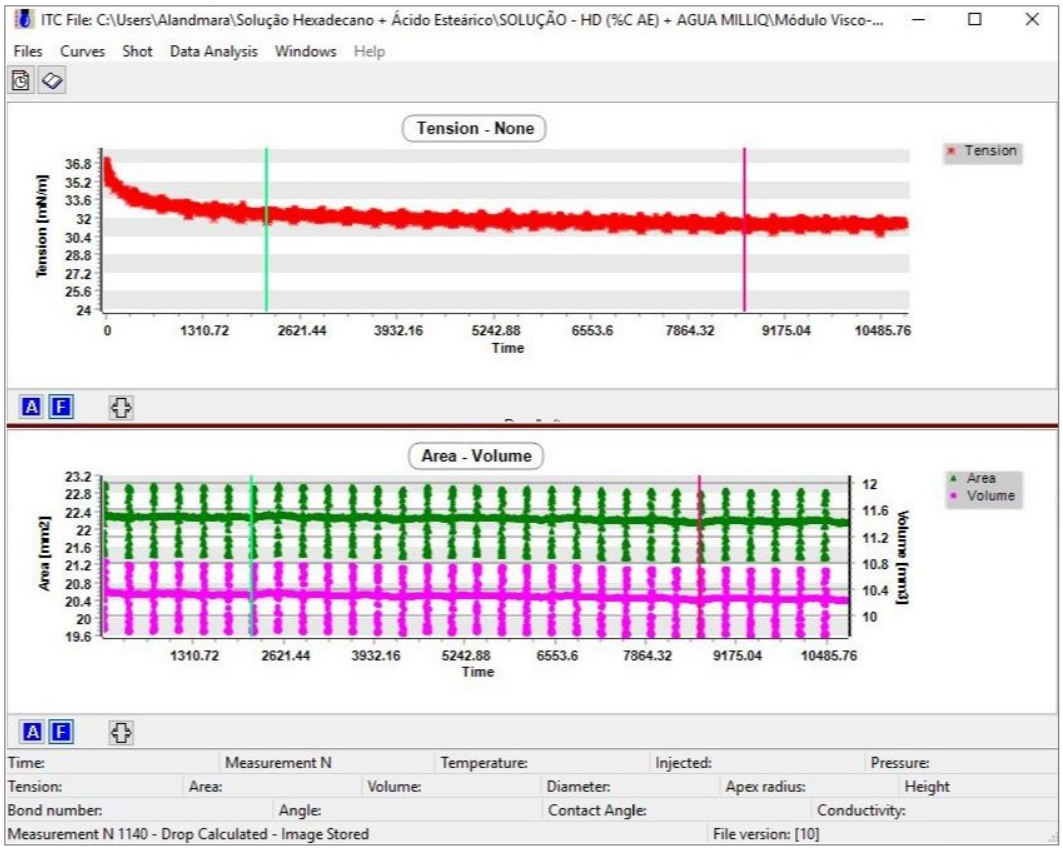

Figure 4.16: Windrop interface of an oscillatory dynamic test.

Input Parameters of the software were established to program the tests, as shown in fig. 4.17: The oscillation amplitude used was 6% in relation to the total drop volume, the oscillation period was set at 10 seconds for all tests, the time varied depending on the aqueous phase used since, in the presence of salts, interfacial film formation behave differently compared to Milli-Q water.

Based on a set time of 3 hours per test, the parameters were calculated to generate 30 points. Five (5) active cycles, which corresponds to the number of sine waves throughout the test, were performed, so that the perturbation time was 50 seconds. Thirty-one (31) blank cycles were performed, which corresponds to the period when the interface is undisturbed and therefore the drop volume is kept at the same value programmed at the start of the test. These are important parameters not to overload the motor of the tensiometer, especially when long tests are scheduled. The sum of the active and blank cycles, shown in fig. 4.18, is a total periodic interval where the number of test points is obtained by the ratio of the total experiment time in that interval. The dynamic elasticity modulus is calculated by selecting the elasticity option

in the software, at which active cycles are selected to be measured and the blanks are eliminated. Figure 4.19 illustrates the steps of processing elasticity data.

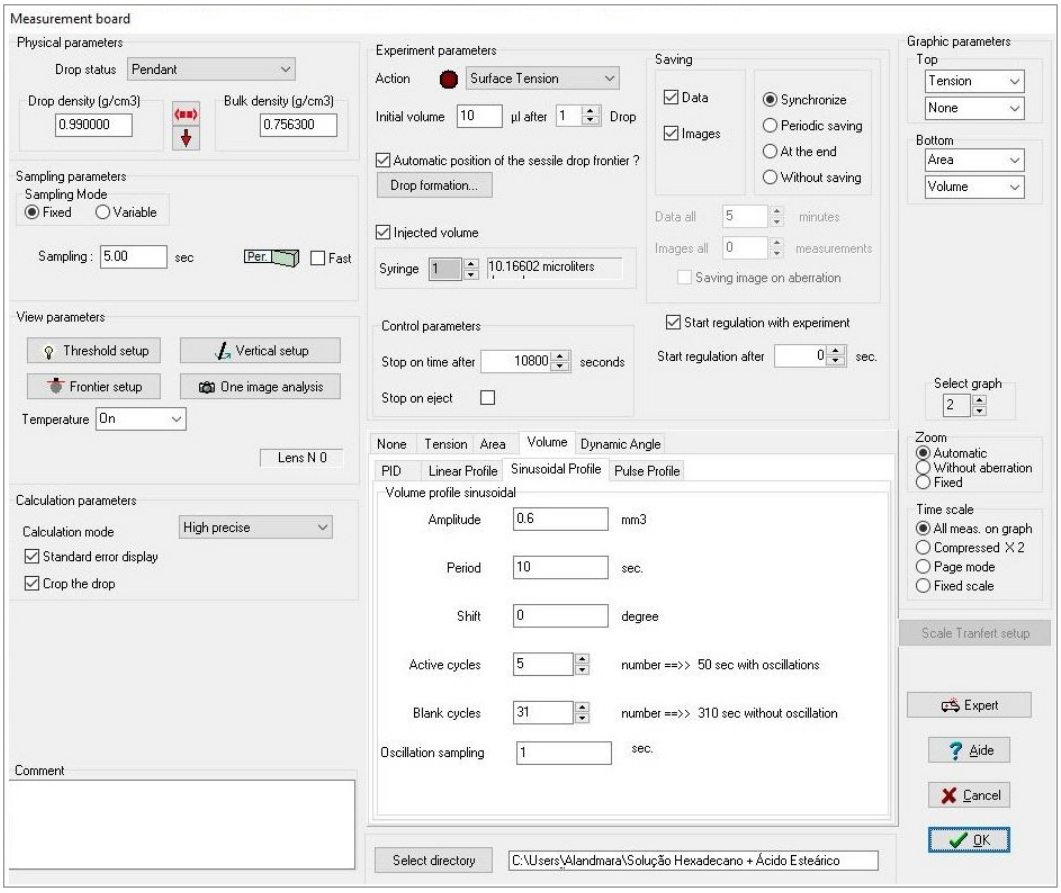

Figure 4.17: Input Parameters of the Windrop software.

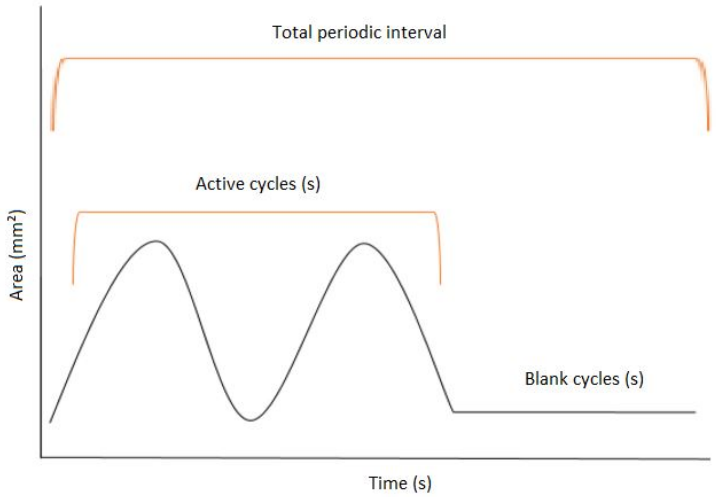

Figure 4.18: Scheme representative of active and white cycles (Soares, 2017) - adapted.

Figure 4.19: Windrop interface in the dynamic elasticity modulus data extraction.

Interfacial tension (IFT) may be determined by both tensiometers (TRACKER and DCAT 25). In the DCAT 25 tensiometer, illustrated in fig. 4.20, the IFT between two liquids can be measured by using a body test, and in contrast to the optical analysis used in the TRACKER tensiometer, it is not necessary enough transparency of the liquids or that the refractive index differs between them.

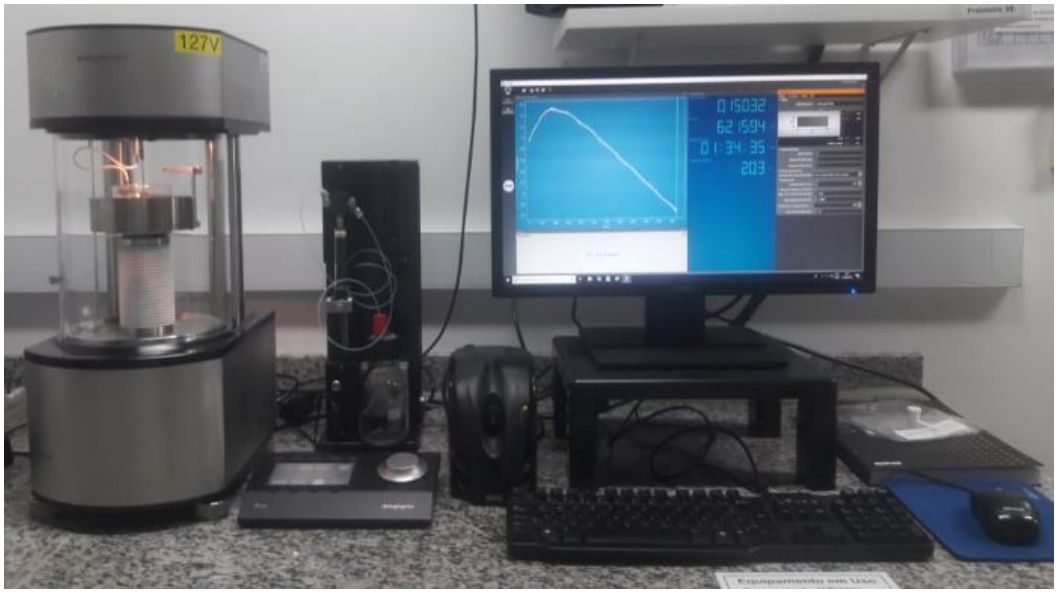

Figure 4.20: DCAT 25 (DataPhysics) tensiometer.

The applied method was the Wilhelmy plate that is made of iridium–platinum and has a few centimeters in length and height, as illustrated to fig. 4.21. The plate is attached to the tensiometer weighing system positioned at the liquid surface. The Wilhelmy equation, shown in fig. 4.22, is applied based on the definition of the surface tension as tensile force per length of the contact line [105].

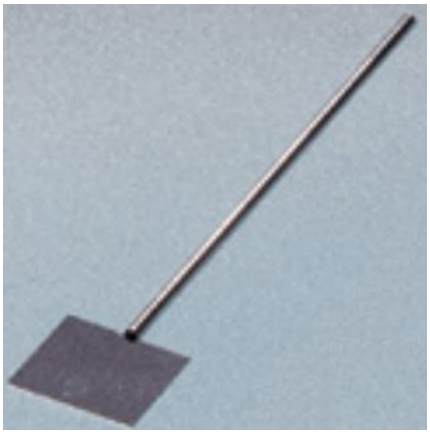

Figure 4.21: Wilhelmy plate used in the DCAT 25 tensiometer.

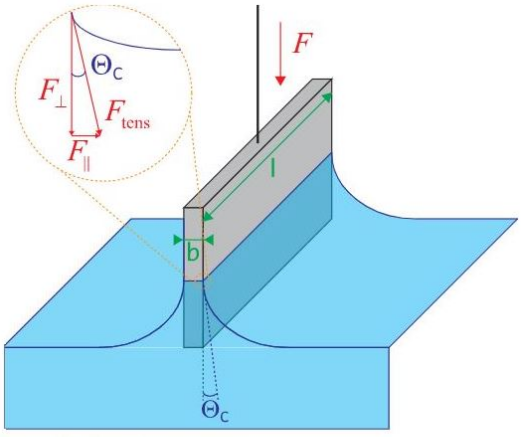

$$\sigma = \frac{F_{\text{tens}}}{L} = \frac{F_{\perp}}{L \cdot \cos\Theta_{\text{C}}} = \frac{F_{\text{G}}}{L \cdot \cos\Theta_{\text{C}}}$$

Figure 4.22: Wilhelmy equation (Dataphysics undestanding interfaces, 2019).

4.4 Porous media

The cores used in the experiments are sedimentary outcrops belonging to the Bentheimer formation, which are light yellow homogeneous sandstones, as shown in fig. 4.23. These samples have 1.5 inches in diameter and 12

inches in length, which were then divided into 3 equal parts. Palombo (2017) performed X-ray diffraction tests and showed that Bentheimer sandstones are composed predominantly of quartz. Tables 4.3, 4.4, and 4.5 list mineralogical characteristics, and petrophysical properties. Figure 4.24 shows the results of Bentheimer sandstone characterization by X-ray microtomography (MRX).

Figure 4.23: Bentheimer sample (Kocurek Industries INC).

Product ID	SS-102
Formation	Valaginian
Permeability	1500-3500mD
Porosity	23-26%
UCS	3500-4500 PSI
Homogeneous	YES
Perm By	KCL/N2

Table 4.3: Bentheimer sample characteristics (Kocurek Industries INC, 2019).

Oxides	[%]
Na_2O	0.05
MgO	0.04
Al_2O_3	1.54
SiO_2	96.3
K_2O	0.49
CaO	0.26
Fe_2O_3	0.60

Table 4.4: Bentheimer sandstone oxide composition (Palombo, 2017) - adapted.

Mineral		[%]
Quartz	SiO_2	92.9
Kaolinite	$Al_2Si_2O_5(OH)_4$	3.2
Microclinium	$KAlSi_3O_8$	2.9

Table 4.5: Bentheimer sandstone mineral estimate (Palombo, 2017) - adapted.

Palombo (2017) estimated the average pore diameter of Bentheimer sandstone by mercury intrusion porosimetry. In these tests, the characteristic curves of the pore throat were obtained using Washburn equation [1]. Palombo found an average pore diameter of 3.5 μm [106].

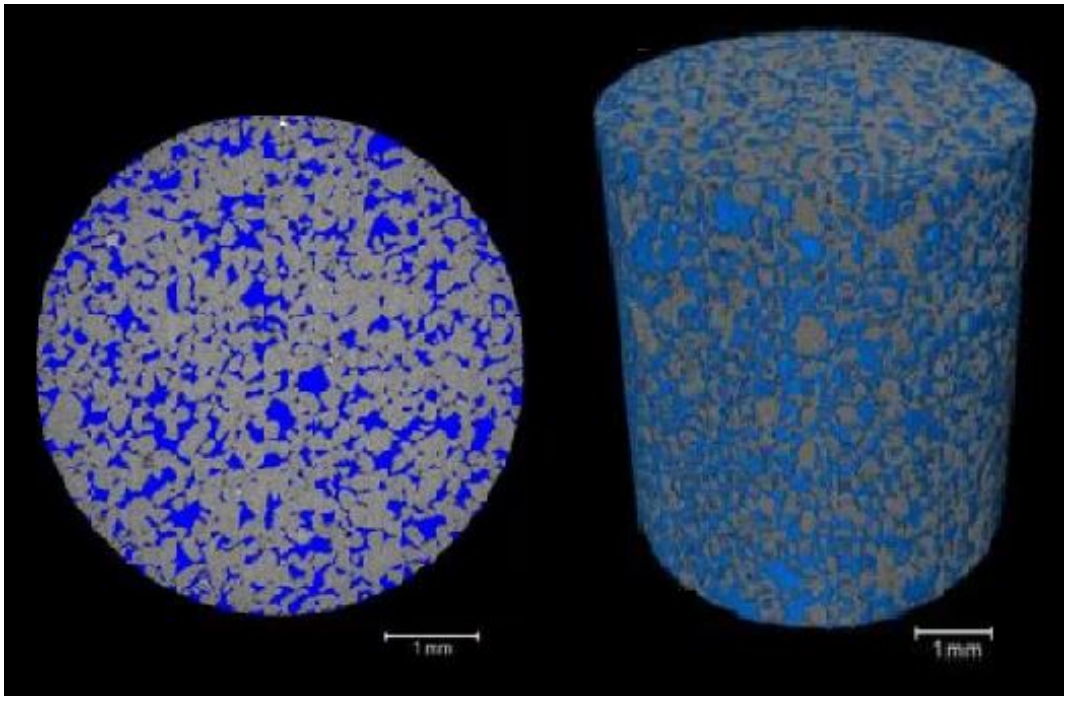

Figure 4.24: 2D section and 3D model of the reconstructed Bentheimer sandstone microtomographic image, with minerals in blue tones and empty spaces in gray (Palombo, 2017) - adapted.

After cutting, the samples used in this study were cleaned with compressed air jets to remove remaining particulate material from the cut, and the permeability was measured in an Ultra-Perm 600 Permeameter. It is a steady state gas permeameter that measures absolute gas permeability of consolidated porous media based on Darcy's law and is configured for measure 3-point considering the Klinkenberg effect. The gas permeabilities in this study were calculated by N_2 injection using the same overburden pressure as the tests performed.

Subsequently, the sample was kept in the oven at 80°C for 12h to remove moisture obeying the APIRP-40 standard (1998) which states that the maximum temperature for drying the sandstones in the conventional oven

[1]The equation describes the capillary flow in a bundle of parallel cylindrical tubes. It is extended with some factors such as size, quantity, pore shape the size of the sample for imbibitions into porous materials. The rate of increase in pressure is a very critical parameter, as increasing mercury pressure will result in gradual mercury penetration into smaller portions of the sample [106].

is 116°C. Then the sample dry mass (m_d) was measured and after that it was saturated with the injection solution such that it covers the entire sample and placed in a vacuum chamber at approximately -670$mmHg$ pressure, as shown in fig. 4.25. The saturation procedure takes at least 12 hours to ensure complete saturation. After saturation, the wet mass (m_w) was measured, and from these data and the fluid density (ρ_w) the sample porous volume (V_p) was calculated by eq. 4-2.

$$V_p = \frac{m_w - m_d}{\rho_w} \tag{4-2}$$

Once placed the saturated sample in the core holder, it is necessary to completely fill all lines with the injection solution so that there are no air bubbles or any other unwanted fluid in the lines, that may impair measurements.

Figure 4.25: Saturation process of the core sample to measure porosity.

4.5 Core flooding system

The device used in the experiments is the Core Flooding System (CFS) available in LMMP at PUC-Rio, and its simplified scheme is illustrated in fig. 4.26. CFS consist of a set of equipments, listed next, that performs permeability

measurements and displacement tests on rock samples under reservoir pressure and temperature conditions.

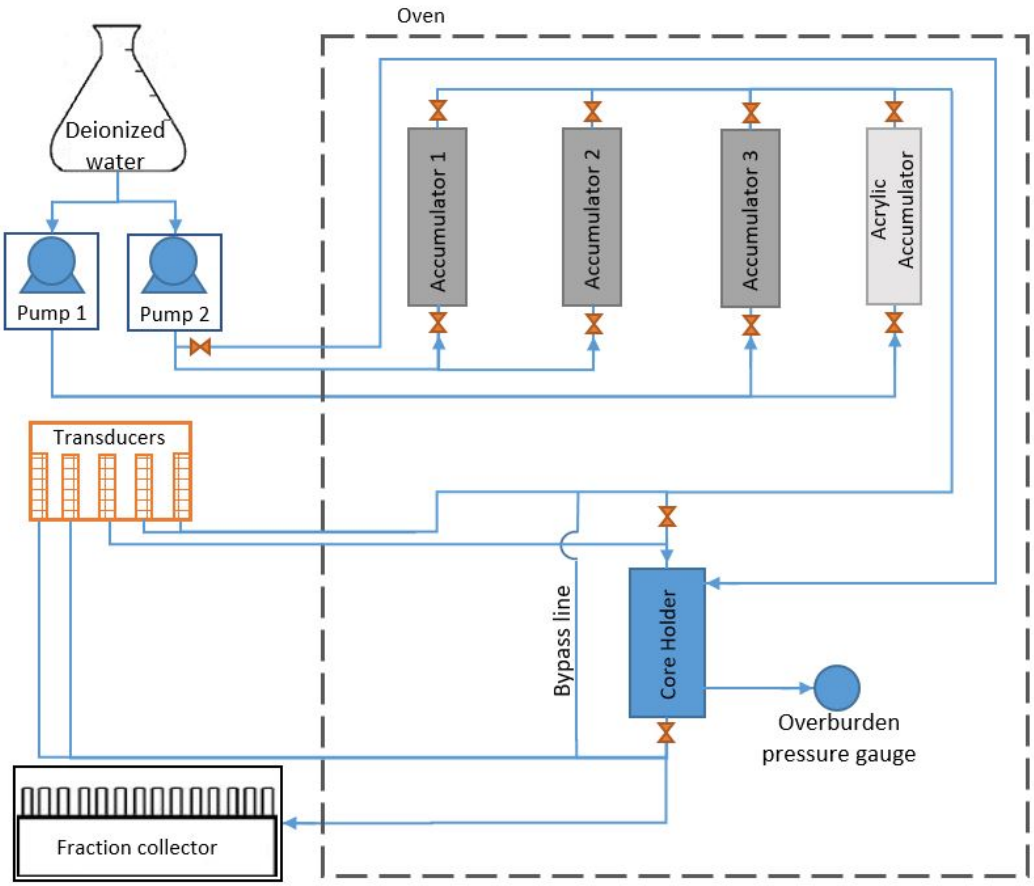

Figure 4.26: Core Flood Experimental Apparatus Scheme.

- A core holder where the rock sample is confined within a nitrile sleeve, subject to the specified pressure and temperature conditions;
- 1/8 inch lines and valves responsible for fluid transport in the system;
- Three 500 ml capacity piston type accumulators made of stainless steel for work fluid injection and one 900 ml capacity acrylic piston type accumulator for emulsion injection into the core holder;
- A magnetic stirrer used to keep the emulsion homogeneous inside the acrylic accumulator; The piston for emulsion injection was made of acrylic for visualization of the internal emulsion, and to verify if the emulsion is visually homogeneous and whether the magnetic stirrer is mixing the emulsion.
- An Ethiktechnology 400-NDE oven used to operate at high temperatures;
- A Gilson - FC 204 fraction collector used to collect volumes of fluids produced as a function of time in 15ml plastic tubes;

- Two Waters - 515 HPLC pumps responsible for injecting fluids into accumulators and overburden pressure;
- Three Velki (0 - 50 PSI) and Two Wika (0 - 145) pressure transducers to measure pressure differentials. Four of them measure inlet and outlet pressures at the injector and producer lines, and one measures the pressure inside the core holder;
- A temperature sensor located inside the core holder;
- A computer for acquisition and storage of data;

Figure 4.27 shows a photograph of the interior of the oven.

Figure 4.27: Inner photo of the oven where is located (a,c,d) three piston type accumulators, (b) the core holder, (e) an emulsion holder acrylic cylinder, and (f) a magnetic stirrer.

Adjustments and overhaul are required before conducting a core flooding experiment to ensure proper equipment operation, which include injection pump and transducer calibration, deionized water line cleaning, valve operation, and line dead volume quantification.

The rock sample was inserted into the core holder and 3600 *psi* was applied as overburden pressure at room temperature ($\approx 24°C$). All the tests were performed without back pressure. The water saturation process was performed by injection of the same aqueous phase used in the preparation of the emulsions. Initially, 20 V_p of the aqueous phase was injected to guarantee that all possible particulate material remained after coring and cutting was removed.

For each core used, the injection pressure was recorded during aqueous phase injection at different flow rates, and the absolute permeability (k) was determined according to the Darcy's law (eq. 2-3), from the slope of the linear correlation of (q) versus (dP) experimental data.

5
Results and Discussion

5.1
Emulsion stability

In this section, the stability results of stearic acid stabilized emulsions are presented. Table 5.1 presents the model systems (aqueous phase and oil phase), stearic acid concentration and temperature analyzed trough dilatational interfacial rheology and bottle tests to check phase separation. Dispersed drops of the emulsions formed were visualized by optical microscopy and their drop size distribution (DSD) was analyzed to check stability.

Model System	Phase		[SA] (%wt/v)	T (°C)
	Aqueous	Oil		
1st	SSW	HD	0	45
			0.5	
2nd	MilliQ	HD	0	45
			0.5	
			1	
			3	
3rd	SSW	HD + TL (9:1)	0.5	45
4th	Buffer	HD + TL (9:1)	0.5	≈24
		HD + TL (8:2)	0.5	
		HD + TL (9:1)	1	
5th	Buffer + NaCL	HD + TL (9:1)	1	≈24
				45

Table 5.1: Model systems analyzed. SSW (Synthetic seawater); HD (Hexadecane); TL(Toluene); SA(Stearic acid).

5.1.1
1st model system

The first system analyzed contained hexadecane as the oil phase, stearic acid as the surfactant, and synthetic seawater as the aqueous phase.

Dilatational interfacial rheology

Dilatational interfacial rheology between synthetic seawater and hexadecane with stearic acid at 45°C was measured using the rising drop technique in the Teclis tensiometer. Figures 5.1, 5.2, 5.3 and 5.4 present the interfacial

tension, the dilatational visco-elastic modulus and their components for 0.0 and 0.5% (wt/v) stearic acid concentration, respectively. Data were extracted in the Teclis tensiometer active cycles and the first acquisition time was t = 25 seconds.

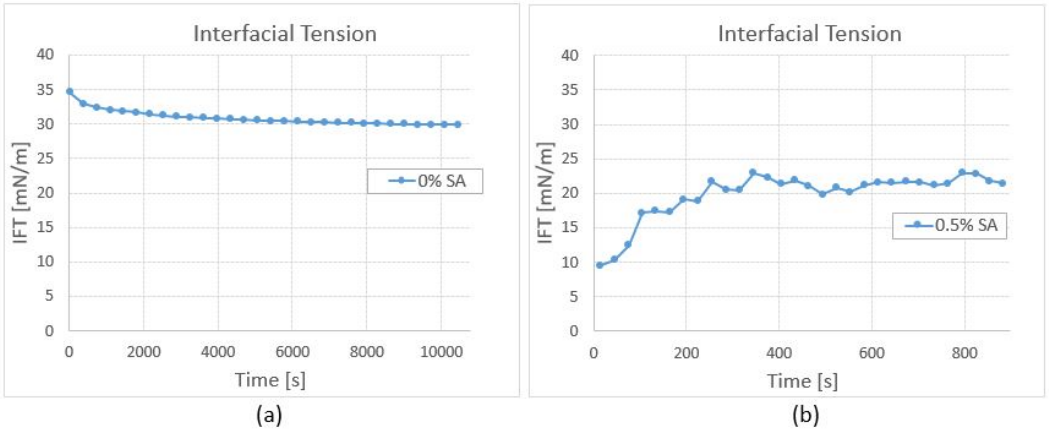

Figure 5.1: Interfacial tension between synthetic seawater and hexadecane at 45°C doped with (a) 0% and (b) 0.5% (wt/v) of stearic acid.

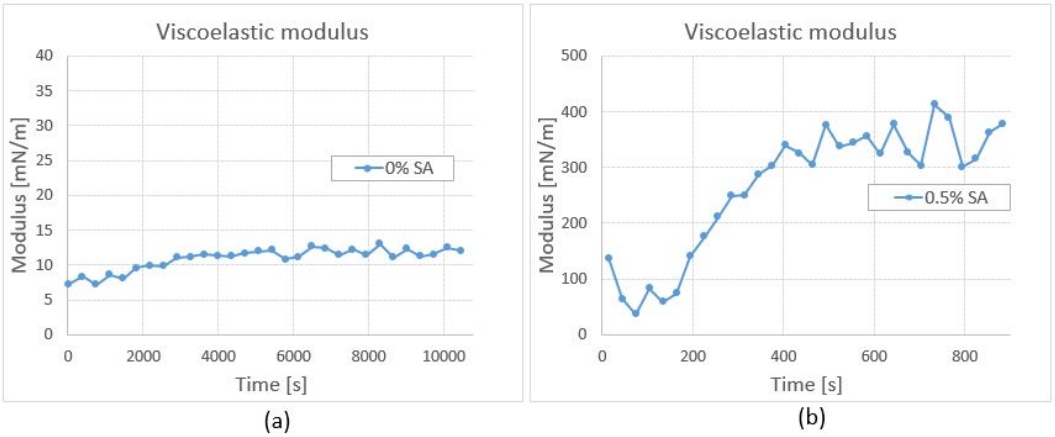

Figure 5.2: Dilatational viscoelastic modulus between synthetic seawater and hexadecane at 45°C doped with (a) 0% and (b) 0.5% (wt/v) of stearic acid.

It is possible to note an important decrease in interfacial tension with the addition of the surfactant and a higher dilatational visco-elastic modulus. Comparison between the visco-elastic modulus components at t=25 seconds suggest that with addition of surfactant, the water-oil interface develops a predominantly elastic behavior almost instantaneously.

As the test goes forward, the droplet lose the Laplacian shape, the IFT value was approximately 10 mN/m (fig.5.1b) in the first 25 seconds, suggesting

a rapid aging of the interface. After that, modulus curves had an irregular behavior, showing values of dilatational elasticity higher than 150 mN/m and negative values of dilatational viscous modulus, as shown in fig. 5.1b, 5.2b, 5.3b, and 5.4b.

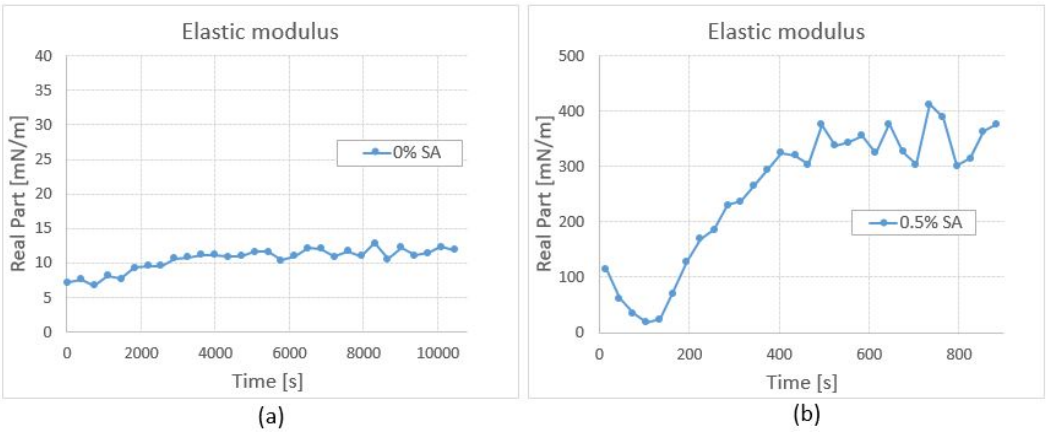

Figure 5.3: Elastic modulus between synthetic seawater and hexadecane at 45°C doped with (a) 0% and (b) 0.5% (wt/v) of stearic acid.

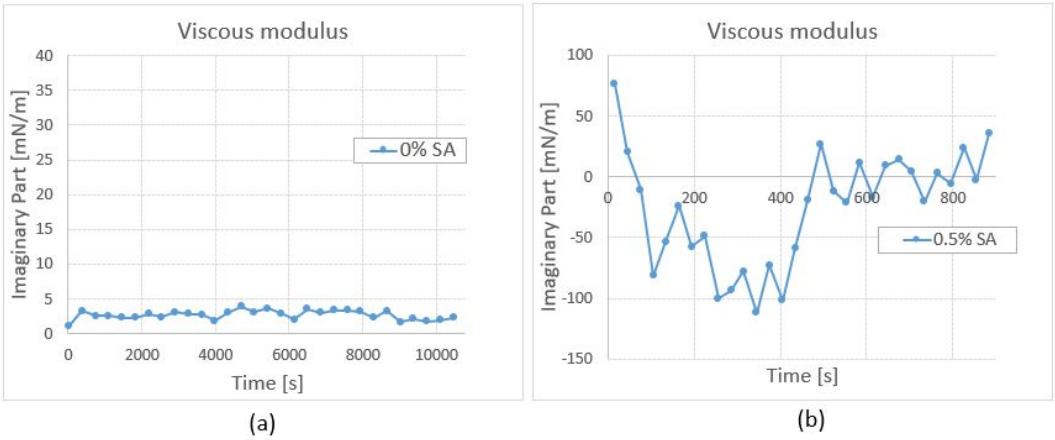

Figure 5.4: Viscous modulus between synthetic seawater and hexadecane at 45°C doped with (a) 0% and (b) 0.5% (wt/v) of stearic acid.

Figure 5.5 shows pictures of the droplet behavior during the oscillation test. The stearic acid adsorbed on the interface and in presence of the saline solution changed the interface rheology/structure forming a solid and rough looking film with increasing aging time. In the oscillatory test, as the area expands and decreases, the surfactant diffusion process occurs and each cycle requires the redistribution of the surfactant at the interface. Increasing the

area causes increased interfacial tension and surfactant molecules migrate from the bulk to the interface, and the opposite occurs with decreasing the area. Depending on the concentration of stearic acid and how it behaves at the interface, this diffusion may have led to the loss of the Laplacian form. As time goes by, it can be noted the gradual loss of the initial Laplacian shape, which made the interfacial properties measured not reliable. As can be seen in the 700 seconds photograph, the film became asymmetric and only one side of the droplet deformed during the oscillation test. The observed interfacial behavior is attributed to interactions between the surfactant and the salts dissolved in the aqueous phase.

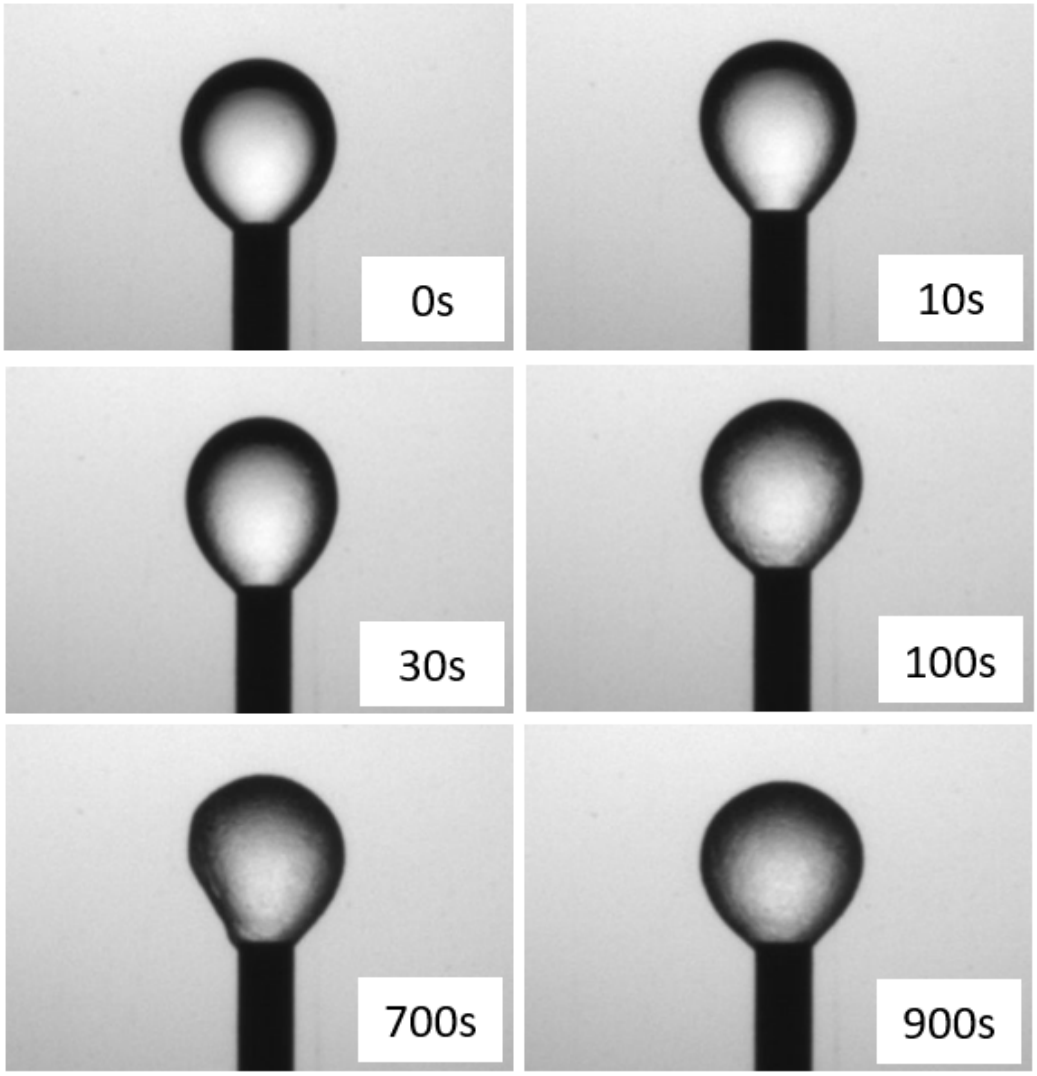

Figure 5.5: Drop shape during dilatational interfacial rheology tests on a drop of hexadecane doped with 0.5% (wt/v) of stearic acid and synthetic seawater at 45°C - First model system.

The rheological tests were performed 3 times for each concentration and

there was no repeatability in any of the interfacial properties with stearic acid. Reproduced tests are available in appendix A (fig. A.1 and A.2).

Emulsions

Table 5.2 shows the working fluids (aqueous and oil phases), surfactant (SA) concentration, temperature (T), rotation speed (Speed), time (t) and the emulsion formed under each condition. Different speed and mixing time values were explored, but none of them were able to form emulsion.

Emulsions	Oil phase	Water phase	SA (% wt/v)	T [°C]	Speed [rpm]	t [min]	Emulsion formed
EM_01	HD	SSW	0	45	6500	2	No
EM_02	HD	SSW	0.5	45	6500	2	No
EM_03	HD	SSW	0.5	45	9000	5	No
EM_04	HD	SSW	0.5	45	24000	2	No

Table 5.2: Evaluation of emulsion formation with and without surfactant at different speed and mixing times - First model system: hexadecane (HD) - synthetic seawater (SSW).

5.1.2
2nd model system

To investigate the system behavior without salinity, Milli-Q water was used as the aqueous phase.

Dilatational interfacial rheology

The interfacial rheology measurements at 45°C are presented in fig. 5.6. The experiments were performed with different stearic acid concentrations, 0.0, 0.5, 1 and 3% (wt/v). According to the results, stearic acid is able to reduce the IFT.

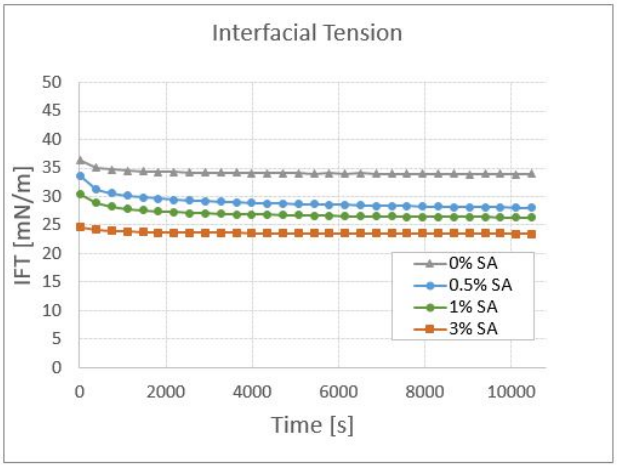

(a)

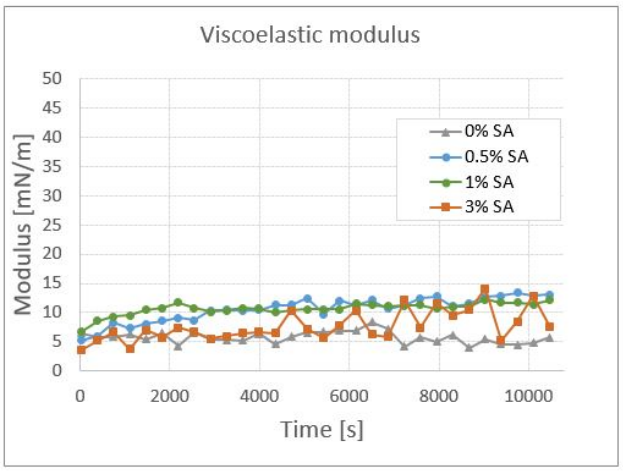

(b)

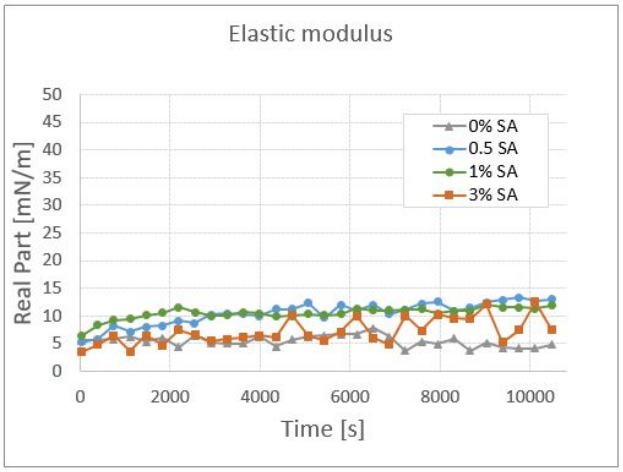

(c)

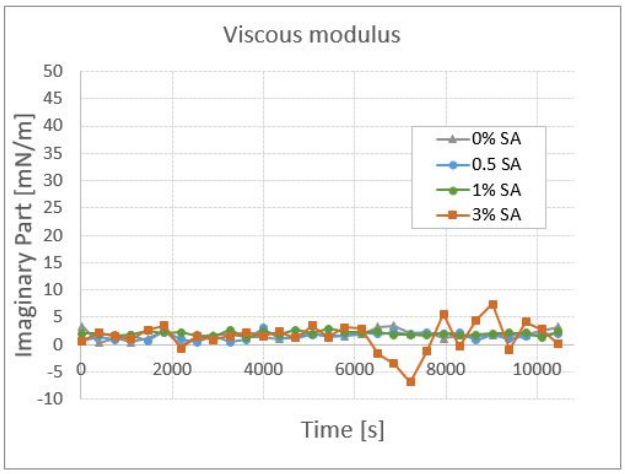

(d)

Figure 5.6: Dilatational interfacial rheology results at different surfactant concentrations for the second model system: hexadecane - Milli-Q water at 45°C (a) Interfacial tension (b) Dilatational visco-elastic modulus (c) Elastic modulus (d) Viscous modulus- Stearic acid (AE).

The viscoelastic results for 3% (wt/v) of stearic acid was inconclusive due to needle clogging during the experiment. It happened due to crystal formation caused by heat loss in the needle. Although the tensiometer was isolated and cuvette and syringe temperature were kept by a temperature controlled bath, it was impossible to avoid heat losses at the needle. This effect can be seen in the graphs by the scatter of the data.

Comparing the IFT results without and with 0.5% (wt/v) surfactant (fig. 5.1a-b and 5.6a.), the reduction with synthetic seawater (from 30 to 10 mN/m) was bigger than that for Milli-Q water (from 34 to 28 mN/m) for the same stearic acid concentration. Besides, the elasticity of the Milli-Q water system was much lower than synthetic seawater. In both cases the interfacial films had higher values of elastic modulus compared to the viscous modulus. The rheological tests were performed 3 times for each concentration and reasonable repeatability was observed. Reproduced tests are available in appendix A (A.3, A.4, A.5, and A.6).

Salt addition decreases electrostatic repulsion between the head groups of the surfactant, interfering with interfacial tension and CMC due to the competition of salt ions present in water with the polar part of the surfactant. In this system, the force that keeps the droplets stable is electrostatic, and salts interfere with these mechanisms, leading to non emulsion formation.

Emulsions

Table 5.3 presents results and conditions used in the preparation of emulsions with the second model system. In none of them stable emulsion was formed.

Emulsions	Oil phase	Water phase	SA (% wt/v)	T [°C]	Speed [rpm]	t [min]	Emulsion formed
EM_05	HD	Milli-Q	0.5	45	10000	5	No
EM_06	HD	Milli-Q	0.5	45	8000	10	No
EM_07	HD	Milli-Q	0.5	45	10000	10	No

Table 5.3: Evaluation of emulsion formation with different surfactant concentrations at different speed and mixing times - Second model system: hexadecane (HD) - synthetic seawater (SSW).

5.1.3 3rd model system

In the third system, the oil phase was composed of a 9:1 ratio of hexadecane (HD) and toluene (TL), and synthetic seawater was used as the aqueous phase. Differently from the previous model systems, in the third model, bottle

tests were performed in the first place instead the dilatational interfacial rheology.

Emulsions

Table 5.4 shows the parameters used and the emulsion stability for the 3rd model system. As can be seen, a W/O emulsion was formed and was stable for about 1h. Since for the same SA concentration and water phase no emulsion were formed in the first model system (see table 5.2), results suggest that toluene addition to the oil phase allowed emulsion formation probably as result of an enhanced solubilization.

Emulsions	Oil phase	Water phase	SA (% wt/v)	T [°C]	Speed [rpm]	t [min]	Emulsion formed
EM_08	HD + TL (9:1)	SSW	0.5	45	10000	10	Yes

Table 5.4: Evaluation of emulsion formation - third model system: 9:1 ratio of hexadecane and toluene doped with 0.5% (wt/v) of stearic acid (SA) - synthetic seawater (SSW).

Figures 5.7 shows the bulk appearance and micro-photographs of the EM_08 emulsion at zero time and 1 hour of aging time. Only few droplets dispersed in the oil phase were observed indicating that a W/O emulsion was formed, however after approximately one hour, they coalesced.

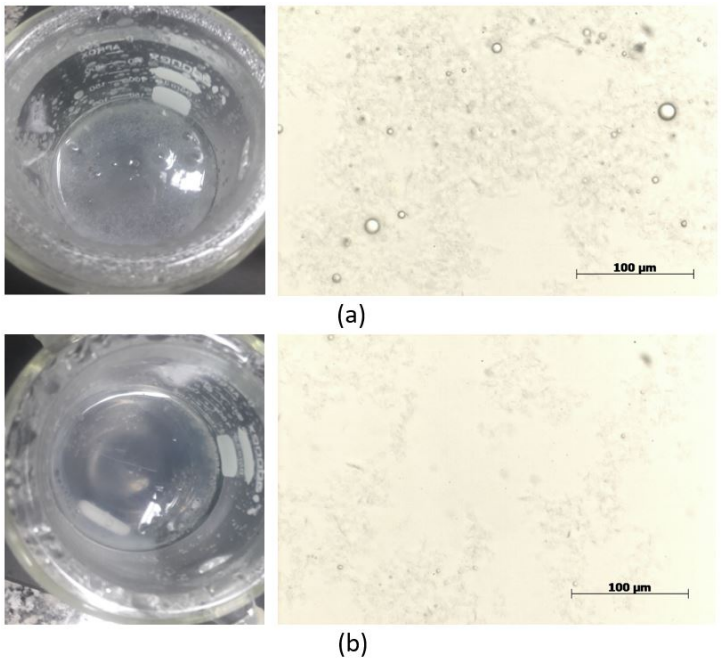

Figure 5.7: Microscopic analysis and photograph of emulsion EM_08 at (a) Zero time (b) and 1 hour of aging time.

5.1.4
4th model system

In this study, hexadecane and toluene were kept as oil phase components and a buffer solution (THAM) was used as the aqueous phase. Studies were performed at room temperature (≈ 24°C).

Stearic acid solubility

To investigate the effect of toluene in the solubility of the stearic acid, the appearance of solutions prepared with different stearic acid (0.5% and 1% wt/v) and toluene (10% and 20%) concentrations were evaluated for different aging times. The prepared solutions are shown in fig. 5.8, 5.9, 5.10. The stearic acid crystallization process was visualized by a Photron FASTCAM Mini UX100 high speed camera due to the crystal movement in the oil phase. In all tests, SA crystals formation/aggregation were observed with aging time at room temperature.

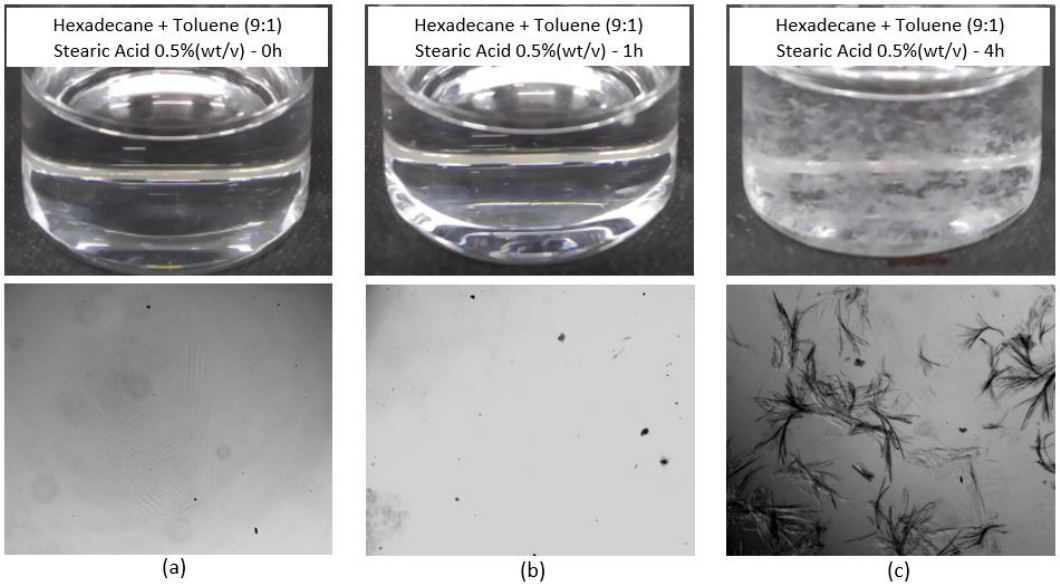

Figure 5.8: Solution composed by 9:1 ratio of hexadecane and toluene doped with 0.5% (wt/v) of stearic acid at room temperature at (a) zero, (b) one hour, and (c) four hours of aging time.

Comparing fig. 5.8-c and 5.9-c with 9:1 and 8:2 ratio of toluene respectively, it can be seen that as toluene concentration increases, there was greater solubility of stearic acid in the model oil. Also, aging time had an important influence on stearic acid solubilization according to fig. 5.10 that shows more acid formation/aggregation with time. As expected, this effect is lost as the SA concentration is increased as noted in fig. 5.8 and 5.9.

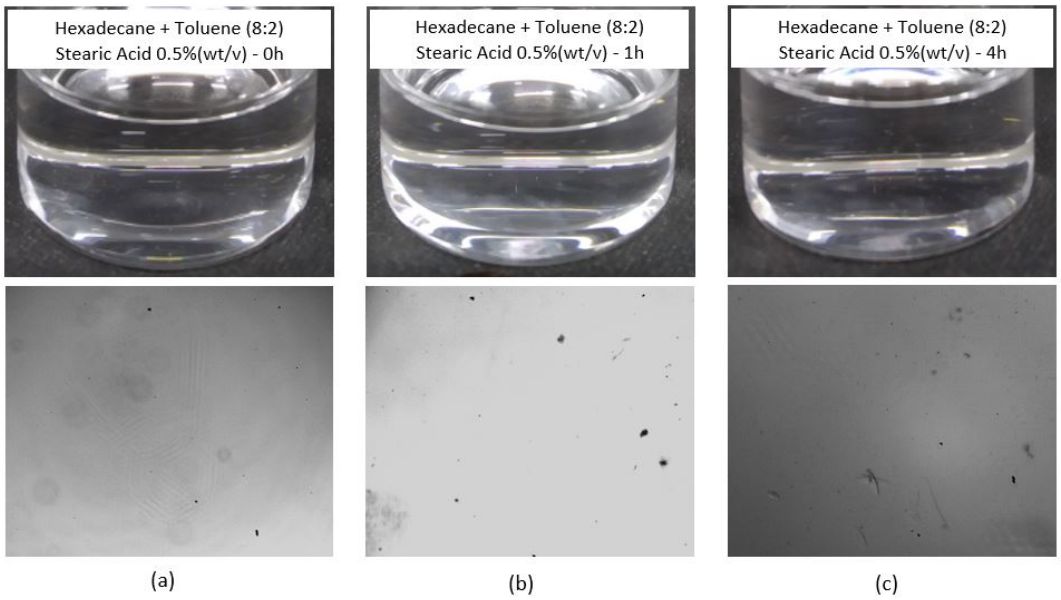

Figure 5.9: Solution composed by 8:2 ratio of hexadecane and toluene doped with 0.5% (wt/v) of stearic acid at room temperature at (a) zero, (b) one hour, and (c) four hours of aging time.

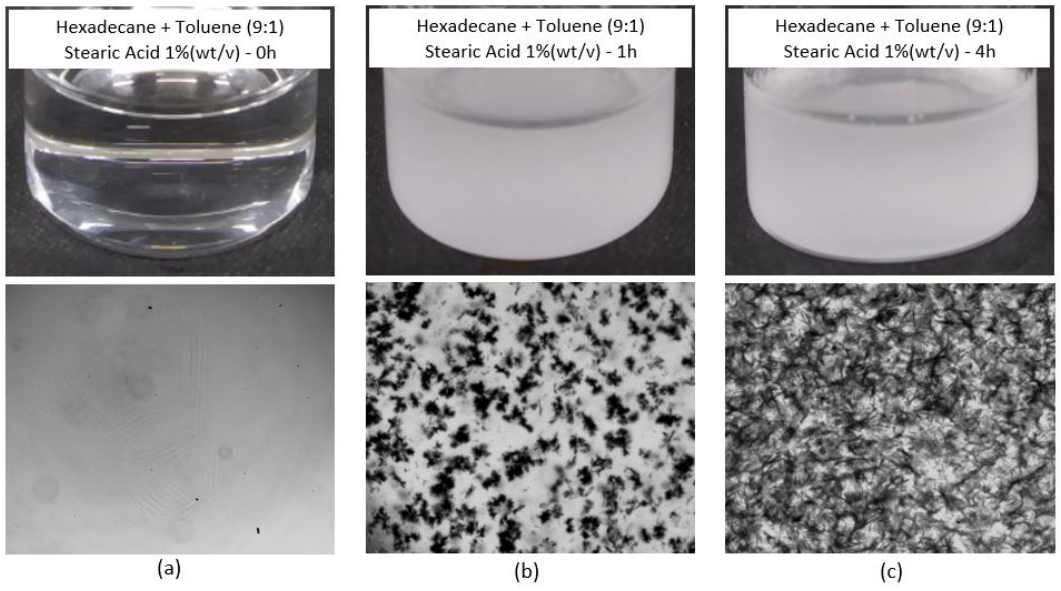

Figure 5.10: Solution composed by 9:1 ratio of hexadecane and toluene doped with 1% (wt/v) of stearic acid at room temperature at (a) zero, (b) one hour, and (c) four hours of aging time.

The crystallization process in the oil phase solution composed by 9:1 ratio of hexadecane and toluene doped with 1% (wt/v) of stearic acid was followed by microscopic analysis at room temperature ($\approx 24°C$). After about one hour

of aging time, micrometer size crystals started to form and aggregates over time, as showed in fig. 5.11.

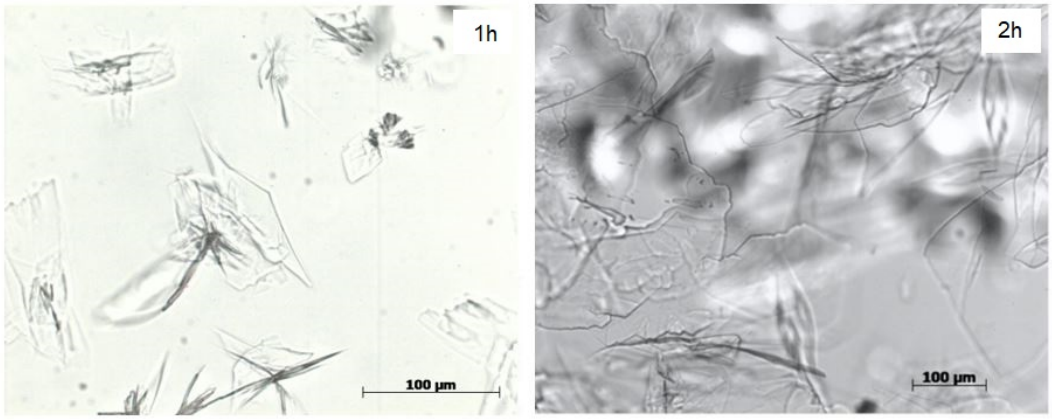

Figure 5.11: Stearic acid crystals formation in a solution composed by 9:1 ratio of hexadecane and toluene doped with 1% (wt/v) of stearic acid at room temperature at (a) one hour and (b) two hours of aging time.

Dilatational interfacial rheology

Dilatational interfacial measurements in the Teclis tensiometer was performed for buffer solution and 9:1 ratio of hexadecane and toluene doped with 0.5% (wt/v) of stearic acid at room temperature ($\approx 24°C$). As can be seen in fig. 5.12, the droplet detached from the needle almost immediately after contact with the buffer solution, indicating that the interfacial tension was too low, which made impossible to carry out the measurements.

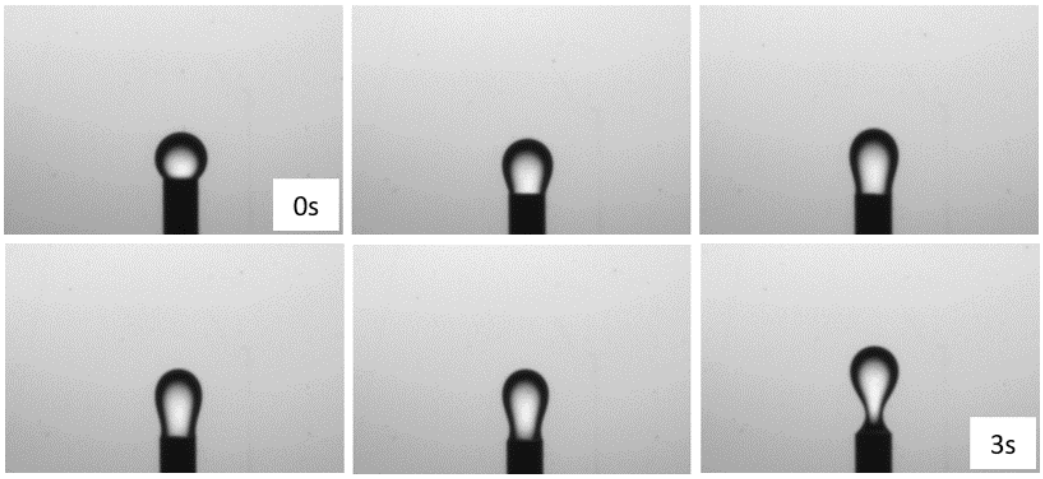

Figure 5.12: Drop detachment during the dilatational interfacial rheology tests performed between buffer solution and 9:1 ratio of hexadecane and toluene doped with 0.5% (wt/v) of stearic acid at room temperature ($\approx 24°C$).

Interfacial tension was measured using the DCAT 25 tensiometer with different stearic acid concentrations in order to find the critical micellar concentration (CMC). The concentrations were 0.00, 0.05, 0.10, 0.25, 0.30, 0.40, 0.50, 0.55, 0.75% (wt/v), adopted in an exploratory way. Since the film formation depends on the time due to the diffusion, adsorption, and rearranging of the surfactant, as discussed in the literature review, for each concentration the interfacial tension was measured for 8 hours.

Figure 5.13 presents the results, it can be noted a decrease in IFT with increasing stearic acid concentration, except for 0.75% of concentration. As can be seen, the IFT value for the concentration 0.5% (wt/v) of stearic acid was low, approximately 2 mN/m, which explains the droplet detachment from the needle during the test realized in the Teclis tensiometer.

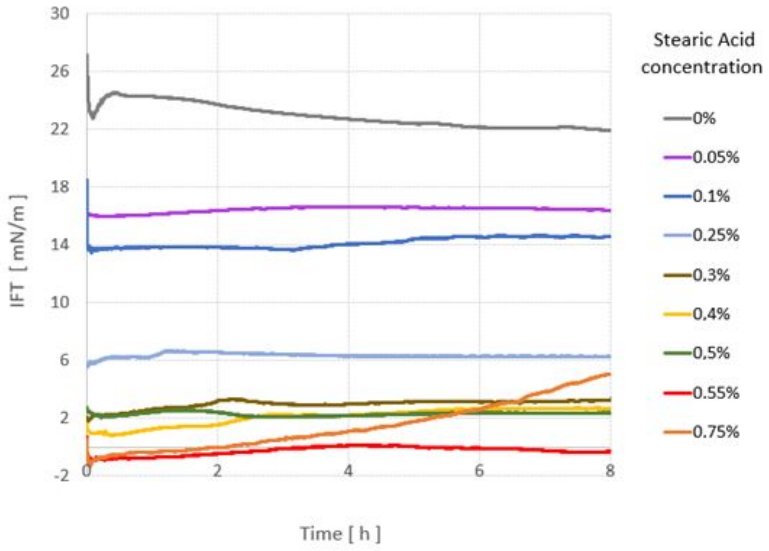

Figure 5.13: Interfacial tension between the oil phase composed by hexadecane and toluene (9:1) and the buffer solution for different concentrations of stearic acid.

As illustrated in fig. 5.14, during tests with 0.55% and 0.75% (wt/v) of stearic acid concentration, stearic acid crystals formed at the interface between the oil and water phases and began to aggregate after approximately one hour of testing. In addition, negative values were obtained for these concentrations and therefore prevented their use in the CMC study. Tests with concentrations of 0.00, 0.10, 0.50, and 0.75% (wt/v) of stearic acid were performed twice and acceptable repeatability was observed.

Table 5.5 shows the IFT values for each concentration. This values were determined by average after the tension reached a plateau for each analyzed concentration, except for 0.55% and 0.75% (wt/v) of stearic acid

concentrations, which the IFT values were taken as the first point before the formation of stearic acid crystals.

Figure 5.14: Stearic acid crystals formation during IFT tests on the DCAT tensiometer with (a) 0.55% and (b) 0.75% (wt/v) of stearic acid.

Stearic Acid [wt/v]	IFT [mN/m]
0.00	22.19
0.05	16.29
0.10	13.84
0.25	6.30
0.30	3.15
0.40	2.68
0.50	2.27
0.55	-0.90
0.75	-1.29

Table 5.5: Interfacial tension of hexadecane + toluene (9:1) and buffer solution as function of stearic acid concentration.

A graph of IFT as function of stearic acid concentration is shown in fig. 5.15. IFT stabilization was observed as stearic acid concentration increases. Addition of surfactants tends to saturate the interface and generates a critical concentration (CMC) at which IFT do not change, regardless of the increase in surfactant concentration. To determine the CMC, two curves were generated, one with the region linearly dependent on the concentration, using 0.00, 0.05, 0.10, 0.25% (wt/v), and the other with the line crossing the plateau, using 0.30, 0.40, 0.50% (wt/v). The CMC was determined by the intersection between both curves, as shown in eq. 5-1.

$$-4.4326x + 4.4709 = -58.648x + 20.567 => x = 0.2969 = CMC \quad (5\text{-}1)$$

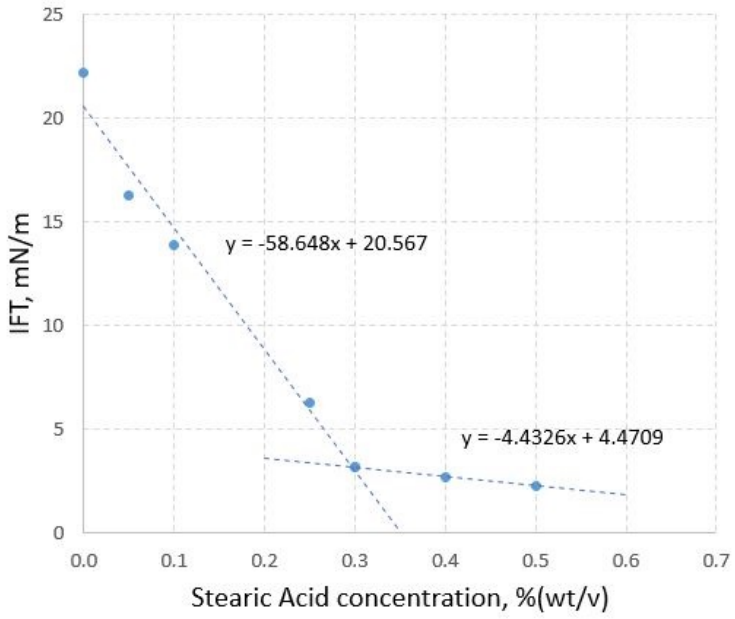

Figure 5.15: Interfacial tension of hexadecane + toluene (9:1) solutions doped with different stearic acid concentration and buffer solution - Fourth model system.

A concentration value of 0.30% (wt/v) of stearic acid was adopted as the CMC for this model system.

Emulsions

Table 5.6 presents results and conditions used in the emulsions preparation. The concentrations chosen were 0.5% and 1% (wt/v) of stearic acid, which correspond to 1.67 and 3.33 times the CMC, respectively. Different speed and mixing time values were explored, and as listed in the tab. 5.6, stable emulsions were formed with the buffer solution as the aqueous phase.

The stearic acid in the aqueous medium has a pH below 7. With the buffer presence, the pH goes to 8 and the acid dissociation balance changes to favor acid dissociation formation. Thus stearic acid behaves as an anionic surfactant. In addition, the dissociated stearic acid plus the ammonic compound THAM acts as a counter-ion. Accordingly, the buffer presence joining to the polar part of the stearic acid enhance its solubility in the aqueous phase. This increases the stearic acid polar part in the aqueous phase, increasing its adsorption at the interface and favoring the formation of emulsions. The use of an aqueous medium at pH 8 does not guarantee that all stearic acid is in dissociated form, that means, ionic and nonionic stearic acid are present, and a surfactant mixture can help stabilize the interface.

Emulsions	Oil phase	Water phase	SA (% wt/v)	T [°C]	Speed [rpm]	t [min]	Emulsion formed	Stability study
EM_09	HD + TL (9:1)	Buffer	0.5 (1.67xCMC)	≈24	10000	4	Yes	15 days
EM_10	HD + TL (9:1)	Buffer	1 (3.33xCMC)	≈24	10000	4	Yes	15 days
EM_13	HD + TL (9:1)	Buffer	1 (3.33xCMC)	≈24	20000	15	Yes	96 days

Table 5.6: Evaluation of emulsion formation with different surfactant concentrations at various speed and mixing times - Fourth model system: hexadecane + toluene (9:1) and buffer solution.

Emulsion type

To identify the type of emulsion formed, the drop dilution method was used. To this end, emulsion samples were dripped into an aliquot of the water and oil phases, and the sample behavior was observed. According to fig. 5.16, in the aqueous phase the sample dispersed rapidly and in the oil phase, the sample retained its shape. Therefore, the outer phase the aqueous and the emulsions formed were O/W.

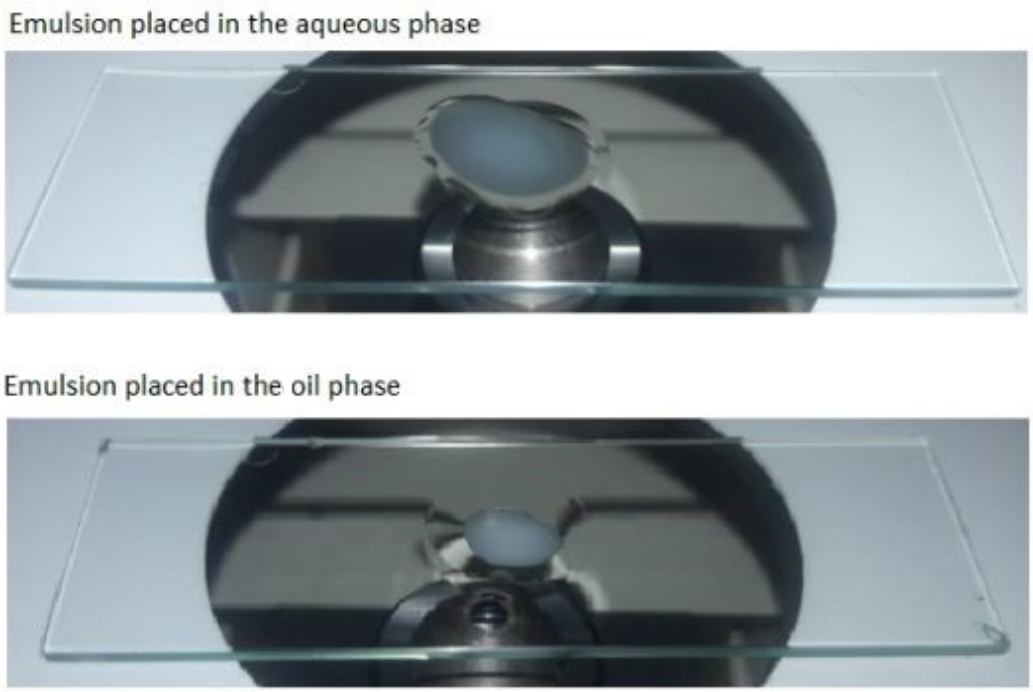

Figure 5.16: Drop dilution method performed to identify the type of the emulsion.

EM_09 emulsion morphology was studied for 15 days. Figure 5.17 and 5.18 show the microscopic analysis and the drop size distribution (DSD), respectively.

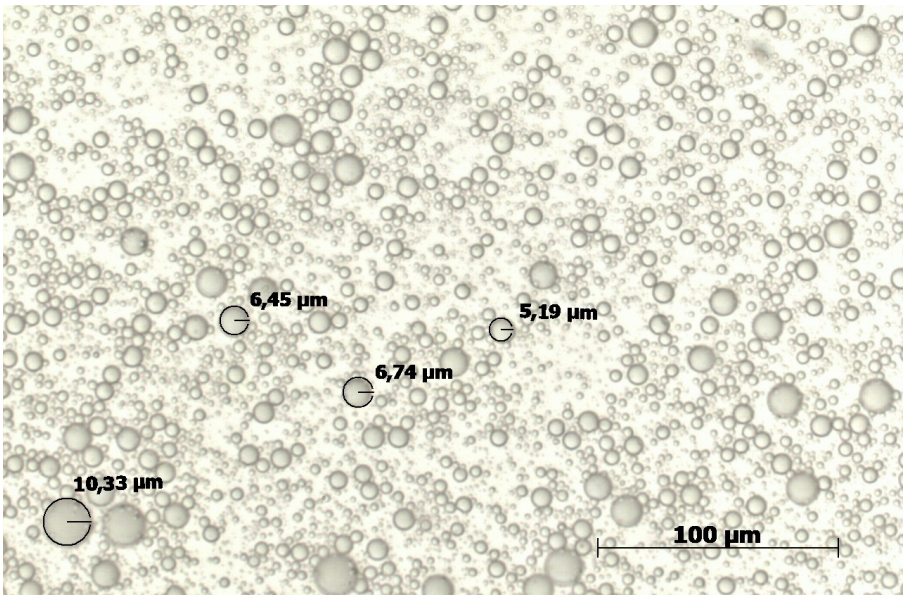

Figure 5.17: Microscopic analysis of EM_09 emulsion - 4th model system: hexadecane + toluene (9:1) doped with 0.5% (wt/v) of stearic acid concentration and buffer solution.

The DSD showed reduction of the smaller drop population and formation of a bimodal distribution over time (coalescence), that means, the curve begins to show a second (bigger drops) distribution. The d(0.5) and d(0.9) values for EM_09 emulsion were 3.9 and 11.7 μm, respectively. In addition bottle tests analysis of this emulsion in a glass cylinder illustrated in fig. 5.19 shows that an oil film was created over time. This results corroborates that this emulsion was in coalescence process.

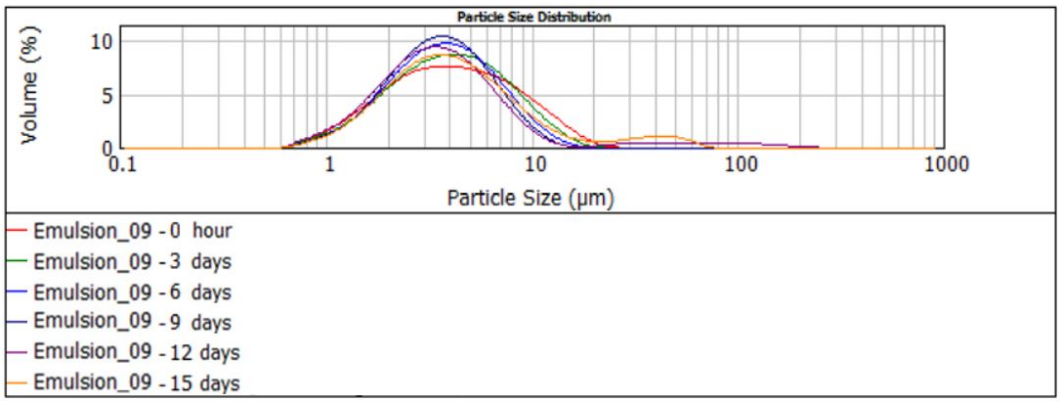

Figure 5.18: DSD of EM_09 emulsion - 4th model system: hexadecane + toluene (9:1) doped with 0.5% (wt/v) of stearic acid concentration and buffer solution.

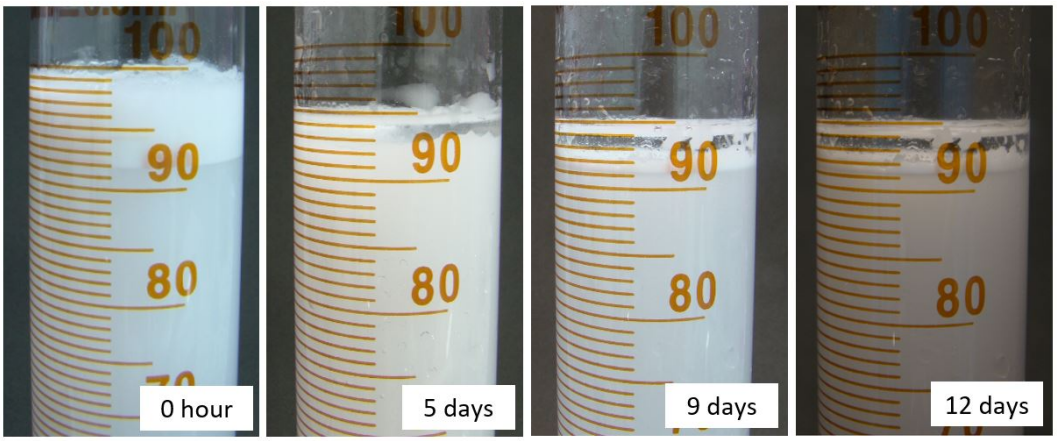

Figure 5.19: Photographs for following the EM_09 emulsion coalescence process during bottle tests.

Morphology of the EM_10 emulsion (with twice the surfactant concentration of EM_09) was studied for 15 days, and fig. 5.20 and 5.21 present the microscopic analysis and the DSD, respectively. The DSD also shows some variation over time, but the curves are more similar to a Gaussian curve, showing that EM_10 emulsion is more stable than EM_09. In the bottle tests results, shown in fig. 5.22, it was not possible to observe the formation of an oily film over time, therefore, neglecting the small variation in the DSD, this emulsion was considered stable for the 15 days analyzed. The d(0.5) and d(0.9) values for EM_10 emulsion were 4.3 and 10.4 μm, respectively.

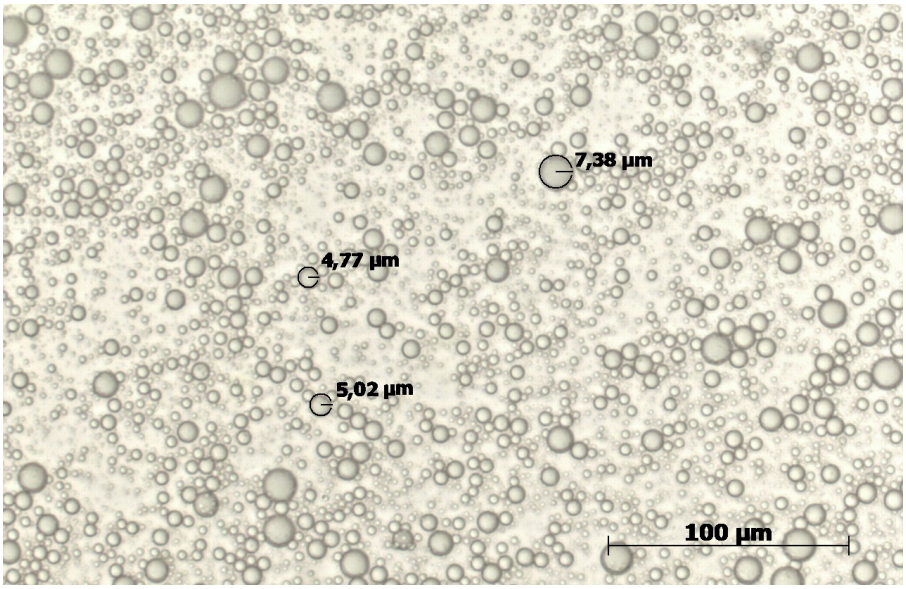

Figure 5.20: Microscopic analysis of EM_10 emulsion - 4th model system: hexadecane + toluene (9:1) doped with 1% (wt/v) of stearic acid concentration and buffer solution.

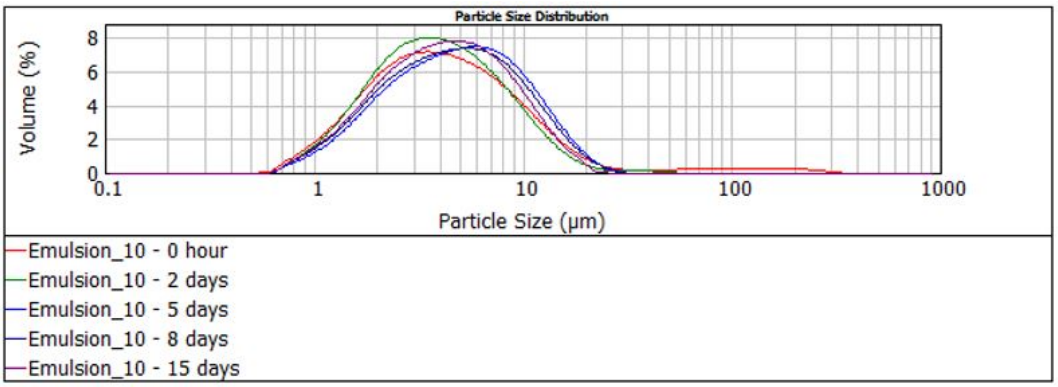

Figure 5.21: DSD of EM_10 emulsion - 4th model system: hexadecane + toluene (9:1) doped with 1% (wt/v) of stearic acid concentration and buffer solution.

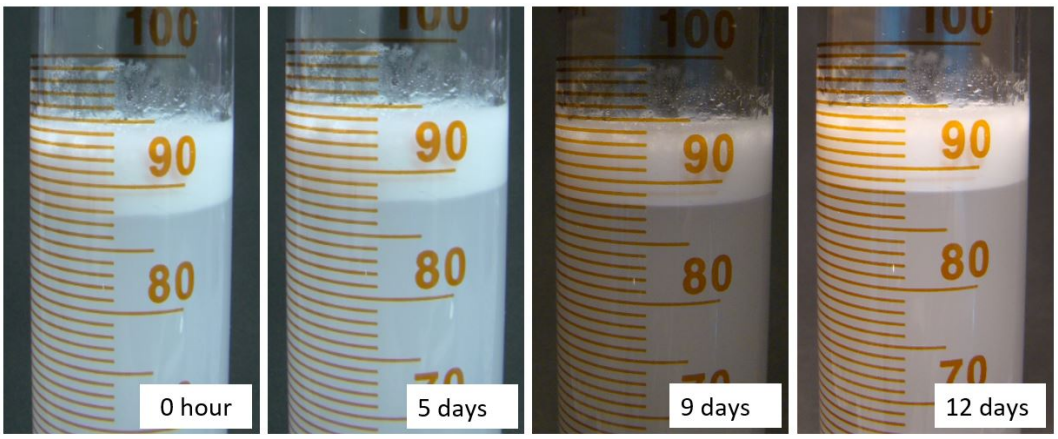

Figure 5.22: Photographs for following the EM_10 emulsion coalescence process during the bottle tests.

EM_13 emulsion was prepared with the same surfactant concentration as EM_10 emulsion, but with higher mixing time and speed. It was stable for 96 days. Figure 5.23 present the microscopic analysis showing a more mono-disperse emulsion compared to EM_09 and EM_10. The DSD and photographs during bottle tests for following the emulsion coalescence process are shown in fig. 5.24 and 5.25, respectively. The d(0.5) and d(0.9) values for EM_13 emulsion were 2.3 and 3.7 μm, respectively.

Results from the three emulsions prepared showed that stearic acid form long-term stable emulsions of hexadecane + toluene in salt-free alkaline solution at $\approx$ 24°C. Due to the formation of stearic acid crystals in the oil solution after approximately 1 hour of aging time, it is believed that the

emulsions formed can be considered as a kind of Pickering emulsion. This type of emulsion is stabilized by solid particles. Therefore, the assumption suggests that after emulsion formation, when crystals begin to aggregate, they may be adsorbed onto the interface between the two phases preventing the droplets from coalescing, making the emulsion more stable.

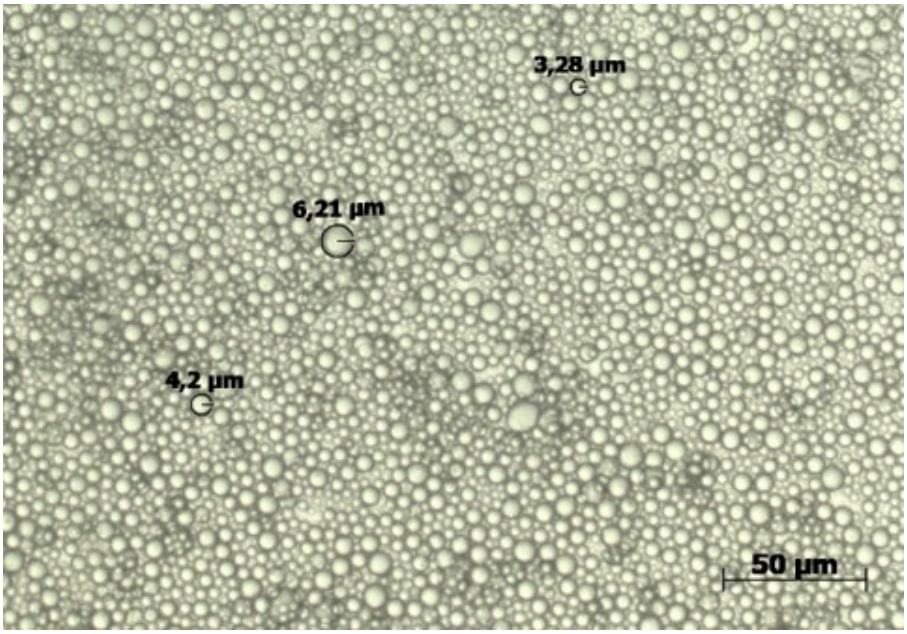

Figure 5.23: Microscopic analysis of EM_13 emulsion - 4th model system: hexadecane + toluene (9:1) doped with 1% (wt/v) of stearic acid concentration and buffer solution (higher mixing time and speed was used).

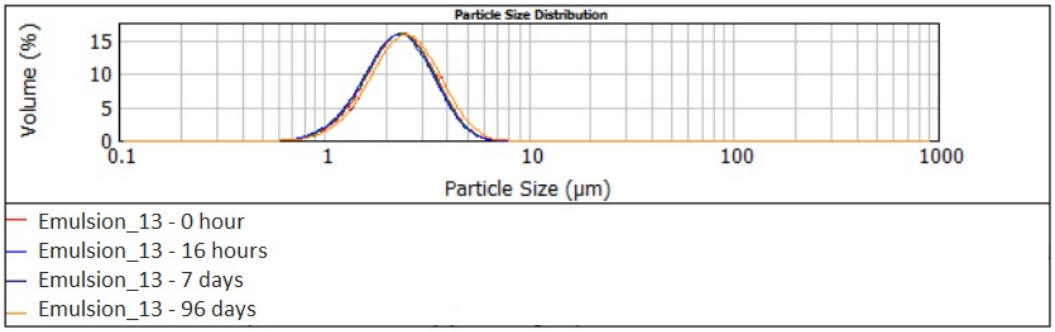

Figure 5.24: DSD of EM_13 emulsion - 4th model system: hexadecane + toluene (9:1) doped with 1% (wt/v) of stearic acid concentration and buffer solution (higher mixing time and speed was used).

Figure 5.25: Photographs for following the EM_13 emulsion coalescence process during the bottle tests.

5.1.5
5th model system

In this system a 9:1 ratio of hexadecane and toluene was used as the oil phase, and a buffered saline solution was used as aqueous phase. To this end, the same $NaCl$ concentration used in the synthetic seawater (24530 ppm) was added to the buffer solution. This choice was made to check whether emulsion may be formed without the divalent salt ions present in seawater. The studies were performed at 45°C and room temperature ($\approx$ 24°C).

Emulsions

Accordingly to tab. 5.7, it was not possible to form emulsion with the system considered. The presence of salts in a dispersion with ionic surfactants (due to the buffer presence) causes a decrease in the electric double layer at the droplet interface, leading to less repulsion between the surfactant heads at the interface, that means, more surfactant molecules will migrate from oil to the interface. So, the interfacial film will have more molecules compacted and there may be a very large reduction in surface area per molecule, decreasing the interfacial tension. The coalescence process is accelerate and the interfacial film resistance falls, what may explain the non-formation of emulsions in the presence of salt. Another explanation may be the Marangoni effect between droplets, which means that surfactant transfer can occur along the droplet interface due to the interfacial tension gradient, so that the surfactant flows out of the low interfacial tension regions, which it may also be accelerating the coalescence process.

Figure 5.26 shows the aspect of the mixture after preparation of EM_11 and EM_12 emulsions. By microscopic analysis, no droplets were found and a layer of aggregated stearic acid was formed, visually similar to a soap.

Emulsions	Oil phase	Water phase	SA (% wt/v)	T [°C]	Speed [rpm]	t [min]	Emulsion formed
EM_11	HD + TL (9:1)	Buffer + NaCL	1	≈24	10000	4	No
EM_12	HD + TL (9:1)	Buffer + NaCL	1	45	10000	4	No

Table 5.7: Evaluation of emulsion formation - Fifth model system: hexadecane + toluene (9:1) doped with 1% (wt/v) of stearic acid concentration and buffered saline solution ($Buffer + NaCl$).

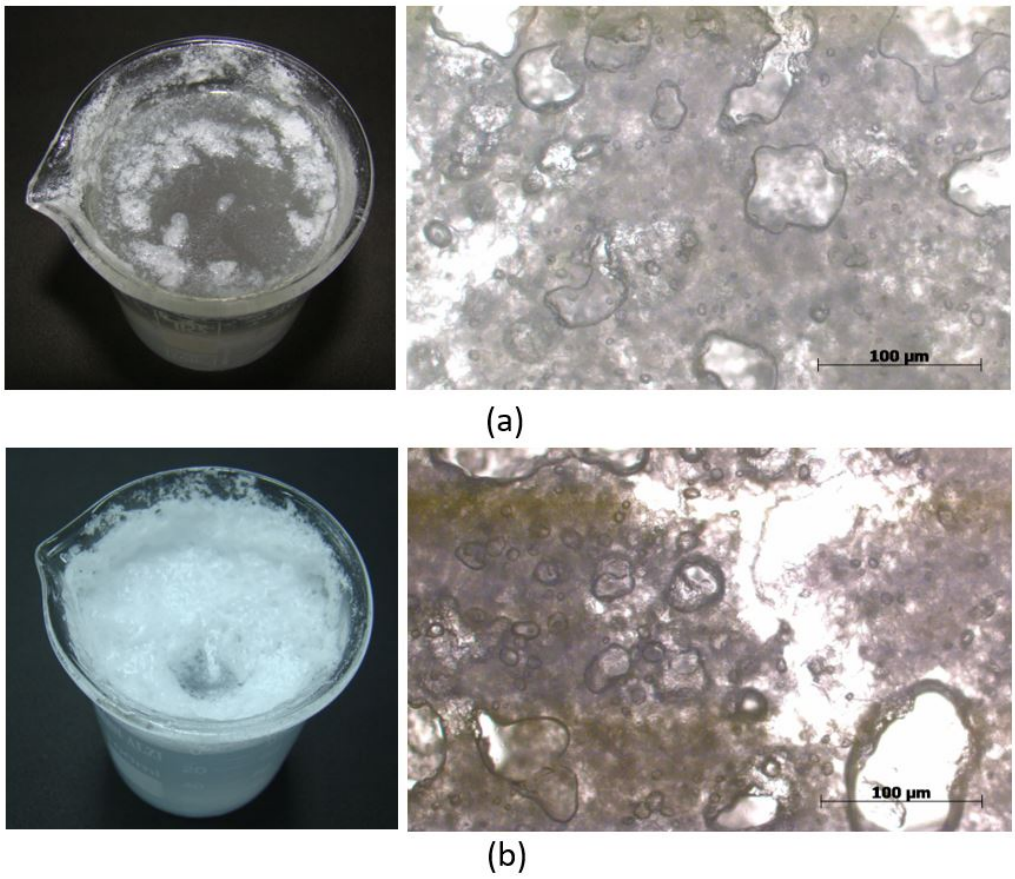

Figure 5.26: Emulsions appearance and microscopic analysis showing the aggregates formed (a) EM_12 emulsion prepared at 45°C (b) EM_11 emulsion prepared at room temperature (≈ 24°C).

Microscopic analysis shows that the aggregates formed were different from the crystals formed when only stearic acid was dissolved into the oil phase (fig. 5.11). Therefore, it may be the result of interactions and/or reactions between stearic acid, the buffer, and the $NaCl$. Emulsion formation was possible in the system with the unsalted buffer because the ammonium cation NH^{3+} ($THAM - HCl$ reaction products - eq. 4-1) acts as a counter-ion and interacts with stearic acid in its dissociated form ($COOH^{-}$). By adding

$NaCl$ to the system, depending on the concentration of the surfactant, it is possible to replace NH^{3+} with sodium cation (Na^{+}) so that the presence of cation type influences emulsion formation. This interaction may be promoting a saponification process, explaining the appearance of the soap in the mixture.

5.2 Injectivity tests

In this section, the flow behavior of emulsion injection experiments will be presented. Table 5.8 shows the petrophysical characteristics and properties of the Bentheimer cores samples used in the injectivity tests, where D is the diameter, L is the length, V_p is the rock pore volume, ϕ is the porosity, and k is the permeability to N_2 injection.

Due to the stability of EM_10 and EM_13 emulsions, the model system and protocol for formulating them were selected to recreate these emulsions and use them in the injectivity tests.

Test	Sample	D [cm]	L [cm]	Vp [cm³]	Ø	k (N_2) [mD]
1st	BH5C	3.815	10.007	26.890	0.235	2663.893
2nd	BH6A	3.829	9.818	26.790	0.237	2092.330
3rd	BH6B	3.825	9.606	26.392	0.239	2501.818

Table 5.8: Petrophysical characteristics and properties of the Bentheimer cores samples used in the injectivity tests.

5.2.1 1st Core flooding test

The absolute permeability of the sample BH5C to buffer solution was determined by using Darcy's law (eq. 2-3). The flow rates adopted were 0.2, 0.5, 0.75, 1, 1.2, 1.5, 2, 2.5 and 3 ml/min. The permeability to buffer injection obtained from the slope of q versus Δp curve (fig. 5.27) was 2505.522 mD. For this injectivity test, a reproduction of EM_10 emulsion was prepared. The drop size distribution (DSD) and D-values of the new EM_10 (namely EM_10a) is shown in fig. 5.28.

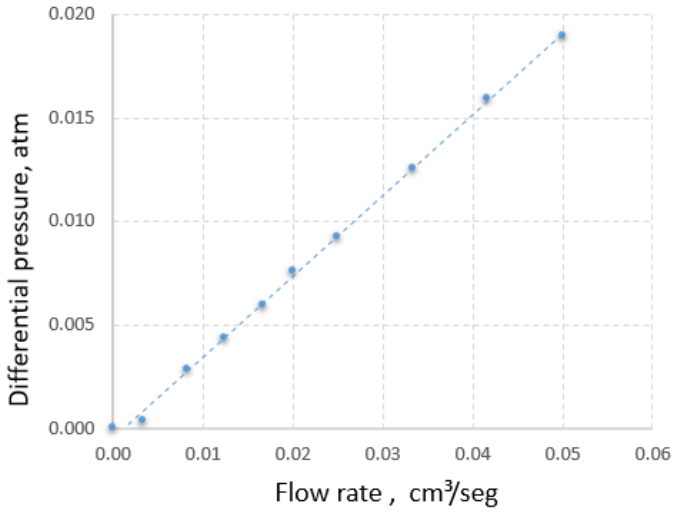

Figure 5.27: Linear correlation of q versus Δp obtained during continuous buffer injection - First Core flooding test.

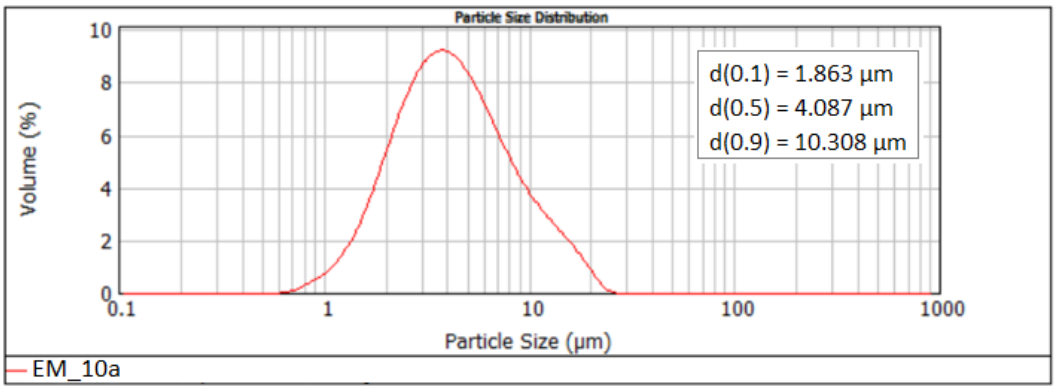

Figure 5.28: DSD of the EM_10a emulsion before the first injectivity test.

Figure 5.29 compares the differential pressure response of the buffer and emulsion injection for the selected flow rates. In both tests, a total of $2V_p$ was injected for each flow rate. Unlike the behavior observed for buffer injection, it is possible to see an important increase in differential pressure during emulsion injection. At low flow rates, the pressure did not stabilize, which evidence drop filtration during emulsion injection. The permeability to the aqueous phase injection was recalculated after the emulsion injection and compared with the initial value to analyze the rock damage caused by emulsion injection. Figure 5.30 compares the differential pressure response of the buffer before and after emulsion injection.

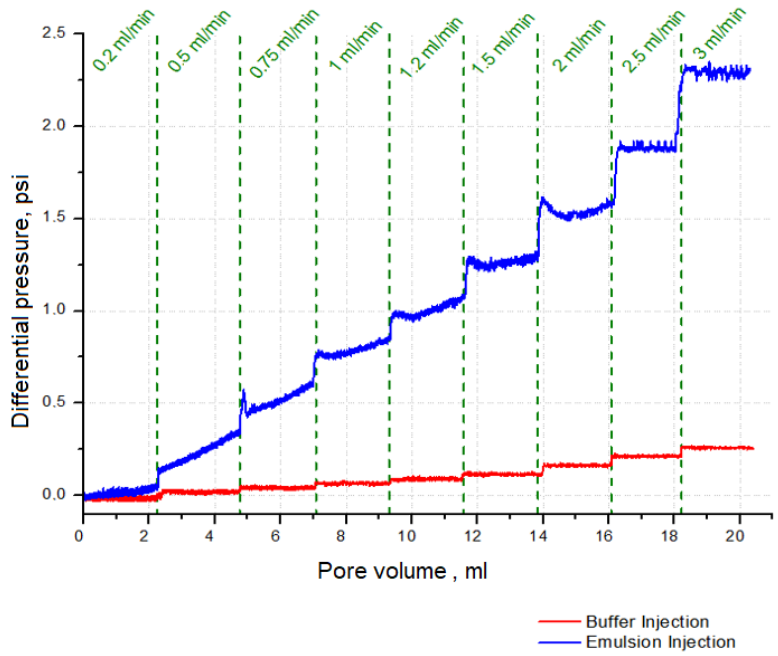

Figure 5.29: Comparison of the differential pressure response during buffer and EM_10a emulsion injection - First injectivity test.

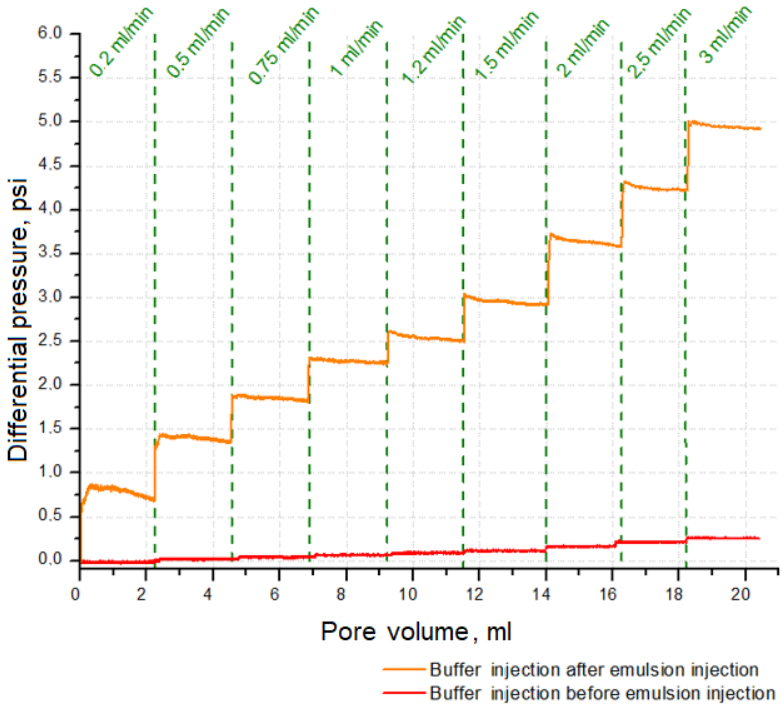

Figure 5.30: Comparison of the differential pressure response during buffer injection before and after EM_10a emulsion injection.

After emulsion injection, absolute permeability was recalculated by using Darcy's law (eq. 2-3). It changed from 2505.522 (before emulsion) to 166.425

mD (after emulsion injection). The permeability reduction, in more than 93%, shows severe rock damage as a result of clogging of the porous media by the emulsion drops.

In order to check the drop break-up, retention and percolation in the porous medium, the drop size distribution of the produced emulsions was compared with the original one (fig. 5.28). To this end, $15ml$ of emulsion effluent were collected for each flow rate, as shown in fig. 5.31, and were analyzed in the MASTERSIZER.

The increased degree of turbidity with flow rate observed in the collect samples, indicates that the dispersed phase was filtered through the porous medium during smaller flow rates and justifies the increased pressure recorded during the test. In addition, as the smaller is the drop, the less scattered is the light, low turbidity may also indicates that at low flow rates only smaller droplets percolates the rock while the larger ones were trapped.

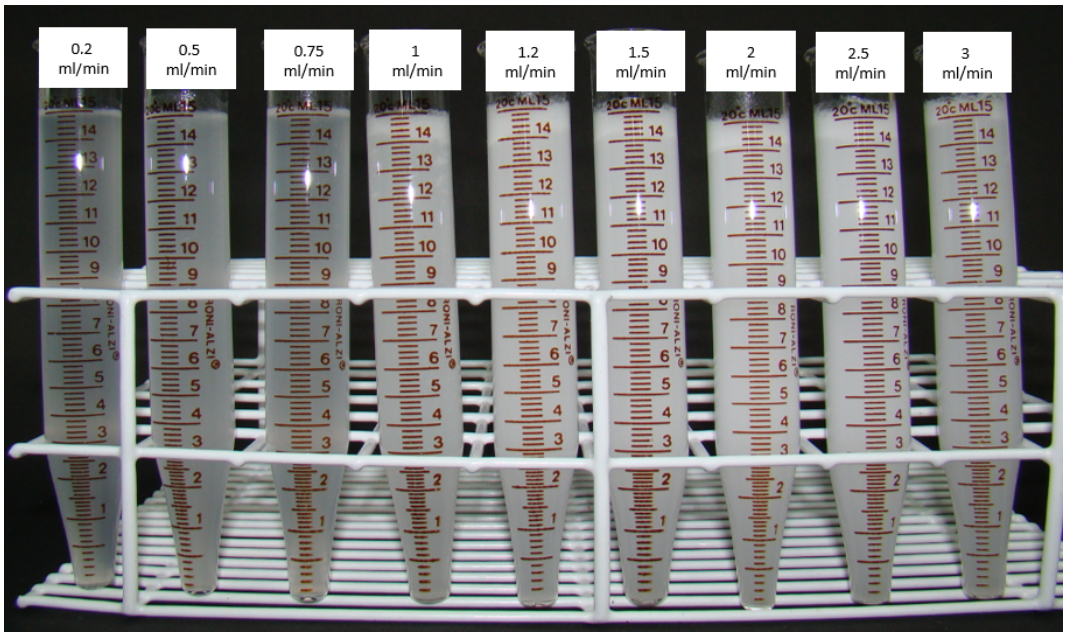

Figure 5.31: EM_10a emulsion effluent collected for each flow rate during the first injectivity test.

Table 5.9 and fig. 5.32 present the diameter values (D-values) for 10%, 50% and 90% of the drop population and the DSD emulsion effluent.

For all flow rates, the DSD showed a multimodal distribution over time, which means that the curves begins to show a second distinct distribution and shifts to the right compared to the emulsion before being injected, evidencing coalescence.

EM_10a	D-values [µm]		
	d (0.1)	d (0.5)	d (0.9)
Before injectivity test	1.863	4.087	10.308
Flow = 0.2 ml/min	1.376	4.051	36.927
Flow = 0.5 ml/min	1.522	3.120	8.537
Flow = 0.75 ml/min	1.279	3.458	29.630
Flow = 1 ml/min	1.639	4.819	30.363
Flow = 1.2 ml/min	1.968	6.810	18.279
Flow = 1.5 ml/min	1.893	6.887	18.773
Flow = 2 ml/min	1.814	7.613	18.053
Flow = 2.5 ml/min	1.924	6.529	19.196
Flow = 3 ml/min	1.828	6.234	23.716

Table 5.9: D-values obtained for the EM_10a emulsion effluent - First injectivity test.

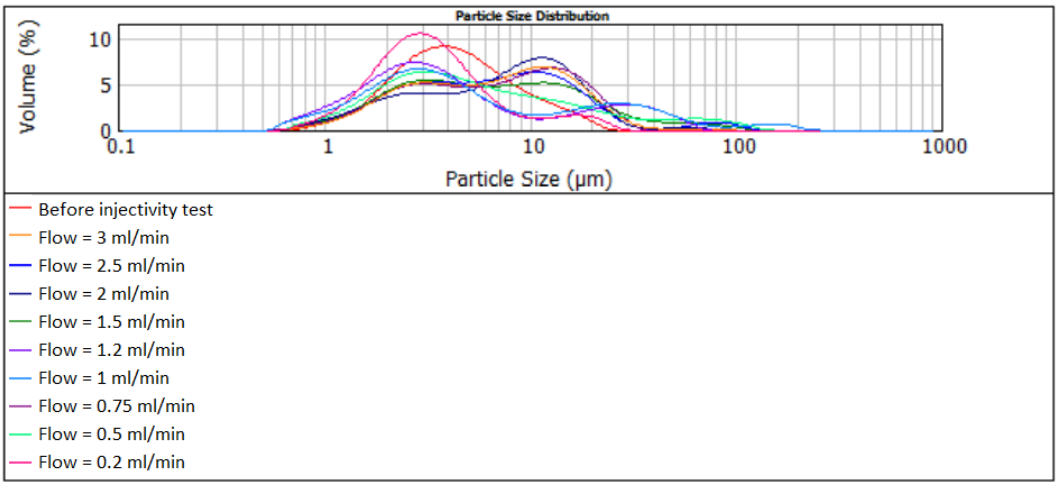

Figure 5.32: DSD of the EM_10a emulsion effluent - First injectivity test.

5.2.2
2nd Core flooding test

Figure 5.33 shows the linear correlation of the q versus Δp data recorded during buffer injection. The permeability obtained by application of the eq. 2-3 was 2194.566 mD.

In this test, a reproduction of emulsion EM_10 (EM_10b) was injected which DSD and D-values are exhibited in fig. 5.34.

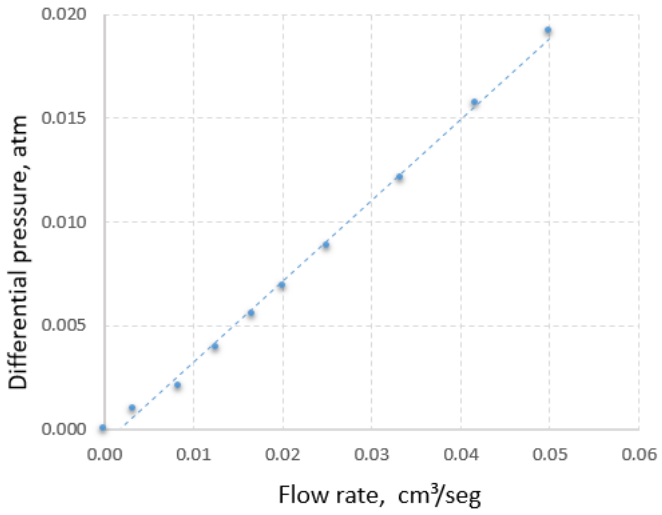

Figure 5.33: Linear correlation of q versus Δp obtained during continuous buffer injection - Second Core flooding test.

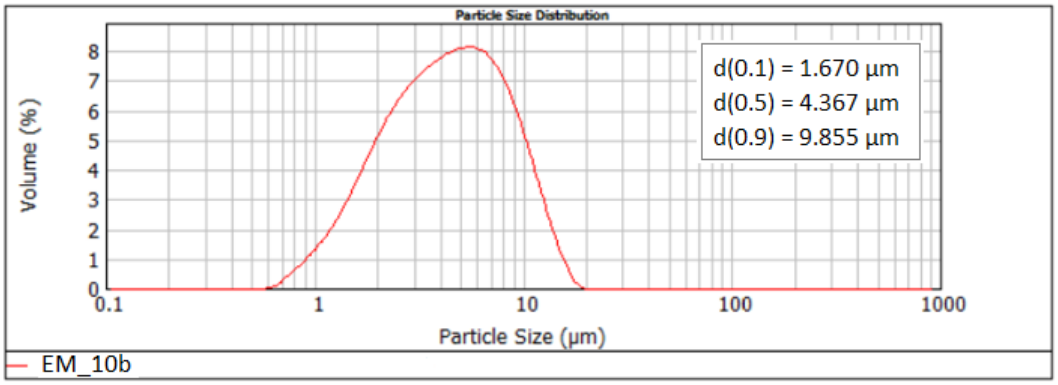

Figure 5.34: DSD of the EM_10b emulsion before the second injectivity test.

In order to confirm the pressure response and the blocking behavior of the emulsion as function of the flow rate in this test, the flow rates varied from highest to lowest values. Results are shown in fig. 5.35. It can be noted that at the highest flow rate (3 ml/min) the pressure did not stabilize even after the injection of more than 40 V_p of emulsion, moment at which the test was stopped.

Similarly to the first injectivity test, the rock damage by emulsion injection was estimated. Figure 5.36 compares the differential pressure response as flow rate varies during buffer injection before and after emulsion injection.

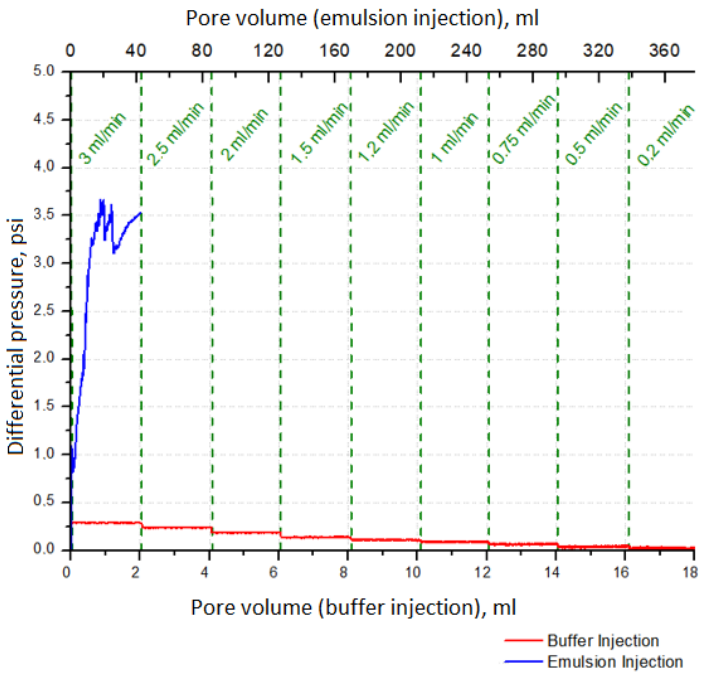

Figure 5.35: Comparison of the differential pressure response during buffer and EM_10b emulsion injection.

By applying the eq. 2-3, the permeability to buffer injection values were calculated resulting in 2194.566 and 146.960 mD before and after emulsion injection, respectively. Similarly to the first injectivity test, there was more than 93% of permeability reduction after emulsion injection.

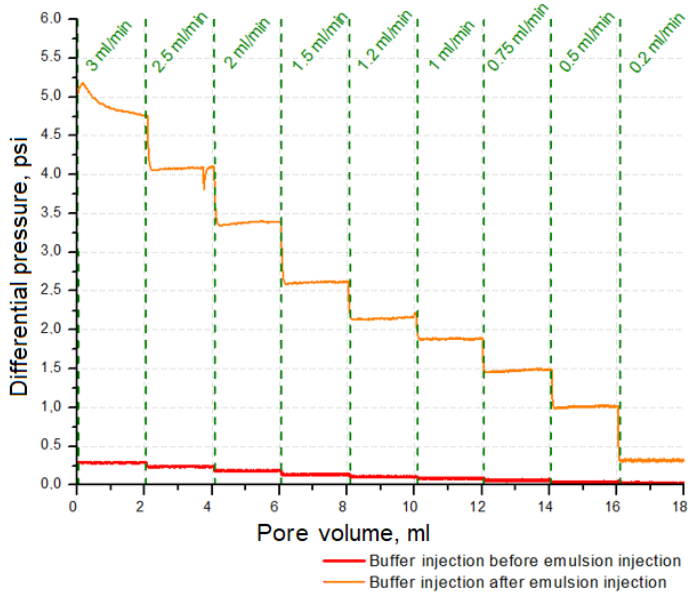

Figure 5.36: Comparison of the differential pressure response during buffer injection before and after EM_10b emulsion injection - Second injectivity test.

Emulsion effluent was analyzed for 4, 8, 12, 16, and 20 V_p injected, and as shown in fig. 5.37, 15 ml were collected for each volume fraction to determine the DSD.

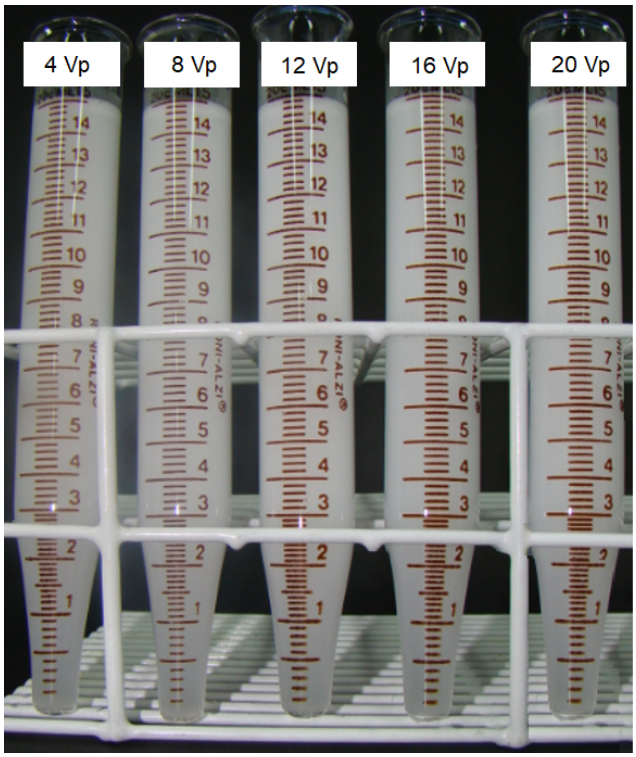

Figure 5.37: EM_10b emulsion effluent collected for 4, 8, 12, 16, and 20 V_p injected during the second injectivity test.

Table 5.10 and fig. 5.38 present the D-values and the DSD of the emulsion effluent, respectively. The large variation in DSD observed in the graph and an increased in the d(0.9) indicates that the droplets coalesced during the test to form drops bigger than $8\mu m$. This can be explained by comparing the curves for the emulsion before and after being injected, the curves were shifted to the right, indicating larger droplets creation.

EM_10b	D-values [µm]		
	d (0.1)	d (0.5)	d (0.9)
Before injectivity test	1.670	4.367	9.855
Flow = 3 ml/min (4 Vp injected)	1.991	8.552	18.049
Flow = 3 ml/min(8 Vp injected)	1.934	6.433	16.881
Flow = 3 ml/min(12 Vp injected)	1.874	6.398	16.866
Flow = 3 ml/min(16 Vp injected)	1.611	5.103	12.950
Flow = 3 ml/min(20 Vp injected)	1.712	5.512	12.696

Table 5.10: D-values obtained for the EM_10b emulsion effluent - Second injectivity test.

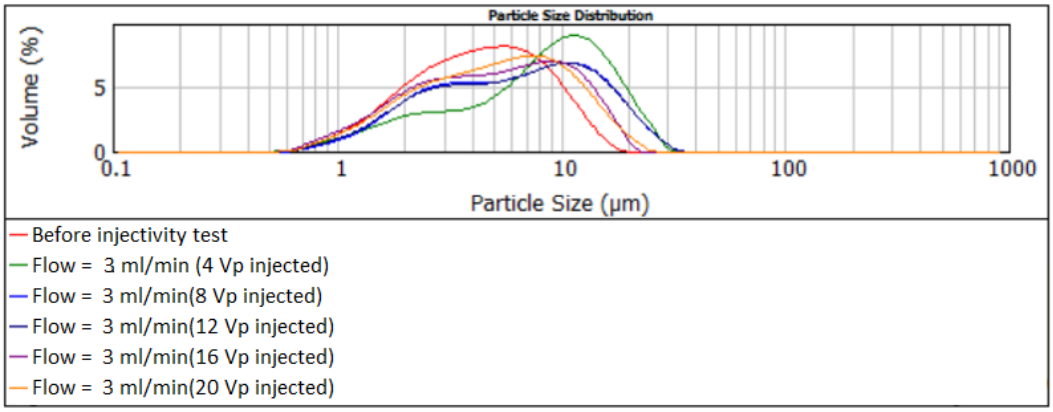

Figure 5.38: DSD of the EM_10b emulsion effluent - Second injectivity test.

After removing the core sample from the core holder at the end of the test, some residue was observed on the inlet end plug (flow distributor) and at the inlet face of the rock sample, as presented in fig. 5.39. By microscope analyses, shown in fig. 5.40, samples from both locations seem to contain emulsion drops and stearic acid crystals.

The presence of acid crystals indicates that the emulsion destabilized during the injection in the porous medium, which means that the interfacial film ruptured and the oil and water phases passed through the rock, leaving behind the surfactant. According to Palombo, the average pore diameter of a Bentheimer sandstone is 3.5331μm [106], and the d(0.9) of the injected emulsion was about 10μm. Since the EM_10b emulsion is approximately three times larger than the pore throat diameter, at the operating conditions the interfacial film would not have sufficient elasticity to deform and cross the pore throat.

Figure 5.39: White residue observed after emulsion injection at the inlet face of the rock sample and inlet end plug - Second injectivity test.

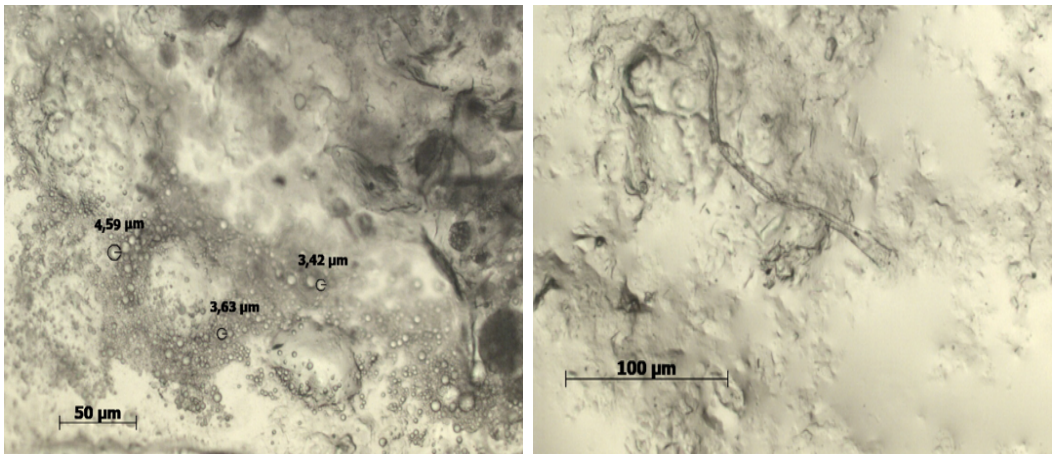

Figure 5.40: Microscope analyses of the residue formed at the inlet face of the rock and inlet end plug after emulsion injection - Second injectivity test.

In order, to study the pressure effect on the stability of the emulsion tested, the EM_10 emulsion was recreated (EM_10c) and subjected for 12 hours to ≈ 10 psi of pressure, which is higher than the highest pressure recorded during the injection of EM_10b (≈ 3.6 psi). Figure 5.41 shows the pressurization set-up used.

Figure 5.41: Experiment set-up used to pressurize the emulsions.

Figure 5.42 and tab. 5.11 show the DSD and the D-values of the emulsion drops before and after being subjected to 10 psi, respectively. It can be noted a large variation in the drop size. Reduction of the smaller droplet volume and increased population of larger drops indicate the emulsion coalescence when submitted at higher pressures.

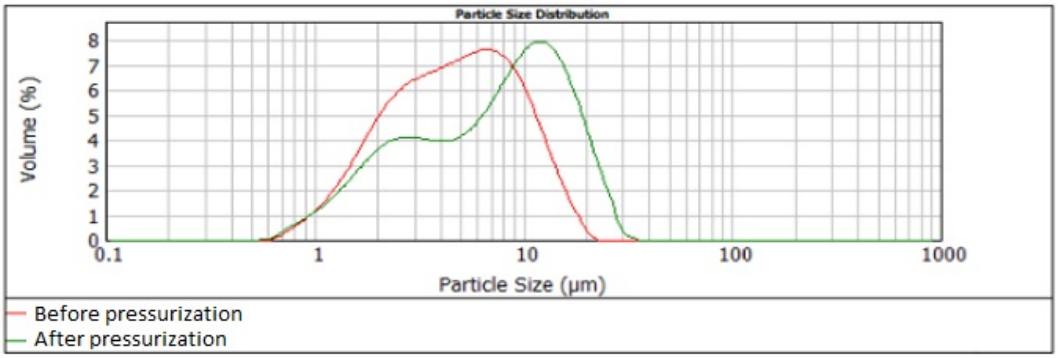

Figure 5.42: DSD of the EM_10c emulsion before and after being subjected to 10 psi.

EM_10c	D-values [µm]		
	d (0.1)	d (0.5)	d (0.9)
Before pressurization	1.728	4.761	11.265
After pressurization	1.823	7.720	17.980

Table 5.11: D-values obtained for EM_10c emulsion before and after being subjected to 10 psi.

5.2.3
3rd Core flooding test

Figure 5.43 shows the linear correlation of the q versus Δp data obtained during buffer injection at different flow rates. The permeability obtained by application of the eq. 2-3 was 2495.173 mD. In order to inject an emulsion with drop diameter in the same range as the average pore diameter of the rock, a recreation of EM_13 emulsion (EM_13a) was injected in the third test. Figure 5.44 shows the DSD and the D-values of EM_13a emulsion. The d(0.9) of the EM_13a emulsion was a little higher than the average pore diameter of the rock (3.5 μm) [106]. Figure 5.45 shows the evolution of differential pressure as function of the flow rate for emulsion injection. In this test, emulsion was injected until the pressure stabilizes. Figure 5.46 compares the last two pore volume of emulsion injection for each flow rate along with the buffer injection.

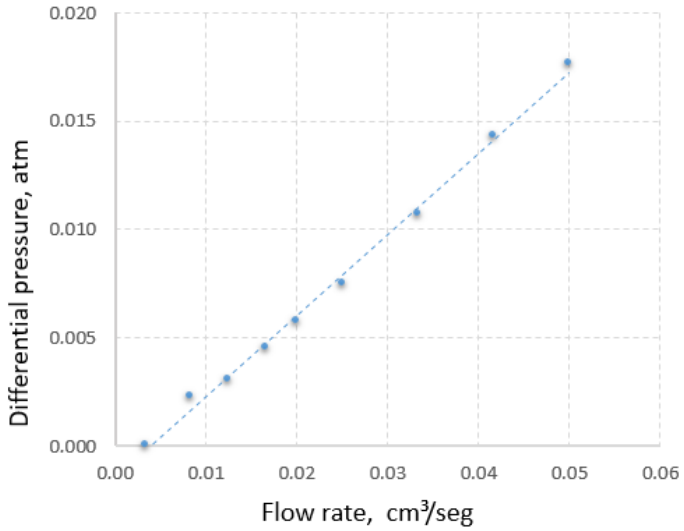

Figure 5.43: Linear correlation of q versus Δp obtained during continuous buffer injection - Third Core flooding test.

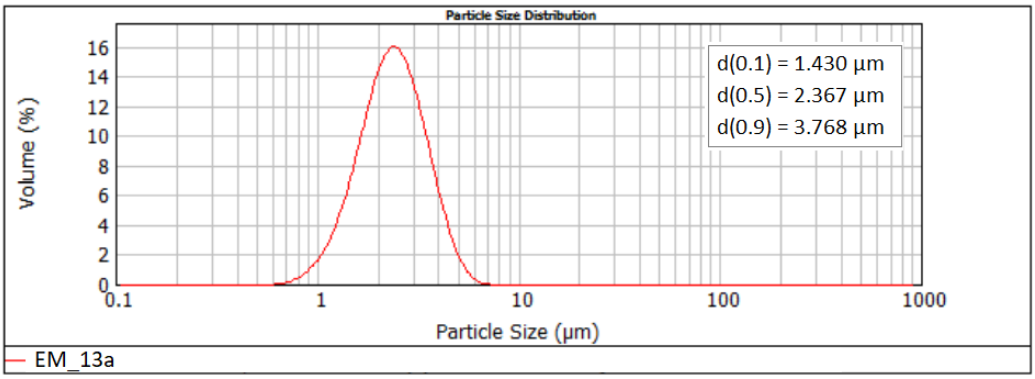

Figure 5.44: DSD of the EM_13a emulsion before the third injectivity test.

As expected, the emulsion pressure response was higher than that for the buffer injection. It can be noted that the pressure fluctuations for the emulsion increases with the reduction of the flow rate. As the capillary number decreases the capillary forces predominates and the drops that formerly percolates the porous media remain trapped. The behavior of the differential pressure during emulsion injection evidence this blockage. The large pressure oscillation shows that the drops block the pores and deform until they can proceed.

The experimental results shown in fig. 5.46 were used to calculate the mobility reduction factor f as a function of Ca for emulsion injection. As discussed in the literature review, f is defined as the ratio of the average pressure measured during continuous phase flow, Δp_c, to that of the emulsion flow, Δp_e, and the improved reservoir sweep occurs when Ca is below a critical value, and above it, the block mechanism is weak. Figure 5.47 shows f as

a function of Ca. Results shows that for Ca above 1.5 x 10^{-8}, the mobility reduction factor stabilizes, this value corresponds to the critical Ca, and the dispersed phase of the emulsion blocks the porous media only for Ca below this value.

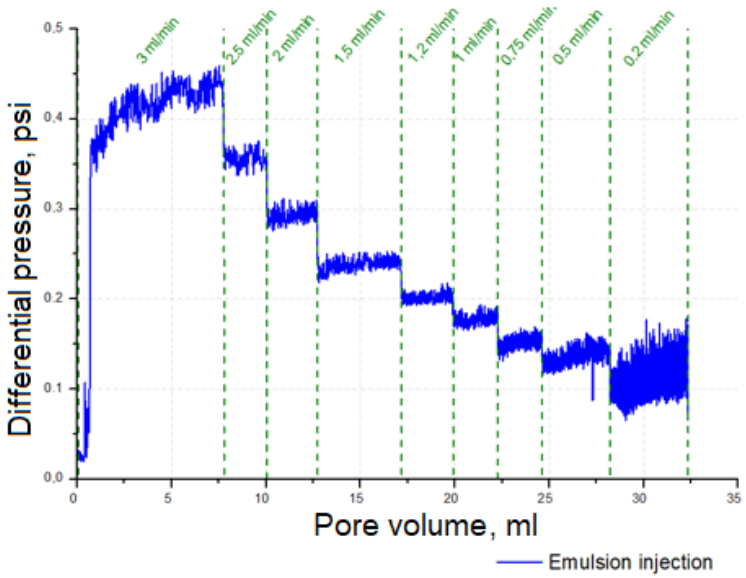

Figure 5.45: Evolution of differential pressure as function of the flow rate for EM_13a emulsion injection - Third injectivity test.

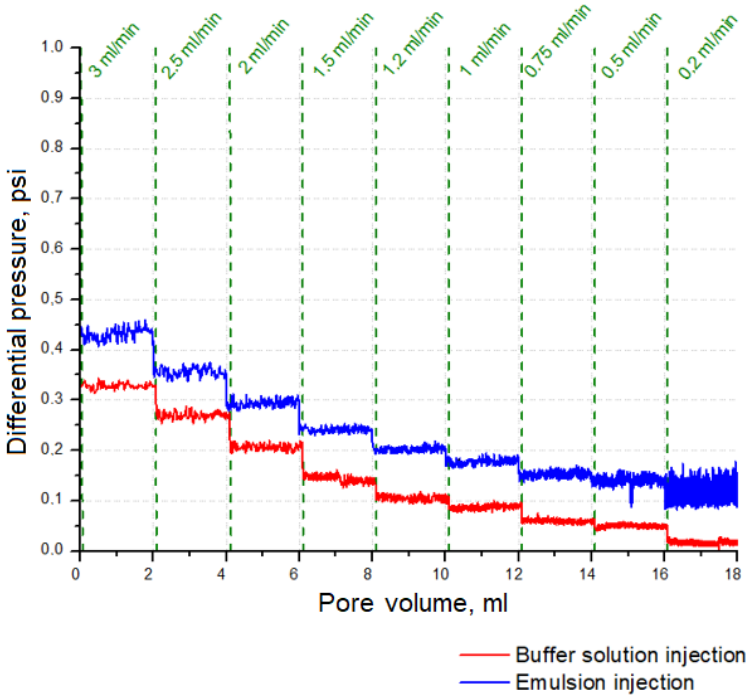

Figure 5.46: Comparison of the differential pressure response during buffer and EM_13a emulsion injection - Third injectivity test.

Figure 5.48 shows the evolution of differential pressure as flow rate varies for buffer injection before and after EM_13 emulsion injection. Similarly to the previous tests, permeability before and after emulsion injection was calculated from this results and compared. Results showed a decrease in permeability from 2495.173 to 2156.208 mD ($\approx$ 16%), a very low damage in comparison with the previous injectivity tests.

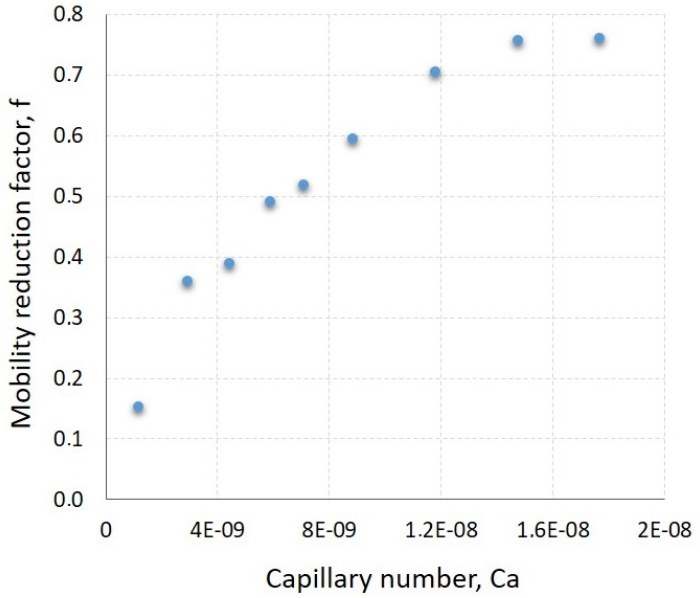

Figure 5.47: Mobility reduction factor f of EM_10c emulsion as function capillary number.

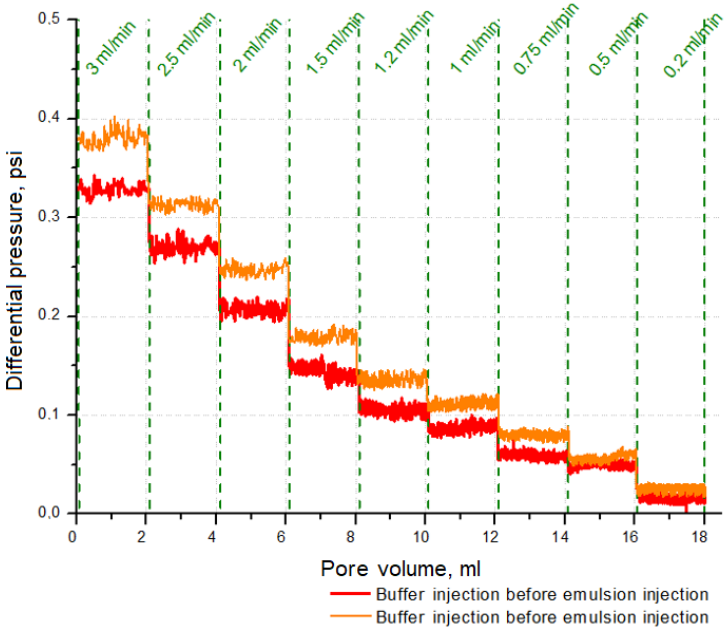

Figure 5.48: Comparison of the differential pressure response during buffer injection before and after EM_13a emulsion injection.

Emulsion effluent collected at each flow rate is shown in fig. 5.49. It is possible to note that there is no visual variation among the samples.

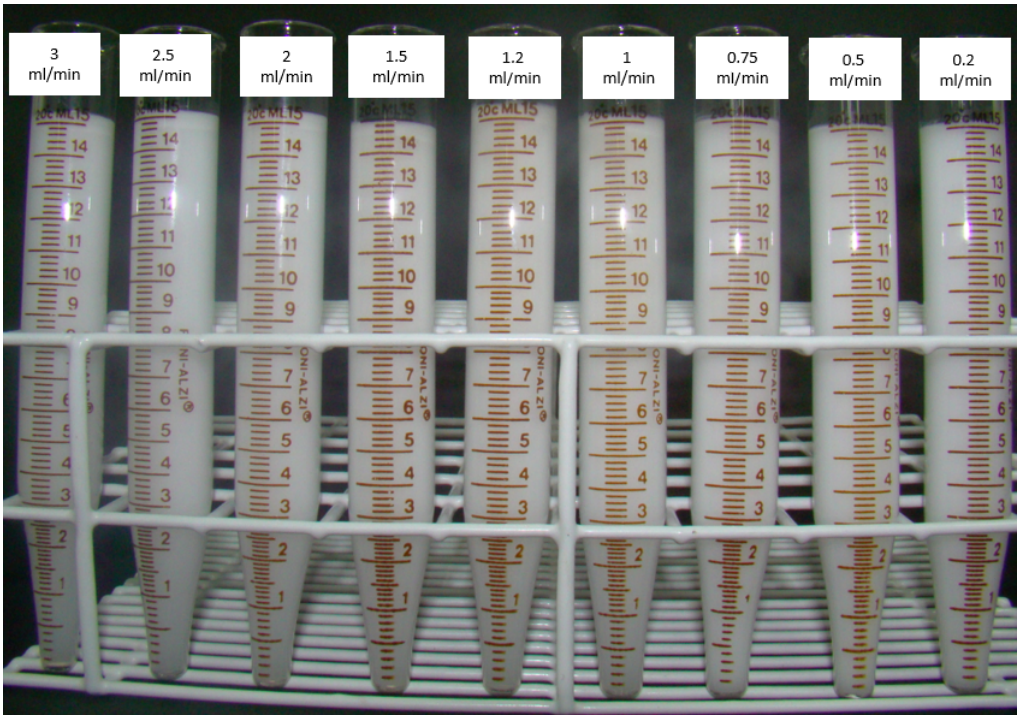

Figure 5.49: EM_13a emulsion effluent collected for each flow rate during the third injectivity test.

Table 5.12 and fig. 5.50 present D-values and the DSD of the emulsion effluent, respectively. No significant variation in the drop diameters and DSD curves was noted.

EM_13a	D-values [µm]		
	d (0.1)	d (0.5)	d (0.9)
Before injectivity test	1.430	2.367	3.768
Flow = 3 ml/min	1.356	2.326	3.801
Flow = 2.5 ml/min	1.439	2.382	3.794
Flow = 2 ml/min	1.420	2.357	3.754
Flow = 1.5 ml/min	1.417	2.351	3.745
Flow = 1.2 ml/min	1.415	2.343	3.723
Flow = 1 ml/min	1.393	2.310	3.656
Flow = 0.75 ml/min	1.361	2.163	3.298
Flow = 0.5 ml/min	1.307	2.111	3.258
Flow = 0.2 ml/min	1.240	2.018	3.121

Table 5.12: D-values obtained for the EM_13a emulsion effluent - Third injectivity test.

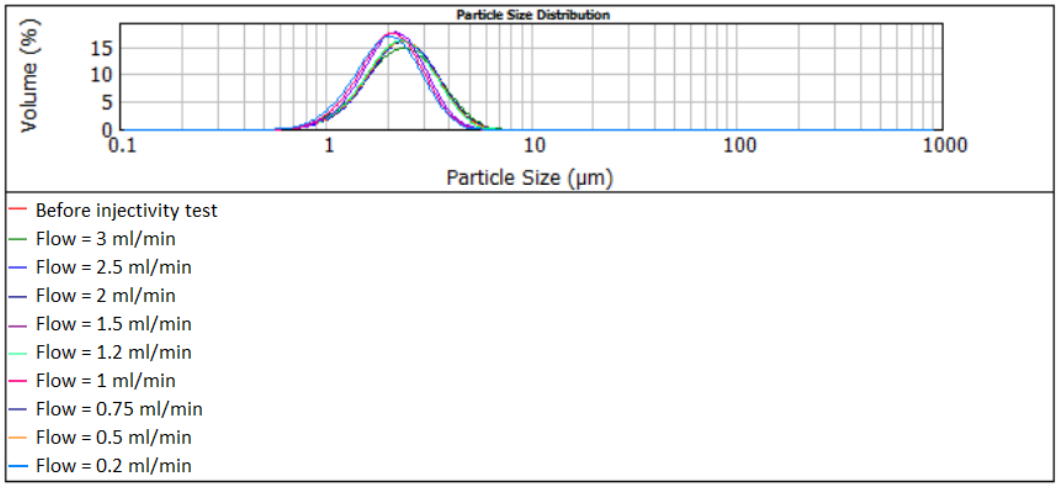

Figure 5.50: DSD of the EM_13a emulsion effluent - Third injectivity test.

At the end of the injectivity test, the inlet end plug and the inlet face of the rock sample were checked. Unlike the second injectivity test (fig. 5.39), no residue was found, as shown in fig. 5.51.

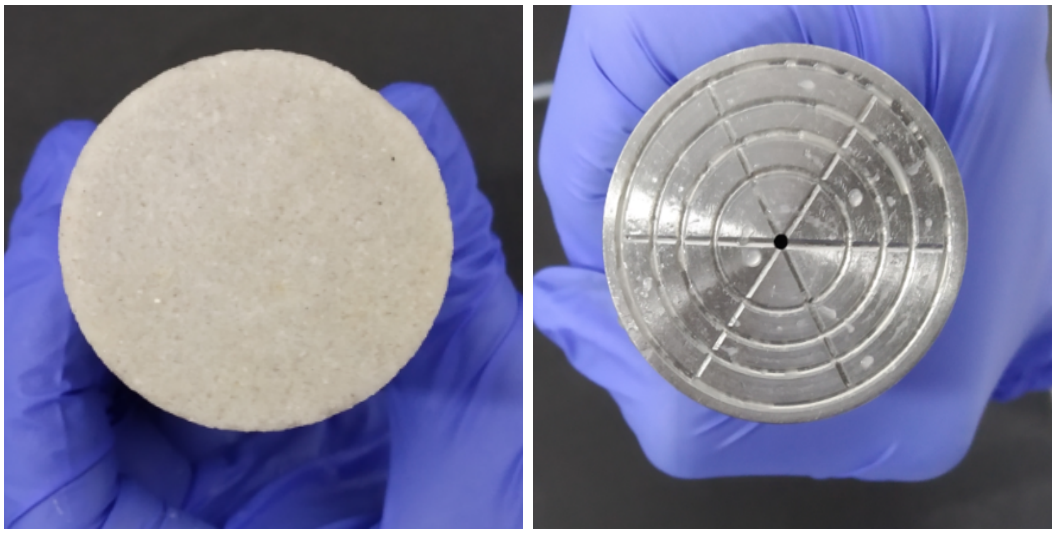

Figure 5.51: Inlet face of the rock sample and inlet end plug - Third injectivity test.

In order to study the pressure effect on the emulsion tested, the EM_13 emulsion was recreated (EM_13b) and subjected to ≈ 10 psi of pressure during 12 hours, to analyze their behavior when subjected to the injection pressure into the porous medium. The pressurization set-up was the same exhibited in fig. 5.41. Figure 5.52 and tab. 5.13 present the DSD and the D-values of the emulsion before and after being subjected to 10 psi. No significant variation was observed among both emulsions. This results and the fact that no residue

was found at the inlet face of the rock sample and inlet end plug indicate that the emulsion remained stable during the third injectivity test.

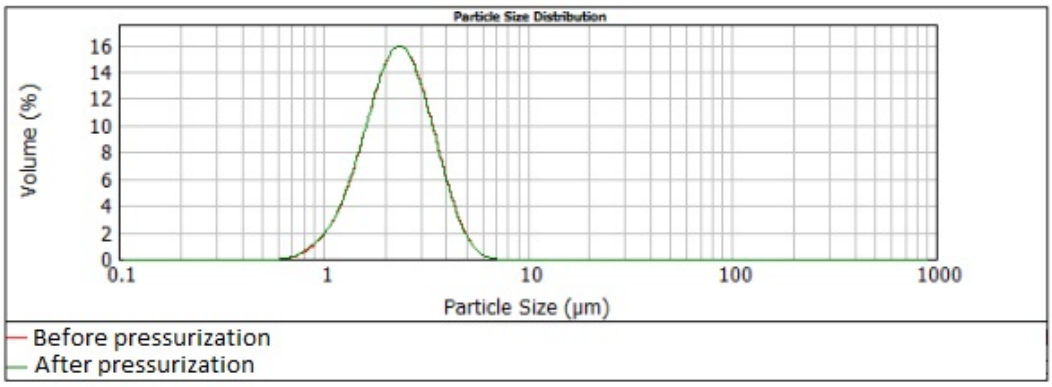

Figure 5.52: DSD of the EM_13b emulsion before and after being subjected to 10 psi.

EM_13b	D-values [µm]		
	d (0.1)	d (0.5)	d (0.9)
Before pressurization	1.407	2.337	3.725
After pressurization	1.399	2.325	3.710

Table 5.13: D-values obtained for EM_13b emulsion before and after being subjected to 10 psi.

5.3 WAE test as EOR method

In this section, the results of water-alternated-emulsion (WAE) injection as EOR method are shown. Table 5.14 presents the petrophysical characteristics and properties of the sample used for WAE injection, where D is the diameter, L is the length, V_p is the rock pore volume, ϕ is the porosity, and k is the permeability to N_2 injection.

Test	Sample	D [cm]	L [cm]	Vp [cm³]	Ø	k (N_2) [mD]
4th	BH5A	3.817	10.505	28.384	0.236	2763.398

Table 5.14: Petrophysical characteristics and properties of the sample used for water-alternated-emulsion injection.

5.3.1
4th Core flooding test

Figure 5.53 shows the linear correlation of q versus Δp obtained during continuous buffer injection. The flow rates adopted were 1, 2, 3, 4, 5 e 6 ml/min, and the permeability obtained by application of the eq. 2-3 was 1993.865 mD.

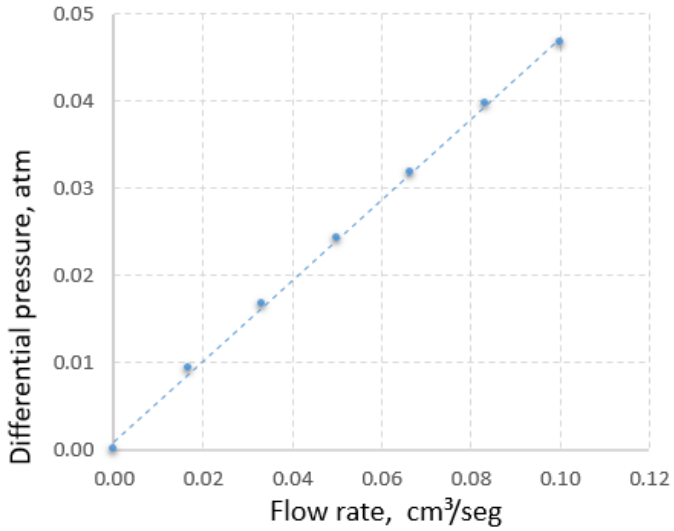

Figure 5.53: Linear correlation of q versus Δp obtained during continuous buffer injection - Fourth Core flooding test.

A recreation of EM_10 emulsion (EM_10d) was injected in this test. Figure 5.54 presents the DSD and D-values before injection in the porous medium.

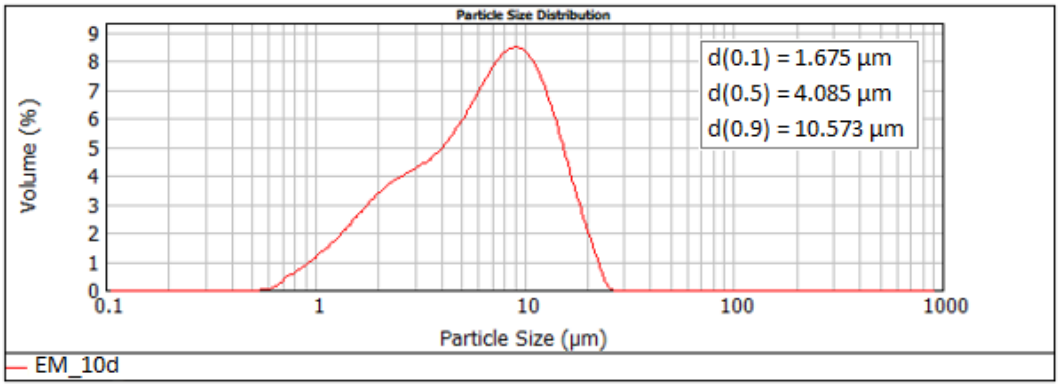

Figure 5.54: DSD of the EM_10d emulsion injected in the WAE test.

In this test, emulsion was injected under two-phase flow, at a flow rate of 0.24 ml/min, which is equivalent to a Darcy velocity of 1 foot per day. The

test consisted in a sequential injection of water (WF1) followed by an emulsion slug chased by a second water flooding (WF2). After buffer saturation, oil phase was injected into the core until reaching the irreducible saturation to the buffer solution (S_{wi}). The S_{wi} was approximately 0.2851 relative to the rock V_p, which means that 8.09 ml of the aqueous phase remained trapped in the rock. The initial oil saturation (S_{oi}) calculated by mass balance was approximately 0.7149, which is equivalent to 20.29 ml.

The first water flooding (WF1) was performed to displace the oil from the porous medium. To this end, 20 V_p of water were injected to ensure oil residual saturation (S_{or}). The oil recovery fraction reached 45.30% , which is equivalent to 9.19 ml.

At this point, 3 V_p of emulsion were injected in the porous media followed by 23 V_p of continuous water injection (WF2). Figure 5.55 shows the production data in terms of differential pressure and oil recovery as function of the pore volume injected. The moment of emulsion injection is represented by the green shaded area. It can be noted an important increase in the differential pressure after emulsion injection which is promoted by the pore blockage during the injection of the slug.

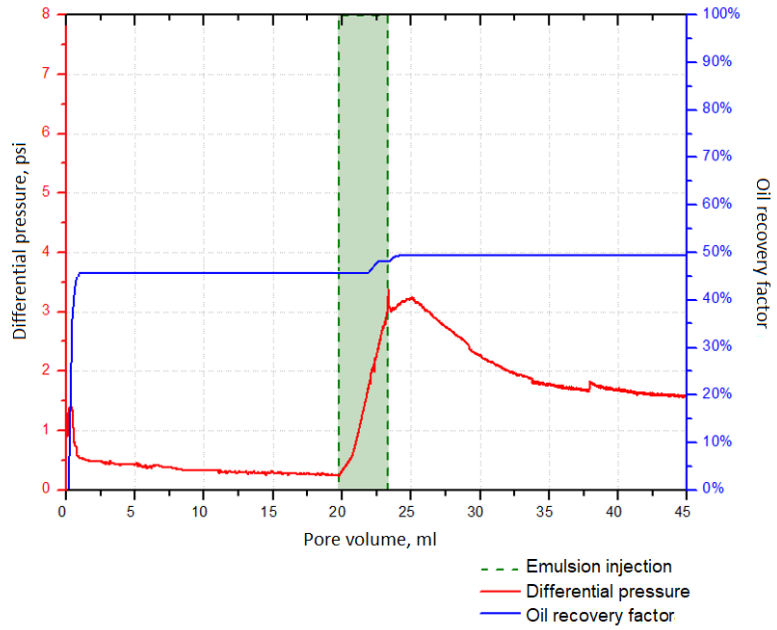

Figure 5.55: Differential pressure and oil recovery factor as function of pore volume injected during WAE process.

After the second water flooding (WF2), oil started to be produced again reaching a recovery factor of 49.49%, denoting that 4.19% of the initial residual oil were produced by emulsion injection. After restarting water injection, differential pressure decreases to a constant value of approximately 1.5 psi.

The difference in the pressure level reached before and after emulsion injection may suggest that an intense pore blockage of the emulsion drops remains in the porous medium after the second water flooding.

At the end of the test the inlet face of the rock sample was checked. As can be seen in fig. 5.56, after the WAE test, part of emulsion was found in the rock face, indicating that the drops were trapped on the injection face causing injectivity loss (rock damage), that explains the high pressure during emulsion injection and the big difference in the pressure level reached before and after emulsion slug. By analyzing fig. 5.54, it can be noted that more than 50% of the EM_10d emulsion drops were larger than the average pore diameter reported for the rock ($\approx 3.5331\mu$m [106]). This suggest that the smaller drops percolates the porous media causing the blockage and flow redistribution that increases oil recovery, while the larger one were trapped in the inlet rock face.

The results of this test were inconclusive, although additional oil was produced by emulsion injection, 3 V_p of emulsion with 5% of the oil phase was injected, which means that 15% of V_p of oil was injected into the porous medium and discounting the produced volume, oil production would be negative. Therefore, it is questionable whether the oil produced comes from the residual oil after the first water injection or if it is from the dispersed phase of the injected emulsion.

Figure 5.56: Injection sample face after WAE test.

6
Conclusions and Suggestions

This dissertation aimed to experimentally investigate the flow and stability of oil-in-water emulsions stabilized by a fatty acid that mimic a lipophilic natural surfactant occurring in crude oils. Stearic acid, a saturated carbon carboxylic acid, was used to represent a natural surfactant. Stability of emulsions was analyzed through the evolution of drop size distribution, and interfacial rheology measurements for different model oil, water systems, surfactant concentration and temperature.

In a system contained hexadecane as the oil phase, stearic acid as surfactant, synthetic seawater as the aqueous phase, and performed at 45°C, the stearic acid adsorbed on the interface and in presence of the salts, a rigid and rough film with increasing aging time was formed. According to the dilatational interfacial rheology, stearic acid is able to reduce the interfacial tension, and the dilatational visco-elastic modulus curves showed irregular behavior, with very high values of elastic modulus and very low values of viscous modulus.

In the same system without salinity, the dilatational interfacial rheology results showed higher values of elastic modulus compared to the viscous modulus. Comparing both systems, the interfacial tension reduction with synthetic seawater was larger than that for Milli-Q water for the same stearic acid concentration, hence the presence of salt leads to a stronger interfacial activity. In neither of both systems stable emulsions were formed, which implies that the formation of an interfacial film does not necessarily promotes emulsion stabilization.

Unstable water-in-oil emulsions were formed in a system contained hexadecane and toluene as the oil phase, stearic acid as surfactant and synthetic sea water as the aqueous phase, and performed at 45°C.

The presence of toluene increases the solubility of stearic acid in the model oil, but with aging time stearic acid crystals forms and aggregates at room temperature ($\approx$ 24°C).

In a buffer solution without salts as the aqueous phase, and with a 9:1 ratio of hexadecane and toluene as the oil phase, the interfacial tension decreased with stearic acid concentration, being the critical concentration

CMC=0.3% (wt/v). All emulsions formed with this system were very stable at room temperature (≈ 24°C). The presence of a monovalent salt in a buffer solution at room temperature (≈ 24°C) and at 45°C, did not form emulsion, so emulsion formation and stability is strongly related to the pH and salt composition of water phase.

The flow behavior of stable emulsions was studied through emulsion flooding in sandstones through injectivity tests at room temperature (≈ 24°C). During emulsion injection in single-phase flow, water mobility control was observed through the reduction of the permeability to aqueous phase injection as a strong function of emulsion drop size distribution and capillary number.

The injectivity results of emulsions with particle size distribution (d(0.9)) larger than the average pore diameter of the porous media, showed permeability reduction, more than 93%, resulting in a severe rock damage by the clogging of the porous media by the emulsion drops. The dispersed phase with diameter larger than the average rock pore diameter was filtered through the porous medium, differential pressure during emulsion injection did not stabilize and was high compared to continuous phase injection. In addition, the emulsion effluent analyzes presented coalescence. In order to study the pressure effect on the emulsion stability, it was subjected to a pressure higher than the highest pressure recorded during the injectivity test and coalescence was noted indicating that large drops do not resist the injection pressure.

The injection of an emulsion with particle size distribution (d(0.9)) in the same order as the average pore diameter of the porous media showed a moderate rock damage (≈ 16%), and during the test the pressure fluctuations for the emulsion injection increases with the reduction of the flow rate. Large pressure oscillation indicates that the emulsion drops are blocking the pores and deforming until they can proceed toward the throats, evidencing the emulsion mobility control effect. The mobility reduction factor f was calculated, and the results show that the emulsion blocks the porous medium for Ca below 1.5 x 10^{-8}.

The efficiency of the emulsions as an EOR method through Water-alternated-emulsion (WAE) injection was analyzed in a two-phase flow. An additional oil recovery of 4.19% was reached after emulsion injection even with drop sizes much bigger than the average pore diameter of the rock, which were filtered in the porous media. There was a difference between the pressure level reached before and after emulsion injection that indicates the pore blockage of the emulsion drops remains in the porous medium after the second water flooding.

The results obtained with the lipophilic natural surfactant had similar

effects already observed in the literature for emulsions stabilized by water-soluble surfactants, and there is potential for the use of water produced without the need for the addition of other chemicals.

To continue this research, some suggestions may be considered as perform emulsion stability studies by evaluating the size of the fatty acid carbon chain molecule and it effect on the surfactant solubility. Study a surfactant similar to resins, asphaltenes, or naphthenic acids because the formation of stable emulsions during the production and transport stages is attributed to their interfacial activity. Study seawater composition to evaluate the effect on salt ion competition with the polar part of the surfactant at reservoir temperature conditions aiming to form a stable emulsion. Perform studies by varying the pH of the aqueous medium to assess which range is least sensitive to salinity. Also, evaluate the effect of temperature and pressure on rheological tests.

To confirm the suspicion of pickering emulsion formation, tests would have to be performed under high-resolution microscopy, such as scanning electron microscopy (SEM) images, in order to identify the crystalline particles at the emulsion droplet interface.

Another proposal is to perform tests under temperature reservoir conditions into an heterogeneous porous media to evaluate the emulsion flow under actual reservoir conditions.

Bibliography

[1] THOMAS, J. E.. **Fundamentos de engenharia de petróleo**. Interciência, 2001.

[2] OUTLOOK, B. E.. **2019 edition**. London, United Kingdom2019, 2019.

[3] PEREIRA, T. D. S.. **Polymer flooding in sandstone cores**. Master's thesis, Pontifícia Universidade Católica do Rio de Janeiro (PUC-Rio) , Rio de Janeiro, Brazil., 2019.

[4] POPE, G. A.; OTHERS. **Recent developments and remaining challenges of enhanced oil recovery**. Journal of Petroleum Technology, 63(07):65–68, 2011.

[5] LIU, Z.; LI, Y.; LUAN, H.; GAO, W.; GUO, Y. ; CHEN, Y.. **Pore scale and macroscopic visual displacement of oil-in-water emulsions for enhanced oil recovery**. Chemical Engineering Science, 197:404–414, 2019.

[6] SADATI, E. Y.; SAHRAEI, E.. **An experimental investigation on enhancing water flooding performance using oil-in-water emulsions in an iranian oil reservoir**. Journal of Petroleum Exploration and Production Technology, p. 1–12, 2019.

[7] ZHOU, Y.; YIN, D.; CHEN, W.; LIU, B. ; ZHANG, X.. **A comprehensive review of emulsion and its field application for enhanced oil recovery**. Energy Science & Engineering, 2019.

[8] FU, C.; ZHU, T.; HUANG, B.; DAI, T.; WANG, Y.; ZHANG, W. ; LIU, X.. **The efficiency of migration and profile control with emulsion systems in class iii reservoirs**. Royal Society open science, 6(5):181634, 2019.

[9] GRUBER, L. D. A.; DAMASCENO, F. C.; CARAMÃO, E. B.; JACQUES, R. A.; GELLER, A. M. ; CAMPOS, M. C. V. D.. **Ácidos naftênicos no petróleo**. Química nova. São Paulo. Vol. 35, n. 7 (2012), p. 1423-1433, 2012.

[10] PERLES, C.; GUERSONI, V. ; BANNWART, A.. **Rheological study of crude oil/water interface–the effect of temperature and brine on interfacial film**. Journal of Petroleum Science and Engineering, 162:835–843, 2018.

[11] ABDEL-RAOUF, M.. **Crude oil emulsions: Composition stability and characterization**. BoD–Books on Demand, 2012.

[12] KAMAL, M. S.; HUSSEIN, I. A. ; SULTAN, A. S.. **Review on surfactant flooding: phase behavior, retention, ift, and field applications**. Energy & Fuels, 31(8):7701–7720, 2017.

[13] JANSSEN, P. H.. **Characterisation of oil-water mixtures produced in high-watercut oil wells**. PhD thesis, Delft University of Technology, 2000.

[14] FU, X.; LANE, R. H.; MAMORA, D. D. ; OTHERS. **Water-in-oil emulsions: flow in porous media and eor potential**. In: SPE CANADIAN UNCONVENTIONAL RESOURCES CONFERENCE. Society of Petroleum Engineers, 2012.

[15] VAN MEURS, P.; VAN DER POEL, C. ; OTHERS. **A theoretical description of water-drive processes involving viscous fingering**. Society of Petroleum Engineers, 1958.

[16] HOMSY, G. M.. **Viscous fingering in porous media**. Annual review of fluid mechanics, 19(1):271–311, 1987.

[17] SORBIE, K. S.. **Polymer-improved oil recovery**. Springer Science & Business Media, 2013.

[18] PARK, S.; LEE, E. S. ; SULAIMAN, W. R. W.. **Adsorption behaviors of surfactants for chemical flooding in enhanced oil recovery**. Journal of Industrial and Engineering Chemistry, 21:1239–1245, 2015.

[19] BORNAEE, A. H.; MANTEGHIAN, M.; RASHIDI, A.; ALAEI, M. ; ERSHADI, M.. **Oil-in-water pickering emulsions stabilized with functionalized multi-walled carbon nanotube/silica nanohybrids in the presence of high concentrations of cations in water**. Journal of Industrial and Engineering Chemistry, 20(4):1720–1726, 2014.

[20] KARAMBEIGI, M. S.; ABBASSI, R.; ROAYAEI, E. ; EMADI, M. A.. **Emulsion flooding for enhanced oil recovery: interactive optimization**

of phase behavior, microvisual and core-flood experiments. Journal of Industrial and Engineering Chemistry, 29:382–391, 2015.

[21] ROSA, A. J.; DE SOUZA CARVALHO, R. ; XAVIER, J. A. D.. **Engenharia de reservatórios de petróleo**. Interciência, 2006.

[22] ANDERSON, W. G.; OTHERS. **Wettability literature survey-part 1: rock/oil/brine interactions and the effects of core handling on wettability**. Journal of petroleum technology, 38(10):1–125, 1986.

[23] AHMED, T.. **Reservoir engineering handbook**. Gulf Professional Publishing, 2018.

[24] PHILIP, J.. **Flow in porous media**. Annual Review of Fluid Mechanics, 2(1):177–204, 1970.

[25] GUILLEN, V. R.; ROMERO, M. I.; DA SILVEIRA CARVALHO, M. ; ALVARADO, V.. **Capillary-driven mobility control in macro emulsion flow in porous media**. International Journal of multiphase flow, 43:62–65, 2012.

[26] HONARPOUR, M.; CHILINGARIAN, G. ; MAZZULLO, S.. **Permeability and relative permeability of carbonate reservoirs**. In: DEVELOPMENTS IN PETROLEUM SCIENCE, volumen 30, p. 399–416. Elsevier, 1992.

[27] GREEN, D. W.; WILLHITE, G. P. ; OTHERS. **Enhanced oil recovery**, volumen 6. Henry L. Doherty Memorial Fund of AIME, Society of Petroleum Engineers . . . , 1998.

[28] DALTIN, D.. **Tensoativos: química, propriedades e aplicações**. São Paulo: Blucher, p. 11–35, 2011.

[29] BLUNT, M. J.. **Flow in porous media—pore-network models and multiphase flow**. Current opinion in colloid & interface science, 6(3):197–207, 2001.

[30] SHENG, J.. **Modern chemical enhanced oil recovery: theory and practice**. Gulf Professional Publishing, 2010.

[31] LEE, R. F.. **Agents which promote and stabilize water-in-oil emulsions**. Spill Science & Technology Bulletin, 5(2):117–126, 1999.

[32] SANTOS, F. K. G.; ALVES, J. V. A.; DANTAS, T. N. C.; DANTAS NETO, A.; DUTRA JÚNIOR, T. ; BARROS NETO, E.. **Determinação da**

concentração micelar crítica de tensoativos obtidos a partir de óleos vegetais para uso na recuperação avançada de petróleo. In: CONGRESSO BRASILEIRO DE PESQUISA E DESENVOLVIMENTO EM PETRÓLEO E GÁS NATURAL, volumen 4, 2007.

[33] **Kruss advancing your surface science, 2019**. `https://www.kruss-scientific.com/services/education-theory/glossary/critical-micelle-concentration-cmc-and-surfactant-concentration/`. Accessed: 2019-08-08.

[34] KILPATRICK, P. K.. **Water-in-crude oil emulsion stabilization: Review and unanswered questions**. Energy & Fuels, 26(7):4017–4026, 2012.

[35] DEHGHAN, A. A.; JADALY, A.; AYATOLLAHI, S. ; MASIHI, M.. **Acidic heavy oil recovery using a new formulated surfactant accompanying alkali–polymer in high salinity brines**. Journal of Surfactants and Detergents, 20(3):725–733, 2017.

[36] TADROS, T. F.. **Emulsion formation, stability, and rheology**. Emulsion formation and stability, 1:1–75, 2013.

[37] CHEN, G.; TAO, D.. **An experimental study of stability of oil–water emulsion**. Fuel processing technology, 86(5):499–508, 2005.

[38] ABDEL-RAOUF, M. E.-S.. **Factors affecting the stability of crude oil emulsions**. In: CRUDE OIL EMULSIONS-COMPOSITION STABILITY AND CHARACTERIZATION. IntechOpen, 2012.

[39] ARIFFIN, T. S. T.; YAHYA, E. ; HUSIN, H.. **The rheology of light crude oil and water-in-oil-emulsion**. Procedia engineering, 148:1149–1155, 2016.

[40] KOKAL, S. L.; OTHERS. **Crude oil emulsions: A state-of-the-art review**. SPE Production & facilities, 20(01):5–13, 2005.

[41] SHARMA, M.; SHAH, D.. **Introduction to macro-and microemulsions, macroand microemulsion: Theory and applications, vol. 272**, 1985.

[42] MORADI, M.; ALVARADO, V.. **Influence of aqueous-phase ionic strength and composition on the dynamics of water–crude oil interfacial film formation**. Energy & Fuels, 30(11):9170–9180, 2016.

[43] PANG, S.; PU, W.; XIE, J.; CHU, Y.; WANG, C. ; SHEN, C.. **Investigation into the properties of water-in-heavy oil emulsion and its role in enhanced oil recovery during water flooding**. Journal of Petroleum Science and Engineering, 177:798–807, 2019.

[44] PANG, J.; DU, S.; CHANG, R.; PEI, Q. ; CUI, D.. **Interfacial rheology of mixed surfactants at the oil/water interface**. Journal of Surfactants and Detergents, 18(5):747–753, 2015.

[45] ALVES, D. R.; CARNEIRO, J. S.; OLIVEIRA, I. F.; FAÇANHA JR, F.; SANTOS, A. F.; DARIVA, C.; FRANCESCHI, E. ; FORTUNY, M.. **Influence of the salinity on the interfacial properties of a brazilian crude oil–brine systems**. Fuel, 118:21–26, 2014.

[46] DJAPAN, M.; MILOSEVIC, M.. **Influence of processing on cosmetic, pharmaceutical and food emulsions quality, stability and rheology**. Center for Quality, 2013.

[47] GOUAL, L.. **Petroleum asphaltenes**. In: CRUDE OIL EMULSIONS-COMPOSITION STABILITY AND CHARACTERIZATION. IntechOpen, 2012.

[48] HAVRE, T. E.; SJÖBLOM, J.. **Emulsion stabilization by means of combined surfactant multilayer (d-phase) and asphaltene particles**. Colloids and Surfaces A: Physicochemical and Engineering Aspects, 228(1-3):131–142, 2003.

[49] ROUSSEAU, G.; ZHOU, H.; HURTEVENT, C. ; OTHERS. **Calcium carbonate and naphthenate mixed scale in deep-offshore fields**. In: INTERNATIONAL SYMPOSIUM ON OILFIELD SCALE. Society of Petroleum Engineers, 2001.

[50] BRANDAL, Ø.; HANNESETH, A.-M. D. ; SJÖBLOM, J.. **Interactions between synthetic and indigenous naphthenic acids and divalent cations across oil–water interfaces: effects of addition of oil-soluble non-ionic surfactants**. Colloid and Polymer Science, 284(2):124–133, 2005.

[51] CHRISMAN, E.; LIMA, V. ; MENECHINI, P.. **Asphaltenes–problems and solutions in e&p of brazilian crude oils**. In: CRUDE OIL EMULSIONS-COMPOSITION STABILITY AND CHARACTERIZATION. IntechOpen, 2012.

[52] NORDGÅRD, E. L.; SØRLAND, G. ; SJÖBLOM, J.. **Behavior of asphaltene model compounds at w/o interfaces**. Langmuir, 26(4):2352–2360, 2009.

[53] DICHARRY, C.; ARLA, D.; SINQUIN, A.; GRACIAA, A. ; BOURIAT, P.. **Stability of water/crude oil emulsions based on interfacial dilatational rheology**. Journal of colloid and interface science, 297(2):785–791, 2006.

[54] BORGES, B.. **Natural surfactants from venezuelan extra heavy crude oil-study of interfacial and structural properties**. In: CRUDE OIL EMULSIONS-COMPOSITION STABILITY AND CHARACTERIZATION. IntechOpen, 2012.

[55] WANG, X.; PENSINI, E.; LIANG, Y.; XU, Z.; CHANDRA, M. S.; ANDERSEN, S. I.; ABDALLAH, W. ; BUITING, J. J.. **Fatty acid-asphaltene interactions at oil/water interface**. Colloids and Surfaces A: Physicochemical and Engineering Aspects, 513:168–177, 2017.

[56] VERRUTO, V. J.; KILPATRICK, P. K.. **Water-in-model oil emulsions studied by small-angle neutron scattering: interfacial film thickness and composition**. Langmuir, 24(22):12807–12822, 2008.

[57] SAUERER, B.; STUKAN, M.; BUITING, J.; ABDALLAH, W. ; ANDERSEN, S.. **Dynamic asphaltene-stearic acid competition at the oil–water interface**. Langmuir, 34(19):5558–5573, 2018.

[58] MACKAY, G.; MCLEAN, A.; BETANCOURT, O. ; JOHNSON, B.. **Formation of water-in-oil emulsions subsequent to an oil spill**. Institute of Petroleum, Journal of, 59(568), 1973.

[59] GAZICKI, M.; JAMES, W. ; YASUDA, H.. **Colloids and surfaces a: Physicochemical and engineering aspects**. Journal of Polymer Science: Letters Polymer Edition, 23:639–645, 1985.

[60] PU, W.; SHEN, C.; PANG, S.; TANG, X.; TIAN, Q. ; SONG, Y.. **Properties of emulsions formed in situ in a heavy-oil reservoir during water flooding: Effects of salinity and ph**. Journal of Surfactants and Detergents, 21(5):699–710, 2018.

[61] ALVARADO, V.; MORADI BIDHENDI, M.; GARCIA-OLVERA, G.; MORIN, B.; OAKEY, J. S. ; OTHERS. **Interfacial visco-elasticity of crude oil-brine: An alternative eor mechanism in smart waterflooding**.

In: SPE IMPROVED OIL RECOVERY SYMPOSIUM. Society of Petroleum Engineers, 2014.

[62] IIDA, P. H.; SCHEER, A. D. P.; WEINSCHUTZ, R. ; SANTOS, B. M. D.. **Estudo do efeito da água em emulsões de petróleo**. UFPR, Curitiba, PR, 83:3322–3222, 2007.

[63] SOARES, I. F.. **Reologia de ácidos orgânicos na interface água/óleo**. Master's thesis, Universidade Federal do Rio de Janeiro, Rio de Janeiro, Brazil., 2017.

[64] CHEN, H.; ZHANG, Y.; LIU, X.; ZHANG, Y. ; FANG, Y.. **Reversibly ph-switchable anionic-surfactant-based emulsions**. Journal of Surfactants and Detergents, 20(5):1115–1120, 2017.

[65] DAAOU, M.; BENDEDOUCH, D.. **Water ph and surfactant addition effects on the stability of an algerian crude oil emulsion**. Journal of Saudi Chemical Society, 16(3):333–337, 2012.

[66] MORADI, M.; ALVARADO, V. ; HUZURBAZAR, S.. **Effect of salinity on water-in-crude oil emulsion: evaluation through drop-size distribution proxy**. Energy & fuels, 25(1):260–268, 2010.

[67] BORGES, B.; RONDÓN, M.; SERENO, O. ; ASUAJE, J.. **Breaking of water-in-crude-oil emulsions. 3. influence of salinity and water-oil ratio on demulsifier action**. Energy & Fuels, 23(3):1568–1574, 2009.

[68] MAAREF, S.; AYATOLLAHI, S.; REZAEI, N. ; MASIHI, M.. **The effect of dispersed phase salinity on water-in-oil emulsion flow performance: a micromodel study**. Industrial & Engineering Chemistry Research, 56(15):4549–4561, 2017.

[69] YANG, X.; VERRUTO, V. J. ; KILPATRICK, P. K.. **Dynamic asphaltene- resin exchange at the oil/water interface: Time-dependent w/o emulsion stability for asphaltene/resin model oils**. Energy & fuels, 21(3):1343–1349, 2007.

[70] VERRUTO, V. J.; LE, R. K. ; KILPATRICK, P. K.. **Adsorption and molecular rearrangement of amphoteric species at oil- water interfaces**. The Journal of Physical Chemistry B, 113(42):13788–13799, 2009.

[71] LAKE, L. W.. **Enhanced oil recovery**. Old Tappan, NJ; Prentice Hall Inc., 1989.

[72] BRANDAL, Ø.. **Interfacial (o/w) properties of naphthenic acids and metal naphthenates, naphthenic acid characterization and metal naphthenate inhibition**. NTNU, 2005.

[73] MORADI, M.; KAZEMPOUR, M.; FRENCH, J. T. ; ALVARADO, V.. **Dynamic flow response of crude oil-in-water emulsion during flow through porous media**. Fuel, 135:38–45, 2014.

[74] COBOS, S.; CARVALHO, M. ; ALVARADO, V.. **Flow of oil–water emulsions through a constricted capillary**. International Journal of Multiphase Flow, 35(6):507–515, 2009.

[75] PONCE, F.; ALVARADO, V.; CARVALHO, M. ; OTHERS. **Water-alternating-macroemulsion reservoir simulation through capillary number-dependent modeling**. JOURNAL-BRAZILIAN SOCIETY OF MECHANICAL SCIENCES AND ENGINEERING, 39(10):4135–4145, 2017.

[76] KUMAR, R.; DAO, E. K.; MOHANTY, K. K. ; OTHERS. **Emulsion flooding of heavy oil**. In: SPE IMPROVED OIL RECOVERY SYMPOSIUM. Society of Petroleum Engineers, 2010.

[77] DE FARIAS, R.; LEOPOLDINO, M.; CARVALHO, M. D. S.; SOUZA, A. S. D.; HIRASAKI, G. J.; MILLER, C. A. ; OTHERS. **A comparative study of emulsion flooding and other ior methods for heavy oil fields**. In: SPE LATIN AMERICA AND CARIBBEAN PETROLEUM ENGINEERING CONFERENCE. Society of Petroleum Engineers, 2012.

[78] PU, W.; SHEN, C.; TANG, X.; PANG, S.; SUN, D. ; MEI, Z.. **Emulsification of acidic heavy oil for viscosity reduction and enhanced oil recovery**. Journal of Dispersion Science and Technology, p. 1–8, 2018.

[79] LANGEVIN, D.; POTEAU, S.; HÉNAUT, I. ; ARGILLIER, J.. **Crude oil emulsion properties and their application to heavy oil transportation**. Oil & gas science and technology, 59(5):511–521, 2004.

[80] ALVARADO, V.; GARCIA-OLVERA, G.; HOYER, P.; LEHMANN, T. E. ; OTHERS. **Impact of polar components on crude oil-water interfacial film formation: A mechanisms for low-salinity waterflooding**. In: SPE ANNUAL TECHNICAL CONFERENCE AND EXHIBITION. Society of Petroleum Engineers, 2014.

[81] ROMERO, M. I.; OTHERS. **Flow of emulsions in porous media**. In: SPE ANNUAL TECHNICAL CONFERENCE AND EXHIBITION. Society of Petroleum Engineers, 2009.

[82] ENGELKE, B. S.. **Determinação das Curvas de Permeabilidade Relativa no Escoamento de Emulsões e Óleo**. PhD thesis, PUC-Rio, 2012.

[83] CARVALHO, M. S.; ALVARADO, V. ; OTHERS. **Oil recovery modeling of macro-emulsion flooding at low capillary number**. Journal of Petroleum Science and Engineering, 119:112–122, 2014.

[84] MCAULIFFE, C. D.; OTHERS. **Oil-in-water emulsions and their flow properties in porous media**. Journal of petroleum technology, 25(06):727–733, 1973.

[85] MCAULIFFE, C. D.; OTHERS. **Crude-oil-water emulsions to improve fluid flow in an oil reservoir**. Journal of Petroleum Technology, 25(06):721–726, 1973.

[86] HOFMAN, J.; STEIN, H.. **Permeability reduction of porous media on transport of emulsions through them**. Colloids and surfaces, 61:317–329, 1991.

[87] ENGELKE, B.; CARVALHO, M. S. ; ALVARADO, V.. **Conceptual darcy-scale model of oil displacement with macroemulsion**. Energy & Fuels, 27(4):1967–1973, 2013.

[88] **Nih u.s. national library of medicine, 2019**. `https://toxnet.nlm.nih.gov/cgi-bin/sis/search2/r?dbs+hsdb:@term+@DOCNO+6854`. Accessed: 2019-08-08.

[89] **Chebi, 2019**. https://www.ebi.ac.uk/chebi/searchId.do?chebiId=CHEBI:45296. Accessed: 2019-08-08.

[90] HAYNES, W. M.. **CRC handbook of chemistry and physics**. CRC press, 2014.

[91] ASTM. **Standard Practice for the Preparation of Substitute Ocean Water**. ASTM International D1141-98 (Re-approved 2013), 2013.

[92] NAHAS, G. G.. **The pharmacology of tris (hydroxymethyl) aminomethane (tham)**. Pharmacological reviews, 14(3):447–472, 1962.

[93] ANDERSEN, N.. **Tris (hydroxym ethyl) amino-m ethane (tham) used as a buffer in bronchoscopy and "apnoeic oxygenation"**. Acta Anaesthesiologica Scandinavica, 6(2):57–69, 1962.

[94] KENKEL, J.. **Analytical chemistry for technicians**. CRC Press, 2013.

[95] XU, L.; YANG, R.. **Stearic acid/inorganic porous matrix phase change composite for hot water systems**. Molecules, 24(8):1482, 2019.

[96] HERYANTO, R.; HASAN, M.; ABDULLAH, E. C. ; KUMORO, A. C.. **Solubility of stearic acid in various organic solvents and its prediction using non-ideal solution models**. ScienceAsia, 33:469–472, 2007.

[97] KILLEN, B. U.; CORRIGAN, O. I.. **Factors influencing drug release from stearic acid based compacts**. International journal of pharmaceutics, 228(1-2):189–198, 2001.

[98] GONÇALVES BONASSOLI, A. B.; OLIVEIRA, G.; BORDON SOSA, F. H.; ROLEMBERG, M. P.; MOTA, M. A.; BASSO, R. C.; IGARASHI-MAFRA, L. ; MAFRA, M. R.. **Solubility measurement of lauric, palmitic, and stearic acids in ethanol, n-propanol, and 2-propanol using differential scanning calorimetry**. Journal of Chemical & Engineering Data, 64(5):2084–2092, 2019.

[99] THENESHKUMAR, S.; GNANAPRAKASH, D. ; NAGENDRA GANDHI, N.. **Solubility and mass transfer coefficient enhancement of stearic acid through hydrotropy**. Journal of Chemical & Engineering Data, 55(9):2980–2984, 2010.

[100] DEMIRBAS, A.; SARI, A. ; ISILDAK, O.. **Adsorption thermodynamics of stearic acid onto bentonite**. Journal of hazardous materials, 135(1-3):226–231, 2006.

[101] LIN, Y.; ZHU, C. ; FANG, G.. **Synthesis and properties of microencapsulated stearic acid/silica composites with graphene oxide for improving thermal conductivity as novel solar thermal storage materials**. Solar Energy Materials and Solar Cells, 189:197–205, 2019.

[102] ROWE, R. C.; SHESKEY, P. J.; OWEN, S. C. ; OTHERS. **Handbook of pharmaceutical excipients**, volumen 1. Pharmaceutical press London, 2006.

[103] SCHMIDT, W. F.; BARONE, J. R.; FRANCIS, B. ; REEVES III, J. B.. **Stearic acid solubility and cubic phase volume**. Chemistry and physics of lipids, 142(1-2):23–32, 2006.

[104] LIU, W. J.; SUN, C.; ZHAO, P. X. ; WANG, S. F.. **Solubility of stearic acid in ethanol, 1-propanol, 2-propanol, l-butanol, acetone, methylene chloride, ethyl acetate and 95% ethanol from (293 to 315) k**. In: ADVANCED MATERIALS RESEARCH, volumen 550, p. 71–74. Trans Tech Publ, 2012.

[105] **Dataphysics undestanding interfaces, 2019**. https://www.dataphysics-instruments.com/products/dcat/tensiometry. Accessed: 2019-08-08.

[106] PALOMBO, L.. **A microtomografia de raios X e a porosimetria por intrusão de mercúrio na determinação de porosidade e densidade de rochas reservatório.** PhD thesis, Universidade de São Paulo, 2017.

A
Dilatational interfacial rheology - Reproduced tests

This appendix shows results of dilatational interfacial rheology tests, with 3 repetitions for each surfactant concentration. Figures A.1 and A.2 show these results for synthetic seawater and hexadecane at 45°C doped with 0 and 0.5% of stearic acid, no repeatability with stearic acid was observed, probably due to Laplacian shape loss. Figures A.3 - A.6 present the rheology tests for Milli-Q water and hexadecane at 45°C doped with 0, 0.5, 1, and 3% of stearic acid. Reasonable repeatability was observed, except for the 3%, which had noisier curves, possibly due to the formation of stearic acid crystals leading to needle clogging due to the high stearic acid concentration.

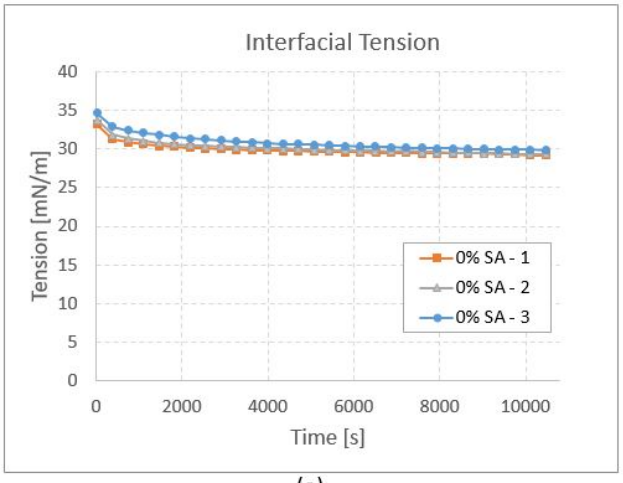

(a)

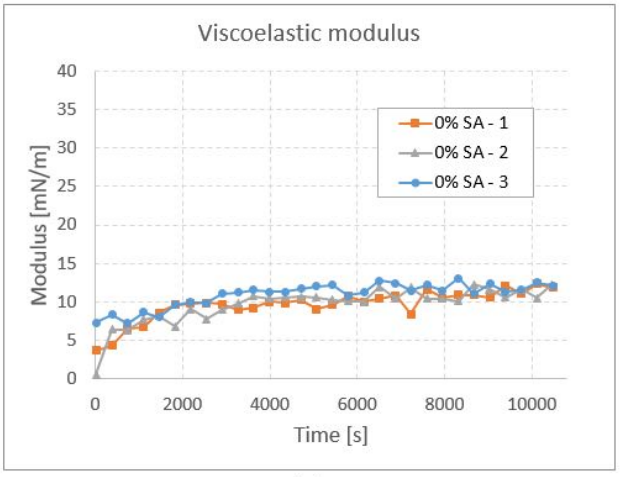

(b)

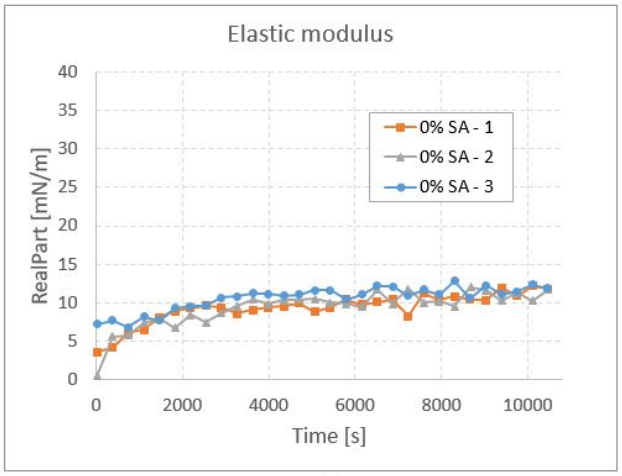

(c)

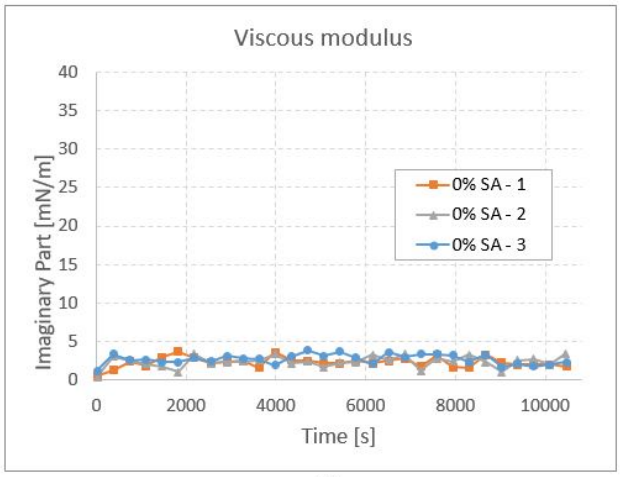

(d)

Figure A.1: Dilatational interfacial rheology results between synthetic seawater and hexadecane at 45°C doped with 0% of stearic acid (SA) (a) Interfacial tension (b) Dilatational viscoelastic modulus (c) Elastic modulus (d) Viscous modulus.

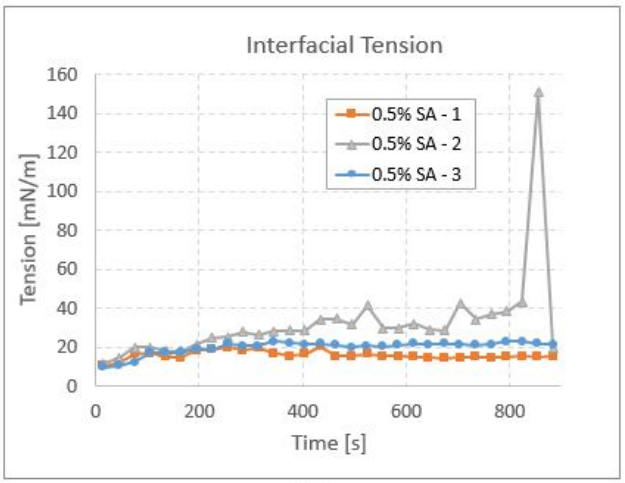

(a)

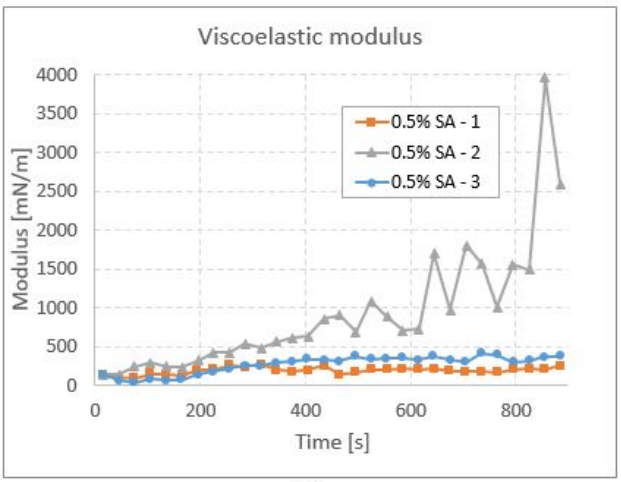

(b)

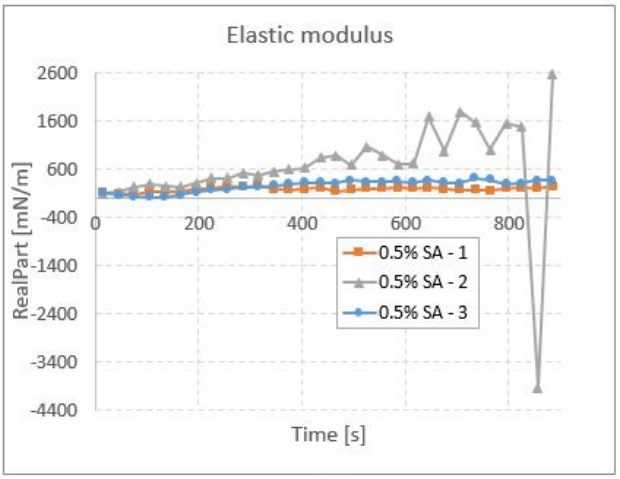

(c)

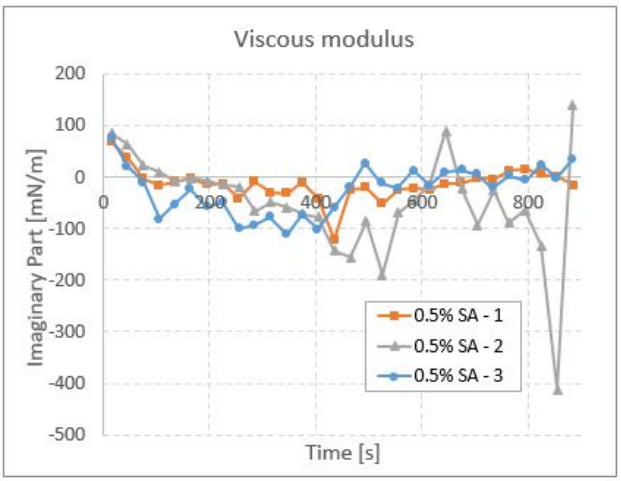

(d)

Figure A.2: Dilatational interfacial rheology results between synthetic seawater and hexadecane at 45°C doped with 0.5% of stearic acid (SA) (a) Interfacial tension (b) Dilatational viscoelastic modulus (c) Elastic modulus (d) Viscous modulus.

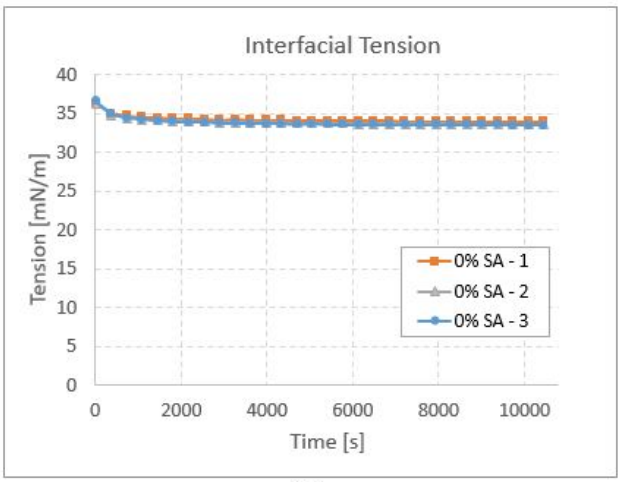

(a)

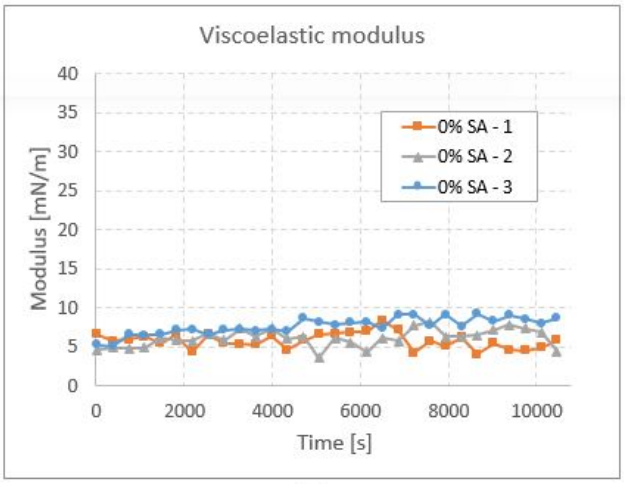

(b)

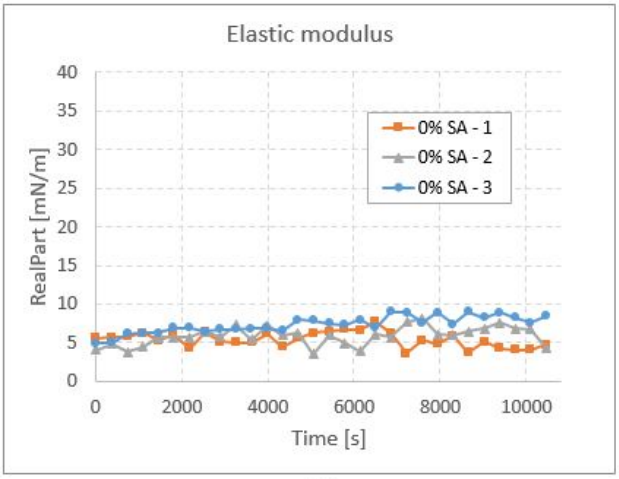

(c)

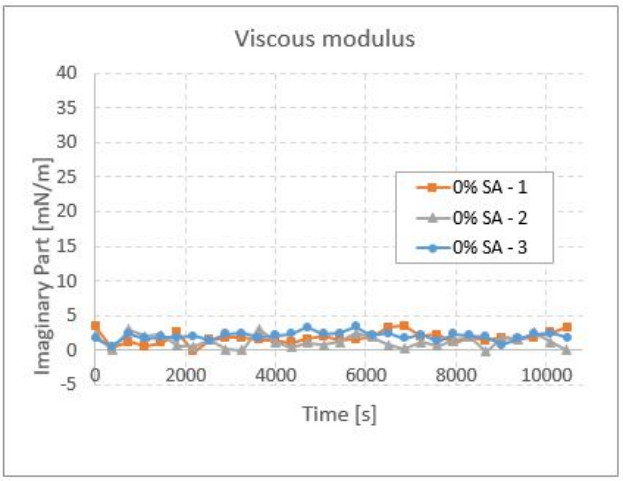

(d)

Figure A.3: Dilatational interfacial rheology results between Milli-Q water and hexadecane at 45°C doped with 0% of stearic acid (SA) (a) Interfacial tension (b) Dilatational viscoelastic modulus (c) Elastic modulus (d) Viscous modulus.

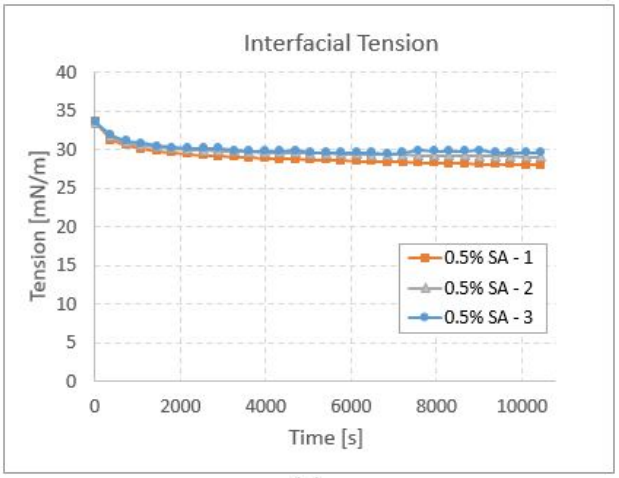

(a)

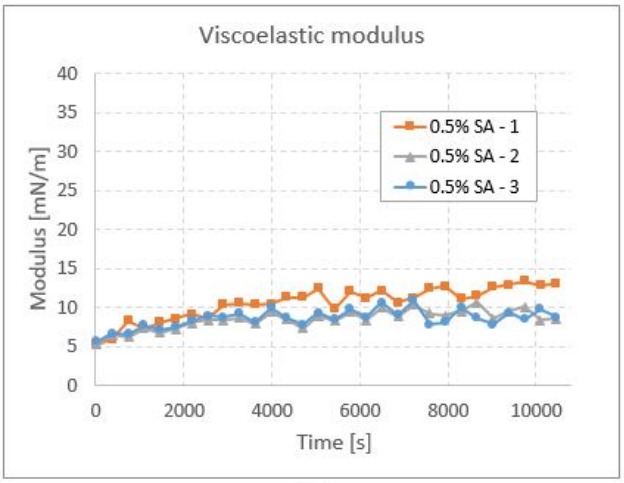

(b)

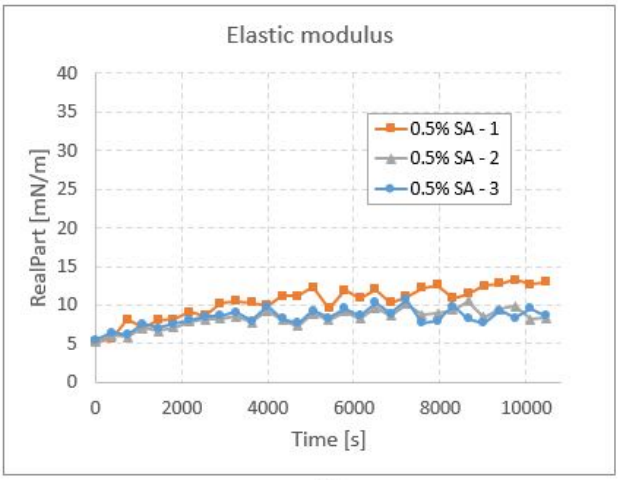

(c)

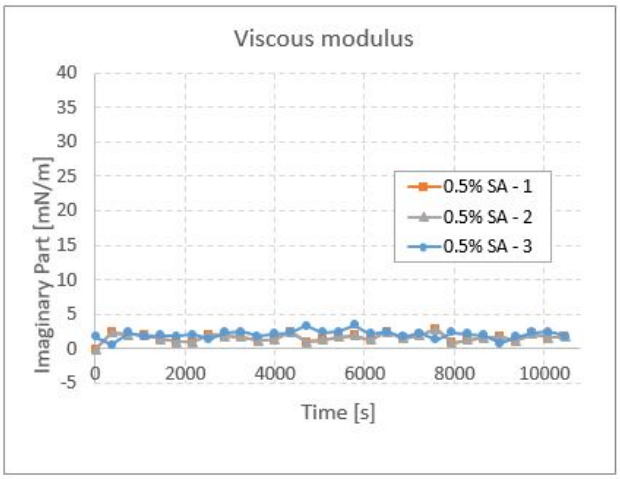

(d)

Figure A.4: Dilatational interfacial rheology results between Milli-Q water and hexadecane at 45°C doped with 0.5% of stearic acid (SA) (a) Interfacial tension (b) Dilatational viscoelastic modulus (c) Elastic modulus (d) Viscous modulus.

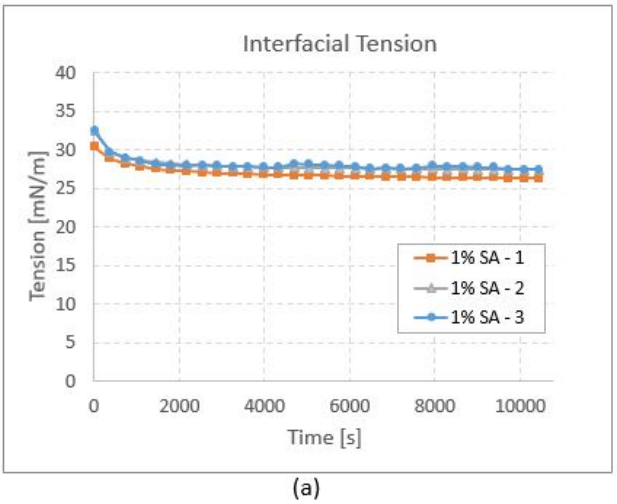

(a)

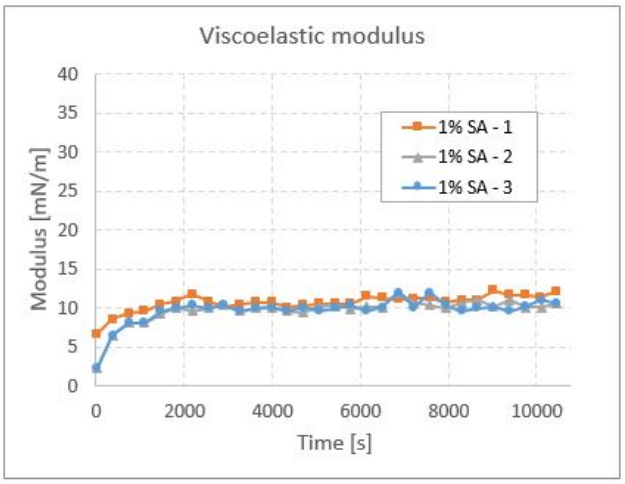

(b)

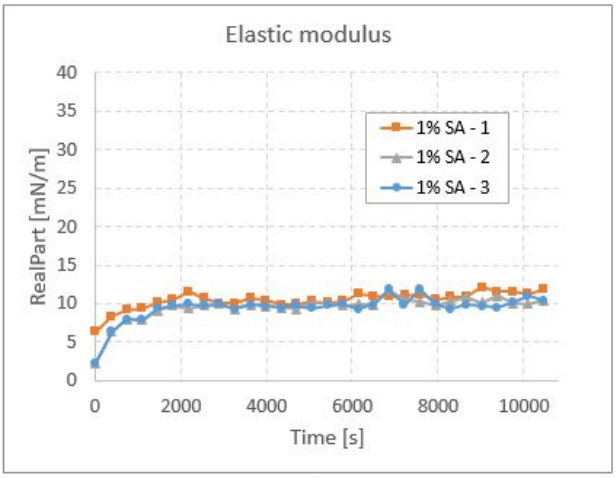

(c)

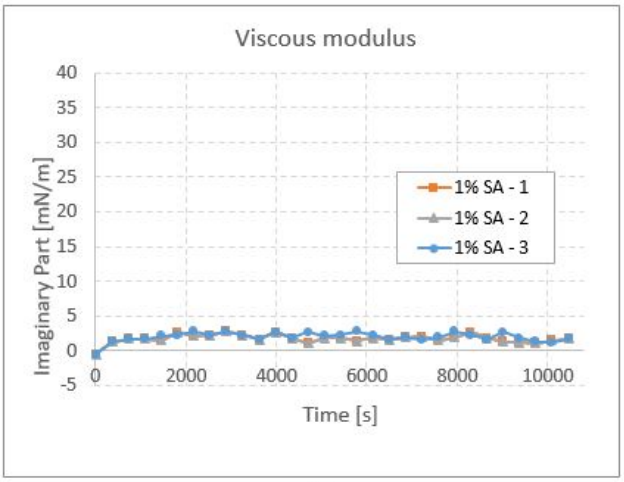

(d)

Figure A.5: Dilatational interfacial rheology results between Milli-Q water and hexadecane at 45°C doped with 1% of stearic acid (SA) (a) Interfacial tension (b) Dilatational viscoelastic modulus (c) Elastic modulus (d) Viscous modulus.

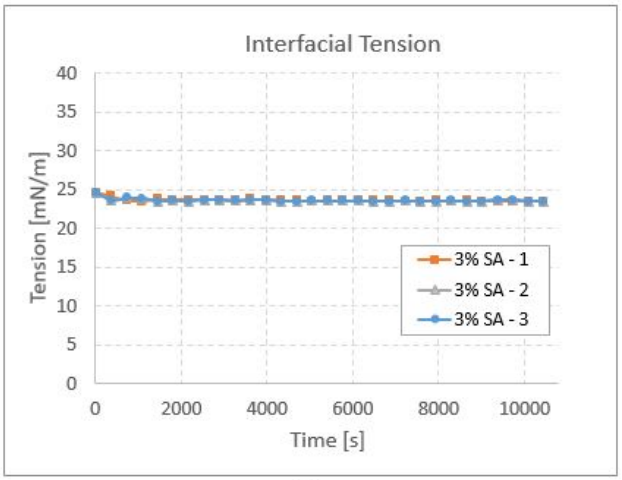

(a)

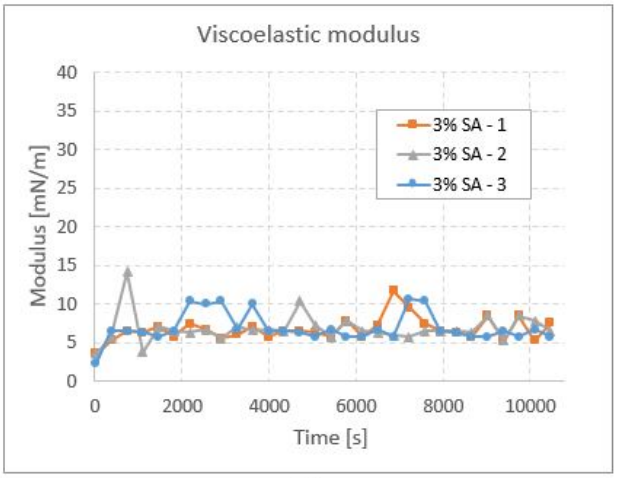

(b)

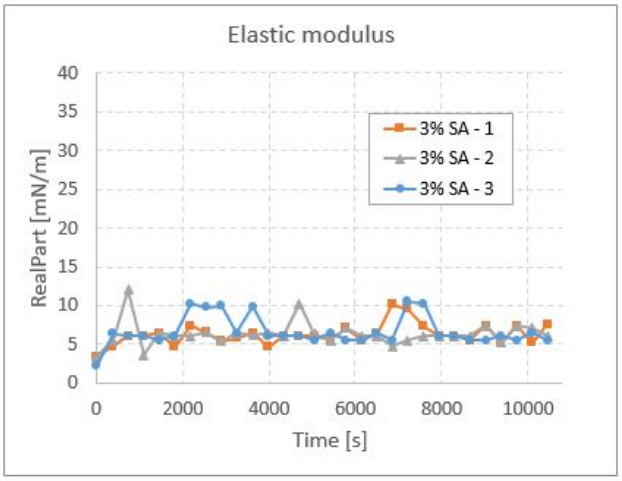

(c)

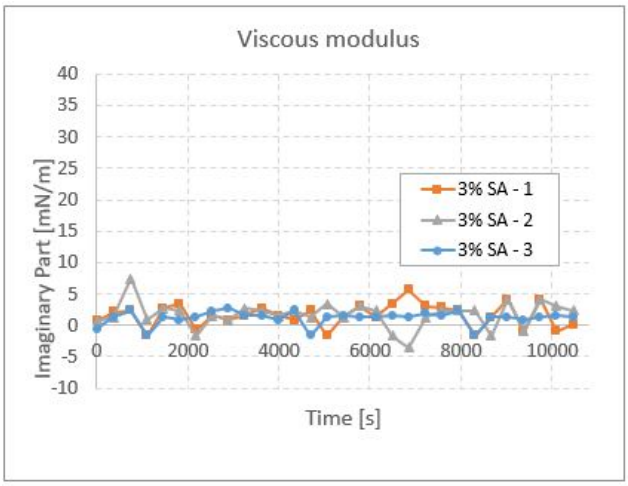

(d)

Figure A.6: Dilatational interfacial rheology results between Milli-Q water and hexadecane at 45°C doped with 3% of stearic acid (SA) (a) Interfacial tension (b) Dilatational viscoelastic modulus (c) Elastic modulus (d) Viscous modulus.